University of Szeged

Faculty of Pharmacy

Department of Pharmaceutical Technology

Head: Prof. Dr. Piroska Szabó-Révész D.Sc.

DEVELOPMENT AND INVESTIGATION OF NANOSTRUCTURED LIPID CARRIERS FOR TRANSDERMAL DRUG DELIVERY

Ph.D. Thesis

by

Blanka Sütő
pharmacist

Supervisors:

Dr. habil. Erzsébet Csányi

and

Dr. Szilvia Berkó Ph.D.

Szeged

2016

PUBLICATIONS RELATED TO THE SUBJECT OF THE THESIS

ARTICLES

I. Szilvia Berkó, Boglárka Balázs, **Blanka Sütő**, Gábor Erős, Brigitta Gál, Anita Sztojkov-Ivanov, Codruta Soica, Piroska Szabó-Révész, Lajos Kemény, István Zupkó and Erzsébet Csányi: Monitoring of skin penetration and absorption with a new *in vivo* experimental model.
Farmacia 62 (6) 1157-1163 (2014)

IF: 1.005 (2014)

II. **Blanka Sütő**, Sabrina Weber, Andreas Zimmer, Gabriella Farkas, András Kelemen, Mária Budai-Szűcs, Szilvia Berkó, Piroska Szabó-Révész and Erzsébet Csányi: Optimization and design of an Ibuprofen-loaded nanostructured lipid carrier with a 2^3 full factorial design.
Chemical Engineering Research and Design 104 488–496 (2015)

IF: 2.348 (2014)

III. **Sütő Blanka**, Berkó Szilvia, Csányi Erzsébet: Nanostrukturált lipid hordozó rendszerek alkalmazása a bőrön keresztüli hatóanyag-penetráció elősegítésére.
Gyógyszerészet 60 (2) 76-85 (2016)

IF: -

IV. **Blanka Sütő,** Szilvia Berkó, Gábor Kozma, Ákos Kukovecz, Mária Budai-Szűcs, Gábor Erős, Lajos Kemény, Anita Sztojkov-Ivanov, Róbert Gáspár and Erzsébet Csányi: Development of Ibuprofen-loaded nanostructured lipid carrier-based gels: characterization and investigation of *in vitro* and *in vivo* penetration through the skin.
International Journal of Nanomedicine (accepted for publication)

IF: 4.348 (2014)

ABSTRACTS

1. **Blanka Sütő**, Sabrina Weber, Szilvia Berkó, Erzsébet Csányi, Piroska Révész and Andreas Zimmer: Ibuprofen loaded lipid nanoparticles (SLN and NLC) for topical delivery. *2nd Pharma DocDay*; Graz, Austria, 04. 07. 2013.
2. **Blanka Sütő**, Sabrina Weber, Gabriella Farkas, Rita Ambrus, Erzsébet Csányi, Piroska Szabóné Révész, Andreas Zimmer, and Szilvia Berkó: Ibuprofén tartalmú nanostrukturált lipid hordozók előállítása és vizsgálata transzdermális kezelés biztosítására. *Congressus Pharmaceuticus Hungaricus XV.*, Budapest, Hungary, 10-12. 04. 2014.
3. Berkó Szilvia, **Sütő Blanka,** Szabóné Révész Piroska and Csányi Erzsébet: Rossz vízoldékonyságú hatóanyagok formulálása szilárd lipid nanohordozók alkalmazásával. *MKE Kristályosítási és Gyógyszerformulálási Szakosztály 7. Kerekasztal Konferenciája*; Szeged, Hungary, 16-17. 05. 2014.
4. **Sütő Blanka**, Budai-Szűcs Mária, Csányi Erzsébet and Berkó Szilvia: Termoanalitika alkalmazása lipid nanorészecskék formulálásában. *MKE Termoanalitikai Szakosztályának Termikus ülése*; Szeged, Hungary, 21. 11. 2014.
5. **Blanka Sütő**, Gabriella Farkas, András Kelemen, Mária Budai-Szűcs, Szilvia Berkó, Piroska Szabó-Révész and Erzsébet Csányi: Optimization of an Ibuprofen loaded nanostructured lipid carrier with 2^3 full factorial design. *Stratum Corneum VIII*. Cardiff, United Kingdom, 17-19. 09. 2014. *International Journal of Cosmetic Science* 37 (1) pp. 159-160. (2015)
6. **Blanka Sütő**, Mária Budai-Szűcs, Péter Sipos, Erzsébet Csányi, Piroska Szabó-Révész and Szilvia Berkó: Characterisation of nanostructured lipid carriers loaded with ibuprofen. *5th International Conference and Exhibition on Pharmaceutics & Novel Drug Delivery Systems*; Dubai, United Arab Emirates, 16-18. 03. 2015. *Pharmaceutica Analytica Acta* 6 (1) p. 82. (2015)
7. **Blanka Sütő**, Nikolett Ungvári, Erzsébet Csányi, Piroska Szabó-Révész and Szilvia Berkó: Factorial design-aided development of salicylic acid loaded nanostrucured lipid carriers. *1st European Conference on Pharmaceutics: Drug delivery*, Reims, France, 13-14. 04. 2015.
8. **Sütő Blanka**, Berkó Szilvia, Csányi Erzsébet: Nemszteroid gyulladásgátlót tartalmazó NLC rendszerek fejlesztése. *Gyógyszertechnológiai és Ipari Gyógyszerészeti Konferencia*, Siófok, Hungary, 15-17. 10. 2015.

TABLE OF CONTENTS

ABBREVIATIONS

AFM – atomic force microscopy
API – active pharmaceutical ingredient
average Z – average height of the particles
BCS – biopharmaceutical classification system
CI(%) – crystallinity index
d(0.1), *d*(0.5), *d*(0.9), *d*(0.95) and *d*(0.99) – diameters of 10%, 50%, 90%, 95% and 99% of the particles are below the measured size value
DDS – drug delivery system
DL% – drug loading
DSC – differential scanning calorimetry
EE% – entrapment efficiency
FT-IR spectroscopy – Fourier transform infrared spectroscopy
GRAS – generally recognized as safe
HLB – hydrophilic–lipophilic balance
HPLC – high-performance liquid chromatography
IBU – ibuprofen
IBU-NLC – ibuprofen-loaded nanostructured lipid carrier
IFT – interfacial tension
LD – laser diffraction
LDC – lipid drug conjugate
LNP – lipid nanoparticle
MWCO – molecular weight cut-off
NLC – nanostructured lipid carrier
NSAID – nonsteroidal anti-inflammatory drug
PBS – phosphate buffer solution
PCS – photon correlation spectroscopy
PDI – polydispersity index
PLN – polymer-lipid hybrid nanoparticle
PS – particle size
RSM – response surface methodology
SC – stratum corneum
SLN – solid lipid nanoparticle
XRD – X-ray diffraction
Z_{ave} – effective particle size
ZP – zeta potential

1. INTRODUCTION

The topical application of drugs is a favorable administration route in the treatment of skin diseases and musculoskeletal disorders. The advantage of dermal preparations is their administration at the site where the effect is needed [1].

Lipid nanoparticles (LNPs) are intensively studied drug delivery systems (DDSs) derived from o/w emulsions; they combine the advantages of polymeric nanoparticles, conventional emulsions and liposomes, while simultaneously avoiding their disadvantages [2-7]. They are capable of improving the insufficient physicochemical properties of biopharmaceutical classification system (BCS) class II (low water solubility and high permeability) active pharmaceutical ingredients (APIs), such as nonsteroidal anti-inflammatory drugs (NSAIDs) [1, 8-13], enhancing their bioavailability. The second generation of LNPs comprises the nanostructured lipid carriers (NLCs). The dermal use of NLC systems offers a number of advantages, such as physical stability of the applied topical formulations, enhancement of the chemical stability of the incorporated APIs, improved dermal bioavailability, the skin targeting of the APIs, and film formation on the skin, accompanied by controlled occlusion and skin hydration *in vivo* [14, 15]. UV-reflecting properties (e.g. the possibility of using these carriers in sunscreens to help increase their protective effect against UV light) and the possibility of modulating API release into the skin have also been reported [2, 16].

However, formulation of an NLC-based drug delivery system is a complex and long-lasting procedure, since the physicochemical properties of NLCs are altered by many factors, such as the quality and quantity of the selected lipids and surfactants or the ratio of lipids to API in the formulation. In view of their significant effects on the physicochemical properties of the nanoparticles, the selection of the proper ingredients is a crucial step in the formulation of NLCs. Optimization of the formulation via a factorial design could facilitate this process [2, 17]. Response surface methodology (RSM) is an appropriate tool with which to evaluate the correspondence between the response and independent variables and to optimize the processes or products [18]. RSM requires less experimentation and provides estimates of the relative significance of the different variables [19].

2. LITERATURE BACKGROUND

2.1 Lipid nanoparticles

LNPs are colloidal carriers which were introduced in the early 1990s. They are derived from o/w emulsions by replacing the liquid lipid with a solid lipid [4, 5, 14, 20, 21]. They range in size from 50 to1000 nm. LNPs are composed of physiologically tolerable lipids and they usually possess the GRAS (generally recognized as safe) grade [6]. The particles are in the solid state at both room and body temperature. The mobility of the incorporated drug is therefore reduced, which predicts controlled drug release from these systems [3].

LNPs possess the advantages of other colloidal carriers and avoid their disadvantages, such as [2]:

- the nanoparticles are not taken up readily by the cells of the reticulo-endothelial system and hence they bypass liver and spleen filtration [22],
- the possibility of controlled drug release and drug targeting [3, 4, 23],
- increased drug stability [24, 25],
- a high drug payload [7],
- the incorporation of both lipophilic and hydrophilic drugs [26-28],
- no biotoxicity of the carrier [29, 30],
- the avoidance of organic solvents [31],
- no problems with respect to large-scale production and sterilization [32-34].

2.1.1 Types of lipid nanoparticles

There are four groups of LNPs: the first generation are called s*olid lipid nanoparticles (SLNs)*. The lipid matrix of this DDS consists of only one type of solid lipid or blend of solid lipids, which is stabilized by surfactant(s) in an outer aqueous phase. The drawback of using lipids in the solid state is that they tend to form a perfect crystal lattice during storage, which will lead to low drug incorporation capacity and drug expulsion [25]. To overcome these limitations of the SLNs, a second generation, *nanostructured lipid carriers (NLCs)* was introduced. The lipid phase of an NLC formulation contains both solid and liquid lipids, which ensures that NLC systems possess certain advantages as compared with SLNs, such as a higher drug-loading capacity and steady drug entrapment during storage [35]. The use of only one lipid as matrix for an SLN tends to lead to the formation of a relatively perfect crystal lattice, which will result in drug expulsion [2, 3, 14, 35, 36]. In contrast, the matrix of

an NLC consists of a mixture of lipids with differently structured molecules, so that the formation of a perfect crystal is limited [14]. Since SLNs and NLCs are highly lipophilic carriers, they can encapsulate lipophilic drugs effectively [21, 37]. Figure 1 depicts the structures of the first two generations of LNPs:

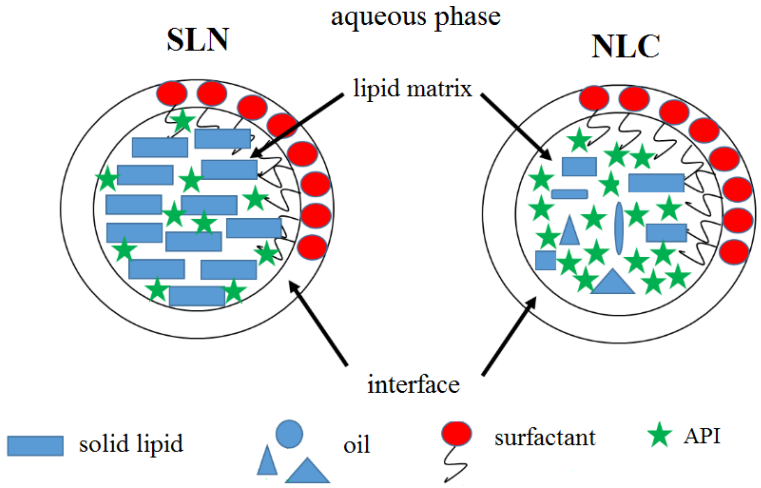

Fig. 1: Structures of solid lipid nanoparticles (SLNs) and nanostructured lipid carriers (NLCs).

Hydrophilic drugs can be incorporated into these DDSs only in very low concentrations. Due to the low drug-loading capacity of hydrophilic drugs, only those with high potency at low concentrations (e.g. proteins and peptides) are appropriate for use in SLNs and NLCs. In order to overcome these limitations of LNPs, *lipid drug conjugates (LDCs)* have been developed. In order to increase the lipophilicity, the hydrophilic drugs are conjugated with a lipid molecule and incorporated into the nanoparticles. *Polymer−Lipid Hybrid Nanoparticles (PLNs)* are suitable for the encapsulation of hydrophilic drugs in their salt forms. The cationic charges of these APIs may lead to low drug incorporation. Through the addition of a counter-ionic polymer, a drug−polymer complex is formed, which demonstrates good partitioning into the lipid matrix [14, 20, 37-39].

2.1.2 Structure of lipid nanoparticles

Depending on the physicochemical properties of the chosen ingredients (the lipid matrix, the surfactant and the API) and on the preparation method, there are three drug incorporation models (Fig. 2) [4, 37]:

- the solid solution (homogenous matrix) model;
- the drug-enriched shell model; and
- the drug-enriched core model.

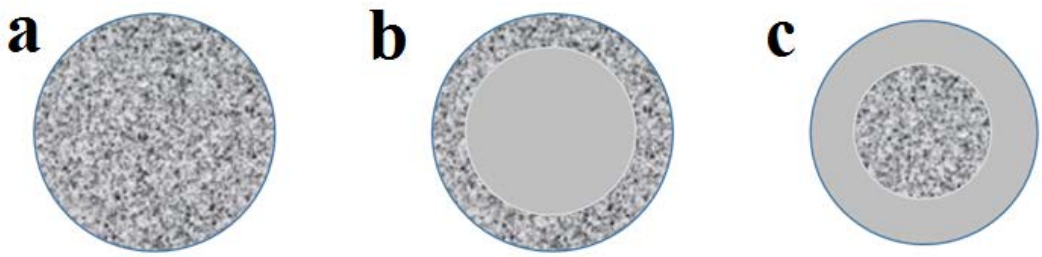

Fig. 2: Drug distribution in the lipid matrix of LNPs: homogenous matrix **(a)**; drug-enriched shell **(b)**; drug-enriched core **(c)**.

The solid solution model can be obtained (the API is molecularly dispersed in the lipid matrix) by the cold homogenization technique [2] without the use of a surfactant or drug-solubilizing agent [4]. API enrichment within the shell occurs when the lipid precipitates, leading to re-partitioning during the cooling process and the lipid can form an API-free core. In contrast, a drug-enriched core may result when the API starts precipitating first and the shell will contain distinctly less of the API. This should be obtained when an API (e.g. prednisolone) is dissolved in the lipid melt at or close to its saturation solubility [40]. The chemical nature and the concentration of any ingredient (API, lipid and surfactant) additionally greatly influence the structure of the LNPs, as do the production conditions (hot or cold homogenization). Depending on the structure, both burst and prolonged drug release can be achieved [4, 15].

2.1.3 NLC models

Based on the lipid compounds used in their production, three NLC models have been proposed (Fig. 3) [21, 37, 41]. These theoretical models have been established based on analytical data, which can be used to physicochemically characterize the matrices of the NLC systems [41].

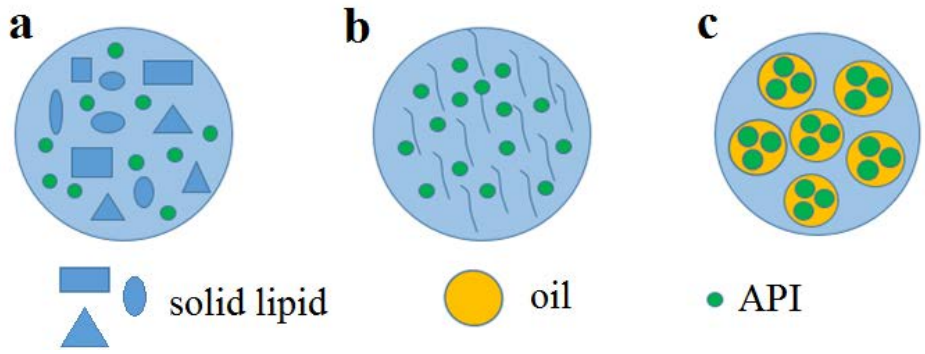

Fig. 3: NLC type I: imperfect crystal model **(a)**, NLC type II: amorphous model **(b)**, and NLC type III: multiple model **(c)**.

The NLC type I is called the imperfect crystal model and can be obtained when solid lipids are mixed with a sufficient amount of liquid lipids (oils). Its matrix consists of many voids and vacancies. High concentrations of API can be incorporated by increasing the number of imperfections. The API is accommodated either in molecular form or as amorphous clusters. Such imperfections can be increased by using glycerides composed of different fatty acids (e.g. mixtures of mono-, di- and triacylglycerols). The matrix of NLC is not able to form a highly ordered structure, thus creating available spaces (structural imperfections) [5, 37, 41]. The NLC type II, or the amorphous model (Fig. 3, b), can be obtained when special lipids are mixed (e.g., hydroxyoctacosanyl-hydroxystearate, isopropyl myristate, dibutyl adipate) that do not recrystallize after homogenization. These lipids create solid, but non-crystalline NLCs, the lipid core congeals in an amorphous nature. The amorphous nanoparticles avoid/delay the recrystallization phenomenon of lipids on cooling and during shelf life, thus minimizing API expulsion during storage time [37, 41].

The NLC type III is defined as the multiple model because it is composed of very small oily nano-compartments created inside the solid lipid matrix of the nanoparticles by a phase separation process [5]. In this type of NLC, higher amounts of oil are blended in solid lipids. At low concentrations, oil molecules are easily dispersed into the lipid matrix. During the cooling of the nanoemulsion the lipid droplets reach the miscibility gap (40 °C), and the oil precipitates forming tiny oil droplets. Subsequent solidification of the solid lipid surrounding these droplets leads to fixation of the oily nano-compartments. Such models allow controlled drug release and the lipid matrix prevents drug leakage. Lipophilic drugs can be solubilized in the oils and multiple types of NLCs are formed during the cooling process of a hot homogenization process. The advantage of this model is the increase of entrapment efficiency (EE%) for APIs of higher solubility in liquid lipids than in solid lipids [37, 41].

2.2 The skin as a possible drug administration route for lipid nanoparticles

The skin is a widely used route of delivery for local and systemic drugs and is potentially a route for their delivery of nanoparticles [16]. The outermost layer of the skin is the stratum corneum (SC), which provides a natural physical barrier against particle penetration, but there are opportunities to deliver therapeutic nanoparticles, especially in diseased skin and to the openings of the hair follicles [42-44].

2.2.1 Drug penetration through the hair follicles

Whilst nanoparticle drug delivery has been touted as an enabling technology, its potential in treating local skin and systemic diseases has yet to be realized. Previously published reports support the hypothesis that nanoparticles >10 nm in diameter are unlikely to penetrate through the SC into viable human skin, but will accumulate in the hair follicle openings (see Fig. 4), especially after massage [43, 44].

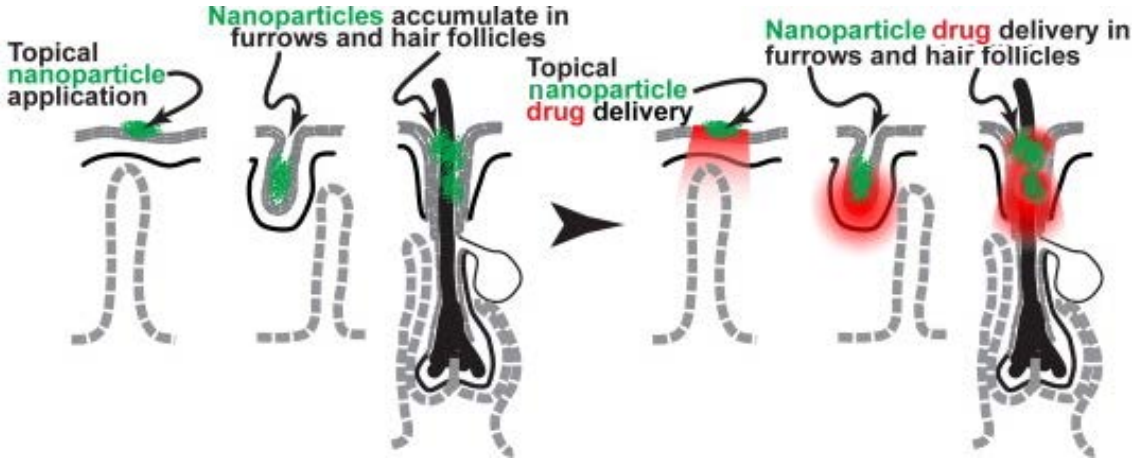

Fig. 4: Accumulation of nanoparticles and drug delivery in the skin [43].

2.2.2 Nanostructured lipid carriers and (trans)dermal drug delivery

NLCs may serve as a solution to overcome the limitations of the dermal permeation of some drugs and to avoid the SC barrier function. This DDS offers numerous advantages for topical application [45, 46]. Figure 5 summarizes the positive effects of NLC systems when applied on human skin.

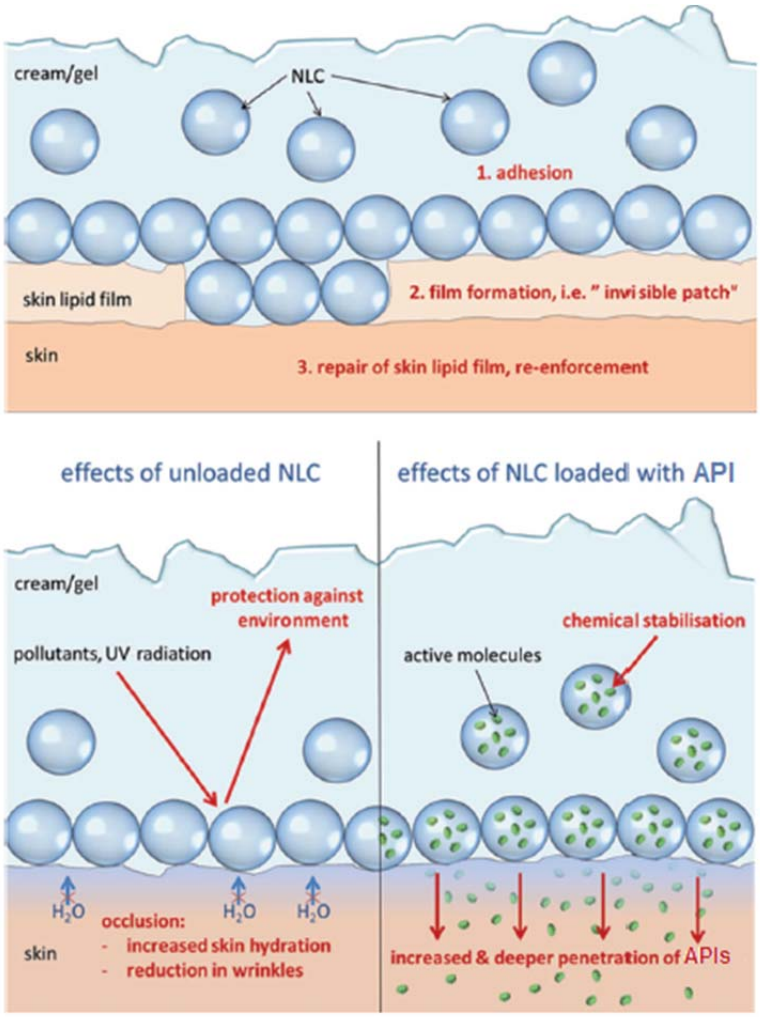

Fig. 5: Effects of NLCs on the skin: NLCs adhere and form a film on the skin, which protects against hazards from the environment and increases the dermal penetration of APIs [46].

The small size of the LNPs ensures close contact between the lipid particles and the lipid bilayer of the SC, resulting in the penetration of an increased amount of drug into the deeper layer of the skin. Sustained and burst release of the drug incorporated in the NLC system may also be achieved [47]. As a result of the film formation that occurs after topical application, occlusive properties have also been reported for NLC formulations [48, 49], and these favor further enhanced penetration through the dermal layers. The NLC particles protect against environmental effects such as UV radiation, and they can function as physical UV filters [46, 50].

3. EXPERIMENTAL AIMS

The aim of my Ph.D. work was to investigate ibuprofen-loaded nanostructured lipid carriers (IBU-NLC), optimizing the composition so as to achieve increased API penetration.

1. In the first part of my Ph.D. work, the excipients were selected and the composition was optimized in order to prepare an NLC system loaded with IBU in the highest concentration. The following aims were set:
    - to select a suitable solid lipid and a suitable liquid lipid which are compatible with IBU and incorporate it in the highest concentration;
    - to select a suitable surfactant which stabilizes the LNPs in the aqueous phase. providing a stable NLC system;
    - to develop an NLC system suitable for transdermal use;
    - to optimize the composition by using a 2^3 full factorial design;
    - to evaluate the drug–excipient compatibility via:
        - differential scanning calorimetry (DSC) measurements,
        - X-ray diffraction (XRD) analysis,
        - Fourier transform-infrared (FT-IR) spectroscopy measurements.
2. The second part of my Ph.D. research was to characterize the properties of the IBU-NLC system. The aims were:
    - to determine the particle sizes (PSs) of the IBU-free (blank) and IBU-NLC formulations by photon correlation spectroscopy (PCS), laser diffraction (LD) and atomic force microscopy (AFM) methods;
    - to measure the zeta potential (ZP), using the electrophoretic mobility method;
    - to examine the crystalline properties of the lipid matrix and the state of the incorporated drug through XRD measurements;
    - to study the occurrence of possible interactions between the components of the prepared samples by using FT-IR and Raman spectroscopy;
    - to localize the drug in the lipid matrix via Raman mapping;
    - to study the permeability of the drug through *in vitro*, *ex vivo* and *in vivo* studies in comparison with a reference formulation.

4. MATERIALS AND METHODS

4.1 Materials

4.1.1 Ibuprofen

NLC formulations were loaded with IBU, a potent NSAID, which was provided by PannonPharma Ltd (Pécsvárad, Hungary). Although IBU is not the most potent active API in this group, it offers the best balance between safety and the therapeutic effect [51]. IBU is less potent than diclofenac, for example, but the higher flux of IBU through the skin means that it is a better candidate for topical delivery [52]. It is relatively lipophilic (log P = 4.0), and has low water solubility (21 mg/l at 25 °C) [51, 53] and low bioavailability [54]. The chemical structure of IBU is shown in Fig. 6:

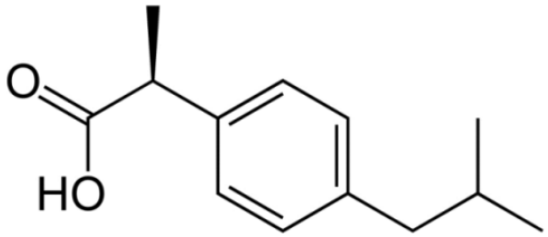

Fig. 6: Chemical structure of ibuprofen (IBU).

4.1.2 Solid lipids and liquid lipids

Since the lipids are the main ingredients of LNPs, they have a huge influence on the drug-loading capacity, the stability and the sustained release behavior of the formulations. A huge variety of lipid materials, such as fatty acids, glycerides and waxes have been investigated to serve as the lipid matrix of NLC dispersions [2, 55-59]. Most of these lipids, with the exception of cetyl palmitate, are GRAS-listed and well tolerated physiologically. Selection of appropriate lipids is one of the key steps before the preparation of lipid-based nanoparticulate systems. No specific guidelines have been proposed, but empirical values, including the solubility of the API in the lipid matrix, seem to be suitable criteria in the selection of the optimal composition [60]. The solubility of the drug in the lipid components is critical as concerns the performance of the NLC system, because it influences the drug EE% and loading capacity, and subsequently the usefulness in drug delivery [61]. A high drug loading (DL%) can be achieved if the API displays high solubility in the lipid(s) used, or a high partition coefficient. Since the solubility of the drug in different types of lipid matrices can vary appreciably, its apparent partition coefficients in those lipids will also differ, leading to

different loading capacities for the same API. In the course of the selection of the optimal composition, lipid polymorphism must also be taken into consideration, since this too influences the properties of an LNP system. Multiple crystalline forms in solid lipids are useful as they provide structural defects in the continuous crystal lattice in which drug molecules can be accommodated. However, they are less thermodynamically stable as compared with the perfect crystalline lattice [62]. These factors pose a significant challenge during the development of an SLN system since transformation of the metastable polymorphs to stable ones can result in drug expulsion during storage or burst release after administration. There are no definitive guidelines that would help in the choice of appropriate lipids on the basis of these properties. It may be noted that lipids with longer fatty acid chains crystallize more slowly than those with shorter fatty acid chains [63]. LNPs produced from waxes are physically more stable, though they can exhibit significant drug expulsion due to their more crystalline nature [64]. As mentioned before, NLC systems were devised in order to overcome such problems with lipid crystallinity and polymorphism [36, 65, 66].

With use of the literature data, lipid screening was performed in order to choose the most appropriate lipids, which would dissolve IBU in the highest concentration and form a stable lipid matrix. The examined solid and liquid lipids with their major properties are listed in Table 1 [67].

Table 1: The main properties of the solid and liquid lipids used.

Lipid type	Examined lipids	Chemical name	Melting point (°C)
solid lipids	Compritol 888 ATO	glyceryl behenate/dibehenate	70-72
	Cutina CP	cetyl palmitate	55-56
	Precirol ATO 5	glycerol palmitostearate	52-55
	Witepsol E85	hard fat – hydrogenated vegetable glycerides	42-44
liquid lipids	Miglyol 812	caprylic/capric triglyceride	< 0
	Oleic acid	oleic acid	13-14
	Walcer	special sunflower-seed oil	-18

4.1.3 Surfactants

Surfactants are the other critical components of the LNP formulations. They adsorb in low concentrations onto the surface or interface of the system, thereby reducing the surface or interfacial free energy, and consequently decreasing the surface or interfacial tension (IFT) between the lipophilic and hydrophilic phases [37, 68].

The surfactants used in the formation of NLCs have two important roles:

- to disperse the lipid melt in the aqueous phase during production; and
- to stabilize the LNPs in dispersions after cooling.

The selection of the surfactants for the nanoparticle preparation depends on a number of factors, including [37]:

- the intended route of administration;
- the hydrophilic-lipophilic balance (HLB) value of the surfactant;
- the effects on the lipid modification and the PS; and
- their role in the *in vivo* degradation of the lipid.

The main properties of the surfactants used during my research work are summarized in Table 2.

Table 2: Main properties of the surfactants used.

Name	Chemical name	Type	HLB value
Tego Care 450	polyglyceryl-3 methylglucose distearate	ionic	12
Cremophor EL	macrogolglycerol ricinoleate	nonionic	12-14
Cremophor RH 60	PEG-60 hydrogenated castor oil	nonionic	15-17
Lutrol F68	Poloxamer 188	nonionic	29
Tween 20	Polysorbate 20	nonionic	16.7
Tween 80	Polysorbate 80	nonionic	15

4.1.4 Other excipients

Carbopol 971P NF supplied by Azelis Hungary Ltd (Budapest, Hungary) was used as gelling agent in the formulation of IBU gels and IBU-NLC gels. Macrogol 400 obtained from Hungaropharma Ltd (Budapest, Hungary) was applied to dissolve the IBU in the reference formulation used in the drug diffusion studies. Purified water high-performance liquid chromatography (HPLC) grade, produced with a TKA Smart2Pure system (TKA GmbH, Niederelbert, Germany) was used to prepare all the formulations.

4.2 Preformulation studies

4.2.1 Lipid screening

To determine the most suitable solid lipid and liquid lipid (oil) which would dissolve IBU in the highest concentration, increasing concentrations of IBU were added to the solid or liquid lipid and the mixture was stirred with a Thermomixer Comfort (Eppendorf, Hamburg, Germany) for 90 min at 500 rpm at a temperature least 5 °C above the melting point of the examined lipid. The solubility of IBU in the examined lipids was analyzed visually. The following step was to evaluate the miscibility of the chosen solid lipid and liquid lipid, and the solubility of IBU in the lipid mixture under the previously mentioned conditions. The details of the experiment were described earlier [61, 69].

4.2.2 Contact angle measurements

Contact angles were measured with an Easy Drop G1 instrument (A.Krüss Optronic GmbH, Hamburg, Germany) to select a suitable surfactant for the NLC composition. Cover slides were coated with a thin film of one or other of the four different bulk lipid mixtures (ratios 10:3, 10:5, 7:3 and 7:5). 10 µl of purified water (as reference) or different 0.5% (w/v) surfactant solutions (in HPLC water) were applied to the lipid film and the contact angle of the droplet was assessed.

4.3 Size measurements and zeta potential analysis

The effective PSs (Z_{ave}) of the prepared NLC formulations were analyzed by PCS, using a Zetasizer Nano ZS (Malvern Instruments, Malvern, UK). The polydispersity index (PDI) was also assessed.

Particles in the micrometer range were excluded through LD measurements with a Mastersizer 2000 (Malvern Instruments, Malvern, UK). The diameters of 10%, 50%, 90%, 95% and 99% ($d(0.1)$, $d(0.5)$, $d(0.9)$, $d(0.95)$ and $d(0.99)$) of the particles were evaluated. The Span value, which corresponds to the width of the PS distribution, was also calculated. The medium was purified water.

To obtain information concerning the stabilities of the prepared samples, their ZPs were determined with a Zetasizer Nano ZS (Malvern Instruments, Malvern, UK). The medium was double distilled water.

4.4 Atomic force microscopic measurements

The PSs of the IBU-NLC samples were also determined by AFM for comparison with the results obtained from PCS and LD measurements. The tapping mode was used on a SOLVER Scanning Probe Microscope (NT-MDT Co., Zelenograd, Moscow, Russia) under ambient conditions. PPP-NVHAuD-10 (NANOSENSORS™, Neuchatel, Switzerland) AFM tips with a nominal radius of curvature of 2 nm and a length of 15 µm were used.

4.5 DSC measurements

To obtain information on the melting behavior of the chosen solid lipid, the lipid mixture and the bulk mixture of IBU dissolved in the lipid mixture were investigated; DSC measurements were performed with a DSC 204 F1 Phoenix instrument (Netzsch Group, Selb, Germany). 2−5 mg samples were measured into aluminum pans which were than sealed; an empty aluminum pan was used as reference. The samples were heated from 20 °C to 65 °C at a heating rate of 5 K/min under constant nitrogen flushing (80 ml/min). The melting point of IBU has been reported to be between 75 and 77 °C, and it immediately starts to decompose on further heating [70]. The lipids and drug compatibilities were therefore monitored up to 65 °C. The crystallinity index (CI(%)) was calculated from the DSC thermograms obtained via Eq. 1 [71, 72]. Before the measurements, the lipid mixtures and lipid−drug mixtures were melted and left to cool to room temperature. The solid lipid was examined as received, without any treatment.

$$\mathrm{CI}(\%) = \left(\frac{\Delta H_{\text{bulk material}} \cdot \text{solid lipid ratio}}{\Delta H_{\text{solid lipid}}} \right) \cdot 100 \qquad \text{Eq. (1)}$$

where ΔH is the enthalpy of the examined material.

4.6 XRD analysis

To characterize the crystalline structures of the raw materials, the physical mixtures and the NLC compositions, XRD analysis was performed with a Bruker D8 Advance diffractometer (Bruker AXS GmbH, Billerica, MA, USA) system with Cu K λI radiation (λ = 1.5406 Å). The samples were scanned at 40 kV and 40 mA from 3 to 40° 2θ, at a scanning speed of 0.1°/s and a step size of 0.010°.

4.7 DXR Raman spectroscopy measurements

Raman spectroscopy was employed to confirm the physical state of the IBU and to study the possible physicochemical interactions between the components. Raman spectra were recorded with a Thermo Fisher DXR Dispersive Raman spectrometer (Thermo Fisher Scientific, Waltham, MA, USA) attached to an Olympus MPlan 10x/0.25 BD microscope (Olympus Corporation, Tokyo, Japan). At least 5 measurements were made at 532 nm with the in-built fluorescence and cosmic ray correction to ensure low background noise. Samples were packed into an aluminum sample holder and spectra were collected for a total of 48 scans at a spectral resolution of 4 cm^{-1}. For the characterization of IBU and NLC samples, the full spectral range (3000−200 cm^{-1}) was used. IBU-NLC and blank NLC compositions were investigated by Raman mapping to localize the IBU inside the formulation. The Raman spectra were then normalized to eliminate the intensity deviation between the measured areas. The detailed parameters were published earlier [73].

4.8 FT-IR spectroscopic analysis

FT-IR spectra of the excipients, the physical mixtures and the prepared NLC formulations were recorded to obtain information about the possible newly formed interactions between the excipients, the IBU and the matrix of the nanoparticles. FT-IR spectra were recorded with a Bio-Rad Digilab Division FTS-65A/896 FT-IR spectrometer (Bio-Rad Laboratories Inc., Hercules, CA, USA) between 4000 and 400 cm^{-1}, with 128 scan size. The detailed parameters were reported previously [69, 73].

4.9 Drug loading and entrapment efficiency measurements

It is essential to investigate the drug DL% and EE% of the nanoparticles, since these have a huge influence on the performance of the nanocarriers. 100 µl of IBU-NLC sample and 400 µl of phosphate buffer solution (PBS) were transferred into a Nanosep 3K ultrafilter Eppendorf tube having a molecular weight cut-off (MWCO) of 3kDa (Pall Co., Port Washington, NY, USA) and centrifuged at 5055 rpm for 10 min [74]. The solution obtained was filtered through a 0.20-µm polyether-sulfone syringe membrane filter and injected directly into the HPLC system [73].

DL% and EE% were evaluated by the indirect method, with measurement of the free API concentration in the external aqueous phase, using Eqs. 2 and 3 [75]:

$$DL\% = \frac{W_{initial\ drug} - W_{free\ drug}}{W_{lipid}} \cdot 100\% \qquad \text{Eq. (2)}$$

$$EE\% = \frac{W_{initial\ drug} - W_{free\ drug}}{W_{initial\ drug}} \cdot 100\% \qquad \text{Eq. (3)}$$

where *W* is the weight in mg.

4.10 Drug permeability studies

4.10.1. *In vitro* release studies

The *in vitro* drug release study was carried out by using the dialysis bag method [76, 77]. Briefly, 200 µl of the IBU-NLC formulation was sealed in a Spectra/Por® 4 dialysis membrane with Spectra/Por® Closures (Spectrum Laboratories Inc., Rancho Dominguez, CA, USA), and placed into 25 ml of PBS (pH = 7.4). The system was held at 32 °C to mimic *in vivo* conditions, and continuously stirred at 450 rpm. At selected time intervals during 6 h, 1 ml of bulk solution was taken. The withdrawn samples were each replaced by 1 ml of PBS to maintain sink conditions. Blank NLC served as blank and was analyzed in the same way as IBU-NLC. A previously prepared 1% IBU suspension was subjected to the same procedure, to serve as a reference.

4.10.2. *Ex vivo* penetration studies

The *ex vivo* penetration studies were performed with a vertical Franz diffusion cell system (Hanson Microette TM Topical & Transdermal Diffusion Cell System, Hanson Research Corporation, Chatsworth, CA, USA). 0.300−0.400 g of 0.5% IBU-NLC gel or 0.5% IBU gel (which served as a reference) was measured as donor phase on pretreated excised human skin [78, 79] supported by a Porafil® CM membrane (pore diameter 0.45 µm; Macherey-Nagel GmbH & Co. KG, Düren, Germany).The detailed description was published earlier [73]. The samples were analyzed at 263 nm with a Unicam Evolution 201 UV/Vis spectrophotometer (Thermo Fisher Scientific Inc., Waltham, MA, USA).

4.10.3. *In vivo* animal studies

The *in vivo* animal studies were performed on 11−13-week-old male SKH-1 hairless mice (body weight: 28–34 g). The procedures and protocols applied were approved by the Ethical Committee for the Protection of Animals in Scientific Research at the University of Szeged (license number: V./145/2013). The modified dorsal skin fold chamber was used to determine IBU penetration through living animal skin by a previously described method [80, 81]. This

experimental setup provides an effective means of performing *in vivo* examinations of permeation. The detailed steps of the experiment were published earlier [73].

4.11 Preparation of ibuprofen-loaded nanostructured lipid carriers

The first batch of IBU-NLCs was prepared by a hot high-pressure homogenization method [5, 14, 76], using a Panda K2 NS1001L Spezial modified for NLC production (GEA Niro Soavi, Germany). Briefly, 5% drug was dissolved in a mixture of the chosen solid and liquid lipid at 65 °C. The surfactant was dissolved in purified water at the same temperature. The aqueous phase was added to the lipid phase and was stirred with an Ultra Turrax T25 (IKA-Works, Staufen im Breisgau, Germany) for 30 s at 12500 rpm. The pre-emulsion obtained was subjected to high-pressure homogenization, applying 5 cycles at 600 bar and 65 °C. The hot oil-in-water pre-emulsion was cooled in an ice bath to recrystallize the lipid and form the NLC [69].

Another series of NLC formulations containing 1% IBU, the solid lipid and the oil in a ratio of 7:3 stabilized by the surfactant Lutrol F68 were prepared by a hot high-pressure homogenization method, using an Emulsiflex C-3 High-Pressure Homogenizer (Avestin Europe GmbH, Mannheim, Germany), with the same method as described above. Blank NLC samples were prepared by the same procedure as for the first and second series of NLC formulations.

An IBU suspension containing 1% of IBU dispersed in purified water was prepared as a reference for *in vitro* diffusion studies of IBU-NLC. For the *ex vivo* permeation and *in vivo* animal studies, IBU-NLC was gelled with a previously prepared 3% Carbopol 971P NF gel in a ratio of 1:1. For comparison, 0.5% IBU was dissolved in Macrogol 400 and gelled with the same polymer [73].

4.12 Experimental design

During the experimental design, 8 different NLC samples (NLC 1−8) were prepared according to the 2^3 full factorial design to evaluate the effects of the three IBU-NLC formulation factors. These factors were: A (the solid lipid concentration), B (the liquid lipid concentration) and C (the surfactant concentration). The optimization parameters (dependent factors) were the measured ZP and mean $d(0.5)$ value of the prepared nanoparticles. The effects of the chosen factors were examined at two levels (+1 and -1). Table 3 shows the

applied factorial table with the values of the independent and dependent factors. Statistical data analysis was performed using Statistica for Windows software version 10.

Table 3: Values of the examined independent factors (A, B and C) and dependent factors (ZP and *d*(0.5)) and compositions of the NLC systems used in the factorial design.

Sample name	Solid lipid concentration % (w/w)	Liquid lipid concentration % (w/w)	Surfactant concentration % (w/w)	Zeta potential (mV)	Particle size (nm)
NLC 1	7 (-1)	3 (-1)	4 (-1)	-14.2	135
NLC 2	10 (+1)	3 (-1)	4 (-1)	-9.5	160
NLC 3	7 (-1)	5 (+1)	4 (-1)	-11.2	143
NLC 4	10 (+1)	5 (+1)	4 (-1)	-11.7	140
NLC 5	7 (-1)	3 (-1)	5 (+1)	-14.2	129
NLC 6	10 (+1)	3 (-1)	5 (+1)	-10.9	152
NLC 7	7 (-1)	5 (+1)	5 (+1)	-11.4	147
NLC 8	10 (+1)	5 (+1)	5 (+1)	-12.1	150

Besides these 8 samples, 8 other formulations belonging in the same parameter space were prepared (Table 4) to check whether there was a possibility of a simpler model with which to optimize these formulations.

Table 4: Values of the examined independent factors (A, B and C) and dependent factors (ZP and d(0.5)) and compositions of the NLC systems randomly picked out from the parameter space.

Sample name	Solid lipid concentration % (w/w)	Liquid lipid concentration % (w/w)	Surfactant concentration % (w/w)	Zeta potential (mV)	Particle size (nm)
blank NLC	10	5	5	-7.54	149
NLC 9	7	3.5	4	-12.4	131
NLC 10	10	4	4	-12.3	137
NLC 11	10	4	5	-15.4	143
NLC 12	7	4.5	5	-9.64	130
NLC 13	10	4.5	4	-12.0	136
NLC 14	10	4.5	5	-12.3	141
NLC 15	7	4	4	-9.97	158

4.13 Statistical analysis

The results were evaluated and analyzed statistically with the 2-way ANOVA test (Bonferroni's multiple comparison), using Prism for Windows 5 software (GraphPad Software Inc, La Jolla, CA, USA). The data are the averages of the results of at least 5 experiments ± standard deviation (*$p \leq 0.05$; **$p \leq 0.01$; ***$p \leq 0.001$; ****$p \leq 0.0001$ versus the control).

5. RESULTS AND DISCUSSION

I. OPTIMIZATION OF THE NLC FORMULATION

5.1 Lipid screening

A large variety of solid and liquid lipids (natural, semisynthetic and synthetic lipids with various structures, e.g. triglycerides, partial glycerides, fatty acids, waxes and steroids) which could be suitable as matrices for NLC production are accessible on the market [2, 5]. However, the lipids used as matrix lipids must be carefully selected as they will directly influence the performance of the carrier system [82]. The properties to be considered: the toxicity and biocompatibility through the selection of well-tolerated physiological and biodegradable lipids; the drug payload and EE% through the choice of lipids which can solubilize high amounts of the drug; drug expulsion during storage, which can be minimized or avoided through the use of lipid matrices with a low tendency to crystallize or a less-ordered structure; controlled drug release properties through incorporation of the drug into the lipid matrix (i.e. a drug-enriched core, a drug-enriched shell or homogenous API distribution in the matrix); and increased chemical drug stability if photosensitive drugs or drugs sensitive to hydrolysis or oxidation are incorporated in the matrix [2, 5, 20].

Apart from oleic acid, all of the investigated lipid melts dissolved IBU in a very high amount (50% (w/w)). The samples were cooled to room temperature and analyzed visually after 24 h. With most of the examined lipids, the IBU underwent recrystallization (Table 5). No IBU crystals were found in Witepsol E85 and Miglyol 812, and these materials were therefore chosen as lipid matrix for NLC formulation. The solid lipid and liquid lipid mixtures were tested in ratios of 10:3, 7:3, 10:5 and 7:5. No oil droplets were observed on the filter paper. No recrystallization was observed visually after the addition of the drug.

Table 5: Results of lipid screening.

Lipid type	Examined lipids	Solubility of IBU	Recrystallization after 24 h
solid lipid	Compritol 888 ATO	soluble	yes
solid lipid	Cutina CP	soluble	yes
solid lipid	Precirol ATO 5	soluble	yes
solid lipid	Witepsol E85	soluble	no
liquid lipid	Miglyol 812	soluble	no
liquid lipid	oleic acid	insoluble	yes
liquid lipid	Walcer	soluble	yes

5.2 Contact angle measurements and determination of surfactant concentration

The nature and the concentration of the surfactant have a great influence on the fineness and physical stability of the NLCs, as the surfactant can reduce the IFT between the lipid particles and the aqueous phase [82, 83]. The IFT can be determined via contact angle measurements. The IFT is directly proportional to the contact angle: the lower the IFT between the lipid matrix and the water phase, the smaller the contact angle. Contact angle measurements were performed to evaluate the surfactant displaying the best wetting with the Witepsol E85 and Miglyol 812 mixture. Contact angle measurements were performed for each of the solid lipid:liquid lipid ratios used in the factorial design (10:3, 7:3, 10:5 and 7:5). Since there was no significant difference between the results, the contact angles measured for films with a solid lipid:liquid lipid ratio of 10:5 are shown in Fig. 7. For all of the examined surfactant solutions, smaller contact angles could be reached than with distilled water (which was used as reference). These results correspond with the fact that surfactant solutions exhibit a smaller surface tension than that of purified water. Cremophor RH60 exhibited the best wetting properties with the lipid mixture (75.02 ± 2.49°), although similar results could be achieved with Lutrol F68 (77.4 ± 4.29°). NLC formulations were therefore prepared with both emulsifiers, and Lutrol F68 was chosen for further investigations on the basis of the $d(0.5)$ and ZP values (Cremophor RH60: $d(0.5)$ = 214.4 nm, ZP = -9.17 mV, and Lutrol F68: $d(0.5)$ = 112.4 nm, ZP = -12.4 mV).

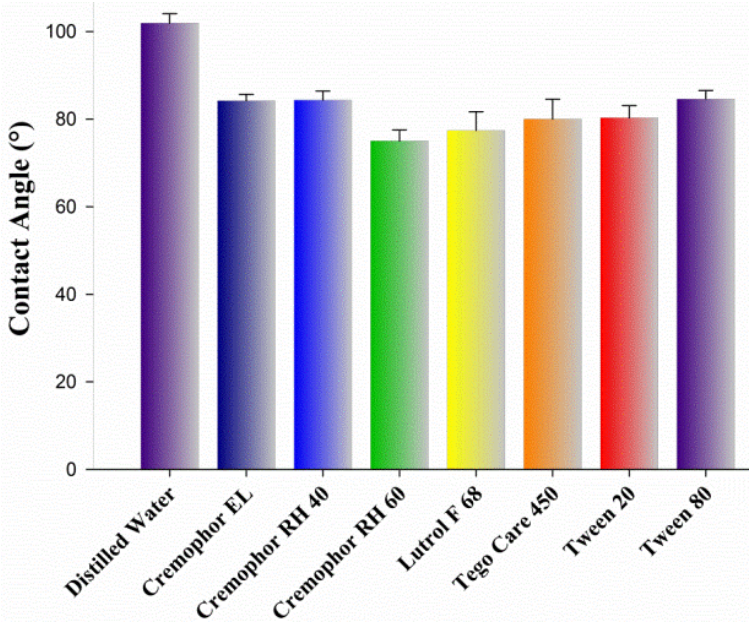

Fig. 7: Contact angles of 0.5% (w/v) surfactant solutions applied to the 10:5 Witepsol E85:Miglyol 812 mixture.

The emulsifier concentration has a great influence on the particle size distribution, stability and toxicological properties of lipid nanoparticles [83-85]. A high surfactant concentration results in a lower particle size, a narrower particle size distribution (which means a smaller PDI and a smaller Span value) and the better long-term stability of lipid nanoparticles, although it simultaneously increases the toxicological potential. Consequently, a balance is needed: the use of a sufficient amount of surfactant that ensures the desired small particle size and appropriate physical stability during storage, but does not demonstrate toxicity. The optimal emulsifier concentration was chosen by factorial design (see section 5.7, B).

5.3 DSC measurements

Lipid crystallization plays a very important role in the performance of NLC carriers. Other research groups have emphasized the importance of the characterization of the degree of lipid crystallinity and the modification of the lipid, because these parameters are closely correlated with the incorporation and release rates of the drug [2, 86].

Figure 8 shows the DSC data of the different samples. Witepsol E85 is a mixture of mono-, di- and triglycerides. It has been reported that the presence of mono- and diglycerides in the matrix of the lipid can facilitate the solubilization of the drug [4, 87]. Lipids which consist of a mixture of different di- and triglycerides or lipids which contain fatty acids of different chain lengths form less perfect crystals with many imperfections, offering spaces to accommodate drugs [87]. Witepsol E85 exhibited a broad endothermic event (melting range:

around 42 °C), as described in the literature [87]. The bulk mixtures of the lipids, Witepsol E85 and Miglyol 812 in all investigated ratios gave a broader endothermic peak, with lower onset and peak values, as expected. The four lipid mixtures yielded similar DSC curves; that of the lipid mixture with a ratio of 10:5 is shown in Fig. 7.

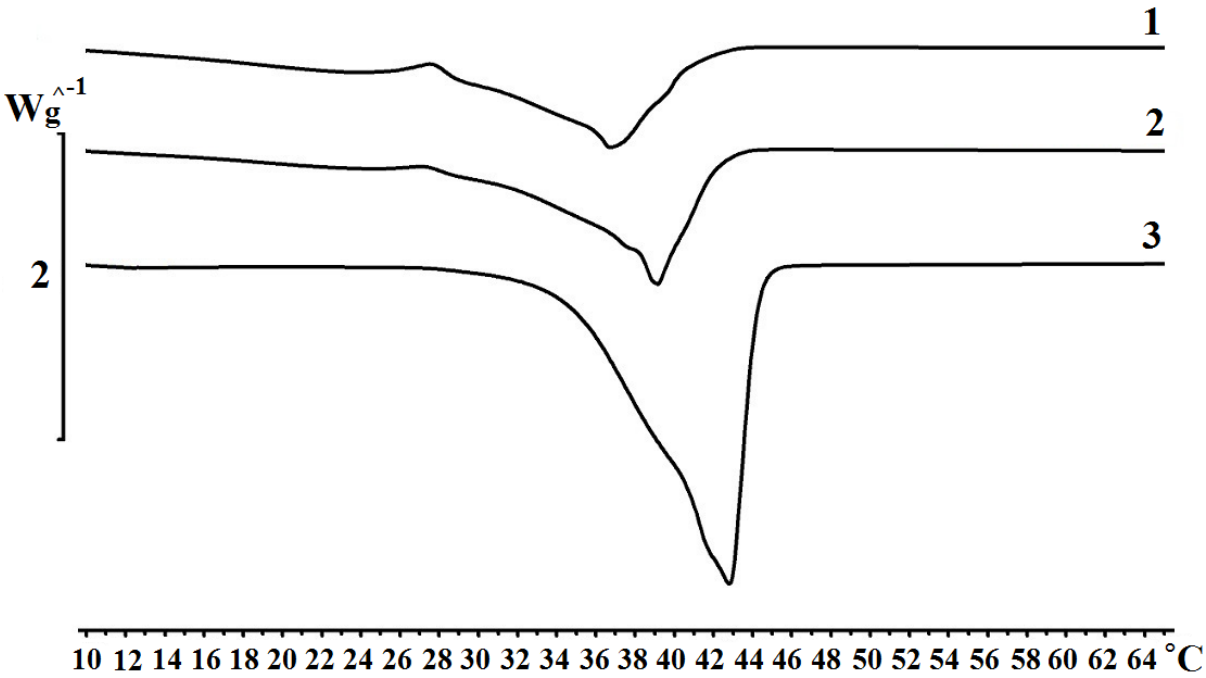

Fig. 8: DSC curves of bulk materials: Witepsol E85:Miglyol 812:IBU 10:5:5 **(1)**, Witepsol E85:Miglyol 812 10:5 **(2)**, and Witepsol E85 **(3)**.

The normalized integral area under the curve, the onset, the peak, the endset and the CI(%) of the pure Witepsol E85, the 10:5 lipid mixture and the lipid mixture with IBU in a ratio of 10:5:5 were evaluated and are listed in Table 6:

Table 6: Normalized integral area, onset, peak, endset and CI(%) of pure Witepsol E85, the lipid mixture in a ratio of 10:5, and the lipid mixture with IBU in a ratio of 10:5:5.

Sample	Integral (normalized) (J/g)	Onset (°C)	Peak (°C)	Endset (°C)	CI(%)
Witepsol E85	-135.29	37.46	42.78	44.24	100
Witepsol E85:Miglyol 812 10:5	-59.60	36.36	39.16	41.95	29.37
Witepsol E85:Miglyol 812:IBU 10:5:5	-42.12	33.03	36.77	41.00	15.57

After the addition of the oil, the melting point of the solid lipid decreased from 42.78 °C to 39.16 °C, and CI(%) fell from 100% to 29.37%. A further decrease in the melting point from 42.78 °C to 36.77 °C was observed after IBU was added to the lipid mixture. CI(%) also fell further from 29.37% to 15.57%. Both the addition of Miglyol 812 and the incorporation of IBU in the lipid matrix can result in an increase in the number of defects in the lipid crystal lattice, causing decreases in CI(%) and the melting point of Witepsol E85 [87]. A less ordered crystalline structure predicts a higher loading capacity of the lipid matrix. A lipid mixture consisting of very differently structured molecules will prevent the formation of a perfect crystal, providing spaces in which to accommodate the drug in molecular form or as amorphous clusters [14].

5.4 XRD analysis

(*RS*)-(±)-IBU, (*RS*)-2-(4-(2-methylpropyl)phenyl)propanoic acid, crystallizes with two molecules in the asymmetric unit to form a cyclic hydrogen-bonded dimer. Within the dimer, each molecule demonstrates subtle conformational differences via rotations about the C(1)---C(2) and the C(10)---C(11) bonds. The bond distances and angles in (*RS*)-(±)-IBU are in close agreement with those found for the structure of the racemic compound [88]. For semisolid fat products (e.g. ice cream, margarine and chocolate), the solid lipids, which normally exist as a 3-dimensional colloidal fat crystal network, determine the physical properties of the product. Upon crystallization, hardstock triacylglycerols aggregate to form fat crystals, which appear to aggregate, in a similar fashion as colloidal gels, to form clusters. These clusters aggregate into flocks, and finally weak links develop between the flocks in the final macroscopic network.

XRD measurements were performed to investigate the effects of the preparation temperature on the structures of the ingredients. The diffractogram of the melted bulk of the 10:5:5 physical mixture of Witepsol E85:Miglyol 812:IBU revealed the characteristic peaks of both the IBU and the lipid mixture. On the addition of Lutrol F68 to the mixture, a further reduction of the IBU peaks resulted (Fig. 9). It is clear from the diffractograms that both the IBU and the excipients retained their crystallinity, but the intensity of the IBU peaks decreased for both the lipid mixture and the physical mixture of the NLC components, which predicts the presence of the IBU in both dissolved and crystalline form.

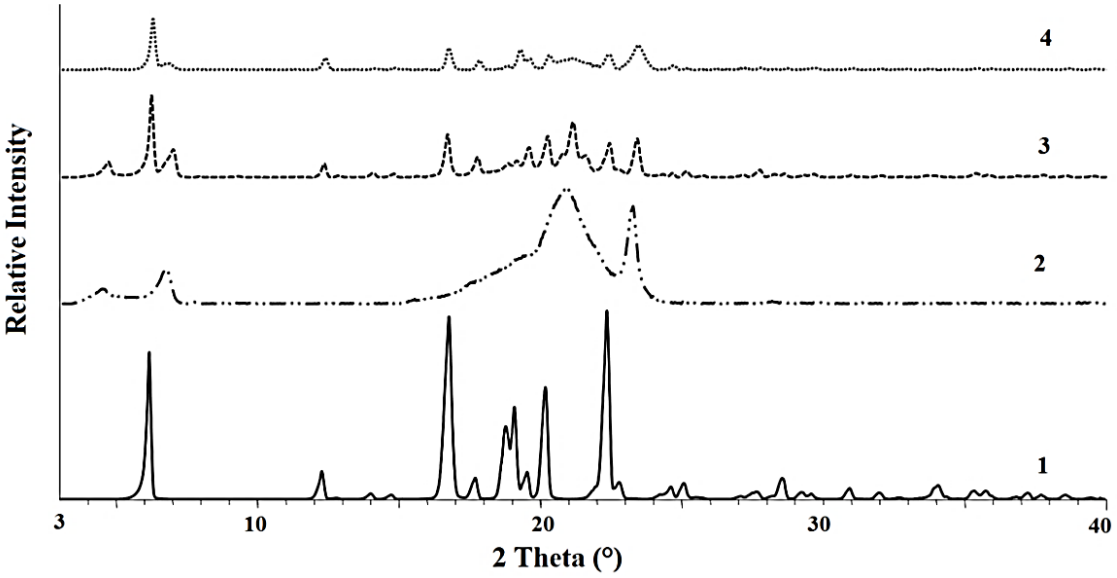

Fig. 9: Wide-angle X-ray diffractograms of IBU **(1)**, the 10:5 bulk mixture of Witepsol E85:Miglyol 812 **(2)**, the 10:5:5 bulk mixture of Witepsol E85:Miglyol 812:IBU **(3)**, and the 10:5:5:5 bulk mixture of Witepsol E85:Miglyol 812:IBU:Lutrol F68 (4).

5.5 FT-IR analysis

The intense band at 2955 cm^{-1} in the FT-IR spectrum of IBU is assigned to CH_3 asymmetric stretching. The very high-intensity peaks at 1721 cm^{-1} and 1231 cm^{-1} are due to C=O stretching and C-C stretching, respectively. The strong-intensity band observed at 779 cm^{-1} is due to CH_2 rocking vibration. The bands at 2955, 1721, 1231 and 668 cm^{-1} were assigned as the fingerprints of IBU in the literature [89-91]. C-O stretching, CH_2 scissoring vibration and CH-CO deformation contribute to their presence. Strong-intensity CH_3 rocking (936 cm^{-1}), CH_3 asymmetric deformation (1462 cm^{-1}), CH_2 asymmetric stretching vibration (3090 cm^{-1} and 2869 cm^{-1}) and CH_2 in-plane rocking vibration (522 cm^{-1}) are also observed. The absorption bands due to C=C stretching vibrations occur at 1507 cm^{-1} and 746 cm^{-1}. The medium-intensity O-H…O valence stretching vibration occurs at 2728 cm^{-1} and 2632 cm^{-1}. Absorption bands due to OH in-plane deformation (1321 cm^{-1}), =C-H in-plane deformation (1268 cm^{-1}, 1123 cm^{-1} and 1071 cm^{-1}), C-H in-plane deformation (1168 cm^{-1}, 1008 cm^{-1}, 636 cm^{-1} and 1092 cm^{-1}), C-H out-of-plane deformation (866 cm^{-1} and 668 cm^{-1}), in-plane ring deformation (407 cm^{-1}), C=C-C ring asymmetric bending (423 cm^{-1}), C-C deformation (588 cm^{-1}), CH_3 symmetric stretching (1380 cm^{-1}) and C-O-C stretching (970 cm^{-1}) have also been noted [92, 93]. FT-IR analysis was used to verify whether any interaction occurred between the excipients and the drug because newly formed bonds can modify the diffusion of IBU from the nanoparticles. Figure 10 presents the FT-IR spectra of the 10:5:5:5 physical

mixture of Witepsol E85, Miglyol 812, IBU and Lutrol F68 and the individual spectra of these bulk components.

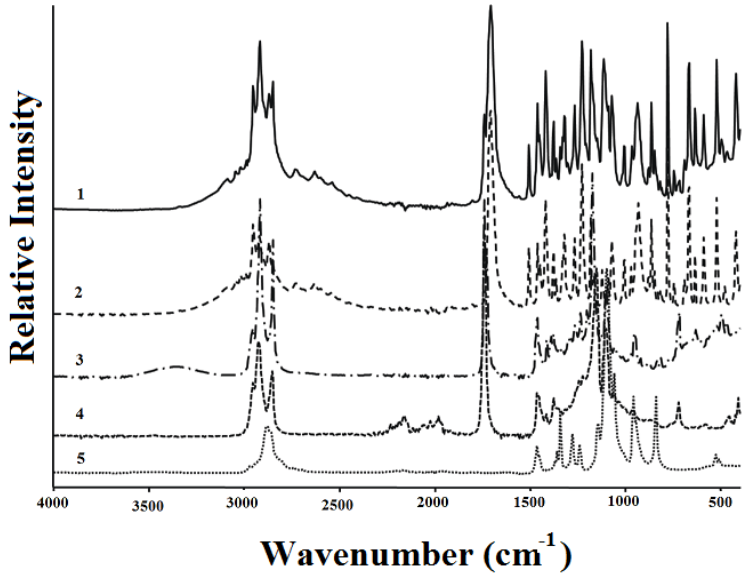

Fig. 10: FT-IR spectra of the physical mixture of the bulk components (Witepsol E85, Miglyol 812, IBU and Lutrol F68 in a ratio of 10:5:5:5) **(1)**, IBU **(2)**, Witepsol E85 **(3)**, Miglyol 812 **(4)**, Lutrol F68 **(5)**.

A comparison of the spectra allows the conclusion that no chemical modification occurred at the temperature of NLC production. Figure 11 depicts the lower wavelength range of the same spectra. No shifts in the major valency vibrations were detected and new peaks did not appear.

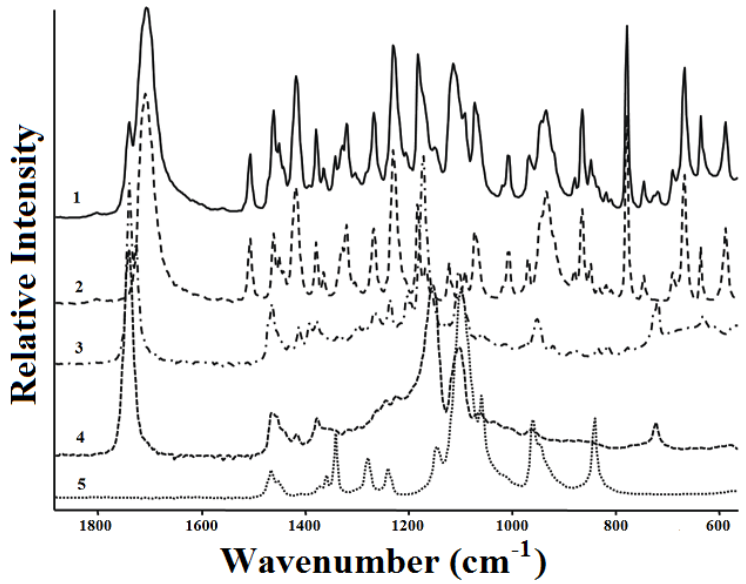

Fig. 11: FT-IR spectra in the lower wavenumber range of the physical mixture of the bulk components (Witepsol E85, Miglyol 812, IBU and Lutrol F68 in a ratio of 10:5:5:5) **(1)**, IBU **(2)**, Witepsol E85 **(3)**, Miglyol 812 **(4)** and Lutrol F68 **(5)**.

5.6 Results of size measurements and zeta potential analysis

The PSs and the PS distribution of the prepared IBU-NLC were measured by PCS and LD. The PS of the NLC systems varied in the interval 108.6−216.3 nm (Table 7). The Z_{ave} and $d(0.5)$ values correlated appropriately with each other, showing the mean PSs of the NLC samples. The PDI and the Span values varied in similar ways, as both relate to the PS distribution of the LNPs.

Table 7: Results of PCS and LD measurements for all the NLC formulations.

Name	ZP (mV)	Z_{ave} (nm)	PDI	$d(0.1)$ (nm)	$d(0.5)$ (nm)	$d(0.9)$ (nm)	$d(0.95)$ (nm)	$d(0.99)$ (nm)	Span value
blank NLC	-7.54	132.2	0.096	91	149	228	250	300	0.919
NLC 1	-14.2	216.3	0.230	97	135	249	280	330	1.126
NLC 2	-9.5	114.5	0.077	87	160	195	210	250	0.675
NLC 3	-11.2	113.1	0.067	86	143	192	210	250	0.741
NLC 4	-11.7	114.5	0.087	89	140	198	220	260	0.779
NLC 5	-14.2	108.6	0.065	86	129	192	210	250	0.822
NLC 6	-10.9	115.8	0.093	91	152	206	230	270	0.757
NLC 7	-11.4	112.7	0.089	85	147	191	210	250	0.721
NLC 8	-12.1	115.0	0.078	87	150	195	210	250	0.720
NLC 9	-12.4	112.4	0.089	87	131	195	210	250	0.824
NLC 10	-12.3	138.2	0.249	74	137	238	270	320	1.197
NLC 11	-15.4	114.7	0.108	90	143	219	240	280	0.902
NLC 12	-9.64	109.7	0.057	86	130	191	210	250	0.808
NLC 13	-12.0	116.1	0.085	90	136	200	220	260	0.809
NLC 14	-12.3	114.8	0.101	92	141	208	230	270	0.823
NLC 15	-9.97	214.4	0.237	91	158	262	300	360	1.082

5.7 Results of the experimental design

5.7.1. Effects of the dependent factors on the ZP values

The results were evaluated according to the 2^3 full factorial design. The three examined independent factors (solid lipid concentration (A), liquid lipid concentration (B) and surfactant concentration (C)) together exerted a significant effect ($p < 0.05$) on the ZP, but individually they did not do so. The coupled factors were also tested, but did not give a significant effect.

The mathematical model is shown in the following equations (Eqs (4), (5) and (6)) of the response surfaces, with the ZP as the dependent factor as a function of factors A and B, factors A and C, and factors B and C, with a good correlation (R^2 = 0.9901):

$$ZP\ (A, B) = 3.61 * A + 6.99 * B - 0.77 * A * B - 43.98 \qquad \text{Eq. (4)}$$

$$ZP\ (A, C) = 1.75 * A + 1.77 * C - 0.27 * A * C - 24.66 \qquad \text{Eq. (5)}$$

$$ZP\ (B, C) = -1.81 * B - 1.33 * C + 0.20 * B * C - 7.25 \qquad \text{Eq. (6)}$$

A positive sign indicates a synergistic effect on the examined dependent factor, whilst a negative sign represents an antagonistic effect.

Factor A (solid lipid concentration) was directly proportional to the ZP, although this effect was not significant. The ZP became lower if factor A was kept on level -1 (7% Witepsol E85). The same effect was observed for factor B (liquid lipid concentration). Lower ZP values were obtained when factor B was kept on a lower level, e.g. when 3% Miglyol 812 was applied. This correspondence is clearly visible in Fig. 12, which depicts 3 response surfaces where the ZP is a function of factors A and B; factor C is given on levels -1 (4% w/w), 0 (4.5% w/w) and +1 (5% w/w) (surfaces 1, 2 and 3).

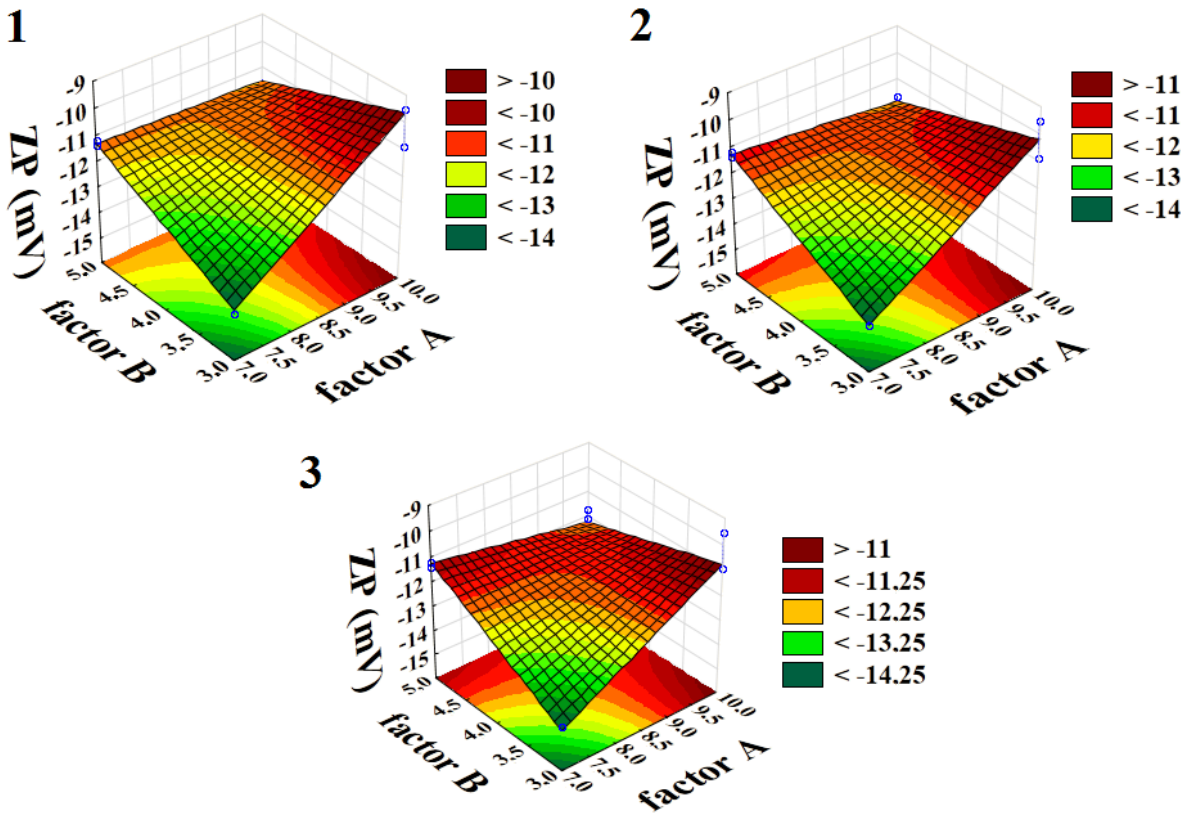

Fig. 12: Measured ZP as a function of solid lipid (factor A) and liquid lipid (factor B). The surfactant concentration was set to 4% w/w **(1)**, 4.5% w/w **(2)** and 5% w/w **(3)**.

The ratio of factors A and B was indirectly proportional to the ZP. The response surfaces exhibited a minimum value at a solid lipid:liquid lipid ratio of 7:3: the ZP was -14.2 mV. This clearly-visible minimum did not change when the surfactant concentration was altered from 4% to 4.5% or 5% w/w; the behavior of the response surface remained unchanged in the examined range. Factor C was indirectly proportional to the ZP. Lower ZP values are expected when higher concentrations of the surfactant are applied; the use of 5% Lutrol F68 is therefore favorable.

5.7.2. Effects of the dependent factors on the PS

Similarly to the results of the statistical analysis of the ZP, the three independent factors (solid lipid concentration (A), liquid lipid concentration (B) and surfactant concentration (C)) together affected the PS significantly ($p < 0.05$), whereas their individual effects did not reach the level of significance (confidence value 95%). No significant effect was observed when the effects of the coupled factors were tested (A and B, A and C and B and C). The mathematical model of the effects of the dependent factors on the PS is shown in Eqs. (7), (8) and (9), with a correlation of $R^2 = 0.9883$:

$$PS(A, B) = 20.02*A + 34.50*B - 4.00*A*B - 27.50 \quad \text{Eq. (7)}$$

$$PS(A, C) = 1.00*A - 5.67*C + 0.67*A*C + 136.00 \quad \text{Eq. (8)}$$

$$PS(B, C) = -31.00*B - 27.97*C + 7.00*B*C + 268.50 \quad \text{Eq. (9)}$$

Factor A (solid lipid concentration) was directly proportional to the PS, but this effect did not reach the level of significance. The PS was lower when factor A was kept on level -1 (7% Witepsol E85). The same effect was observed with factor B (liquid lipid concentration), i.e. the PS of the nanoparticles was lower when 3% Miglyol 812 was used in the formulations. The ratio of factors A and B was indirectly proportional to the PS. In Fig. 13, the response surfaces exhibit a minimum value at a solid lipid:liquid lipid ratio of 7:3; the PS is < 125 nm.

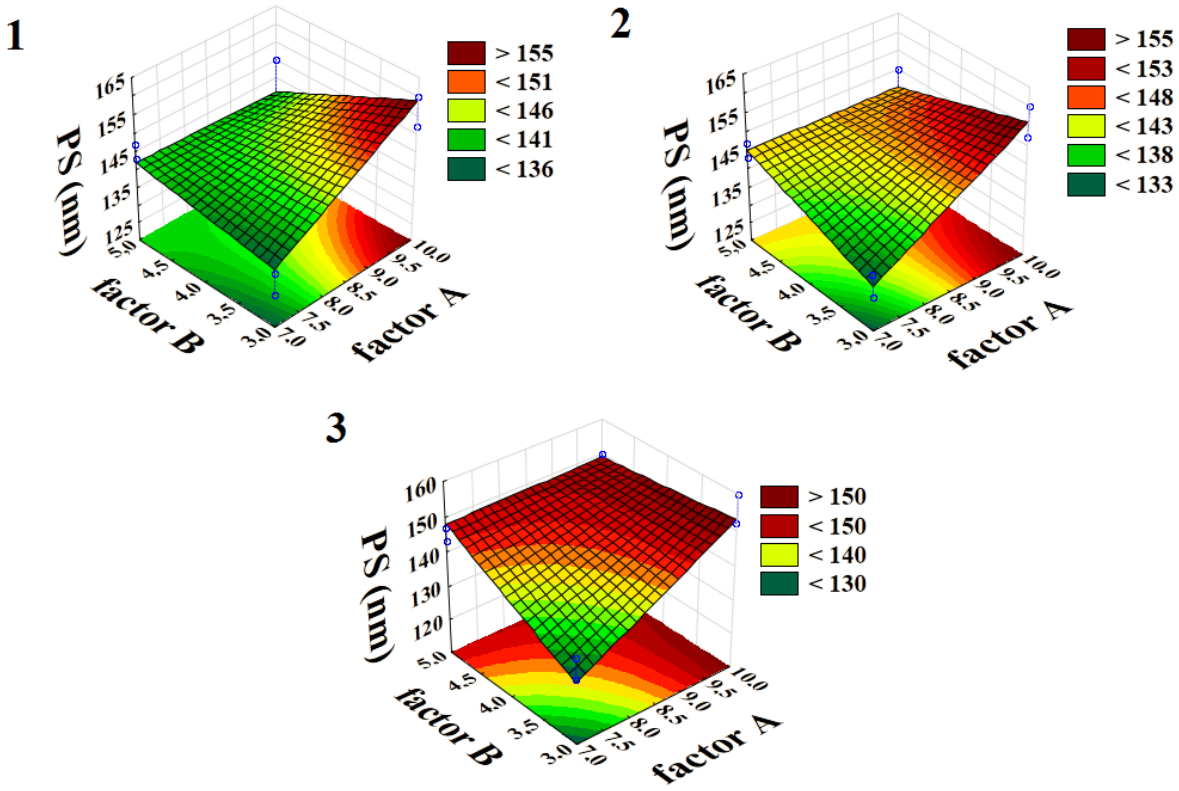

Fig. 13: Measured PS as a function of solid lipid (factor A) and liquid lipid (factor B). The surfactant concentration was set to 4% w/w **(1)**, 4.5% w/w **(2)** and 5% w/w **(3)**.

The surface plot retained its minimum value regardless of the surfactant concentration. The difference between the maximum and minimum points of the surfaces became more explicit at higher surfactant concentrations (Fig. 13 (1), (2) and (3)) in the range of the factorial design.

Factor C (surfactant concentration) did not have an impact on the PS in this range.

The results of the applied factorial design indicate that NLC 5 was the most suitable for IBU delivery, together with 7% Witepsol E85, 3% Miglyol 812 and 5% Lutrol F68.

Table 7 (section 5.6) gives data on NLC formulations randomly picked out from the factorial design space. By measuring the ZP, Z_{ave}, PDI and Span values of these NLC systems, a simpler function (Eq. 10) could be defined to choose the optimal formulation. Factorial design requires a large number of samples, which may be decreased through use of the following equation if the response surface has a minimum value. The aim was to find a simpler correspondence to evaluate the optimal ratio of the compounds. The following equation gives the optimum as a non-dimensional number with a minimum value at the optimal compound.

$$\text{Optimum} = \min\left[\text{ZP} + Z_{ave} + \text{PDI} + \text{Span} + \frac{\text{SL}}{\text{LL}} + \frac{\text{SL}/\text{LL}}{\text{S}}\right] \quad \text{Eq. (10)}$$

where ZP is the zeta potential, Z_{ave} is the mean particle size measured by PCS, PDI is the polydispersity index, Span is the Span value ($\frac{d(0.9)-d(0.1)}{d(0.5)}$), $\frac{\text{SL}}{\text{LL}}$ is the solid lipid:liquid lipid ratio and $\frac{\text{SL/LL}}{\text{S}}$ is the solid lipid:liquid lipid ratio proportional to the surfactant concentration.

As regards the optimum equation, NLC 5 (7% Witepsol E85, 3% Miglyol 812, 5% Lutrol F68 and 5% IBU) proved optimal for the formulation of a stable IBU-NLC system. This method appears suitable for the design of NLC formulations.

II. CHARACTERIZATION OF THE IBU-NLC FORMULATION

The IBU concentration of the optimized NLC 5 formulation was decreased from 5% to 1% in order to decrease the side-effects in diseases demanding prolonged treatment, such as the therapy of musculoskeletal disorders such as osteoarthritis. Furthermore, it was noticed that decreasing the concentration of IBU led to an increase in the stability of the formulation (the ZP values decreased from −14.2 to −18.4 mV).

5.8 Results of particle size and zeta potential measurements

PS determination by PCS demonstrated that both samples were in the nanometer range, with an effective PS (Z_{ave}) of 114 nm for the blank NLC, and 106 nm for IBU-NLC. LD measurements confirmed that larger particles (> 1 μm) were not present in the formulations, and 90% of the particles measured < 205 nm. The surface charge was negative for both the blank (-15.9 mV) and IBU-NLC (-18.4 mV). The PDI was small for both formulations, meaning that the PS of the nanoparticles were in a narrow range. This parameter is important for steady drug diffusion. Parameters measured with PCS, LD and electrophoretic mobility measurements are presented in Table 8.

Table 8: PSs, PS distributions (PDI and Span) and ZPs of the blank NLC and IBU-NLC formulations.

Sample	Z_{ave} (nm)	ZP (mV)	PDI	*d*(0.1) (nm)	*d*(0.5) (nm)	*d*(0.9) (nm)	Span value
blank NLC	114 ± 2.2	-15.9 ± 0.7	0.15 ± 0.1	67 ± 0	118 ± 0	204 ± 0.6	1.16 ± 0
IBU-NLC	106 ± 1.7	-18.4 ± 1.3	0.18 ± 0.3	74 ± 0	122 ± 0	205 ± 0.6	1.07 ± 0

5.9 Results of AFM measurements

AFM has been widely used to acquire information on the size, shape and surface morphology of nanoparticles [94]. Both the blank and the IBU-NLC samples were measured by AFM to confirm the PCS and LD results. The data were evaluated by grain analysis, and size distribution histograms were made (Fig. 14 A, B). The *Z* values of the blank NLC particles were between 109 and 124 nm, with an average of 113.67 ± 15.5 nm, while those of the IBU-NLC were between 95 and 118 nm, with an average of 107.47 ± 14.4 nm (Fig. 14 C, D), verifying the PCS and LD results.

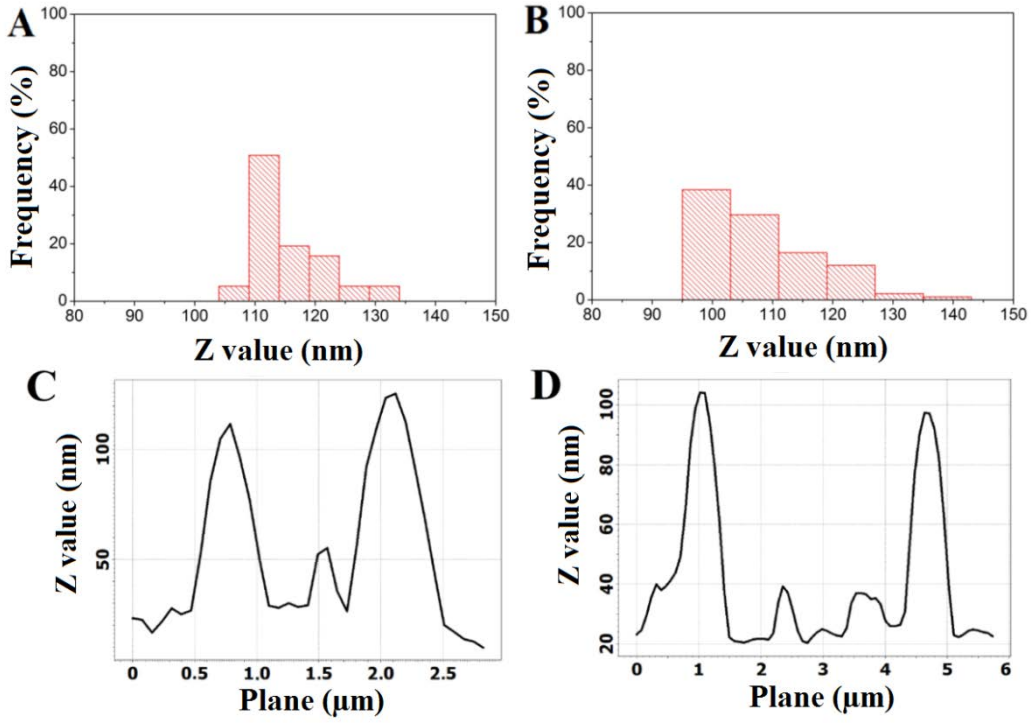

Fig. 14: *Z* value (height) distribution of blank NLC **(A)** and IBU-NLC **(B)**; and Z values (height) of blank NLC **(C)** and IBU-NLC **(D)**.

In the present samples, the separated lipid particles were spherical or nearly spherical with a smooth surface (Fig.s 15 and 16).

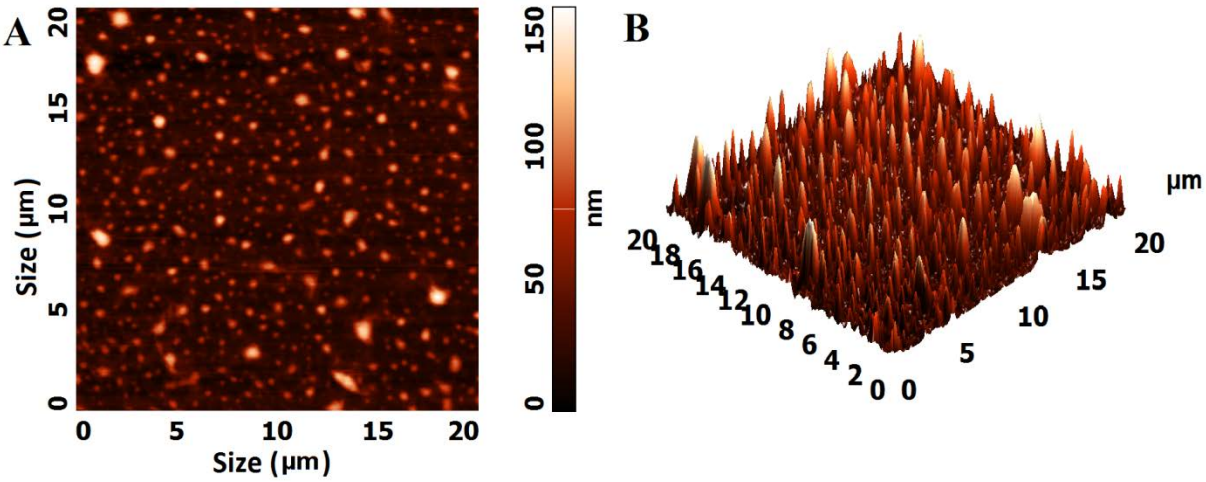

Fig. 15: 2D **(A)** and 3D **(B)** images of blank NLC.

No major differences were detected between the blank and IBU-NLC samples, although some larger lipid agglomerates were found in the IBU-NLC. This is probably due to the sample preparation process: the sonication was unable to disperse the previously dried lipid particles completely.

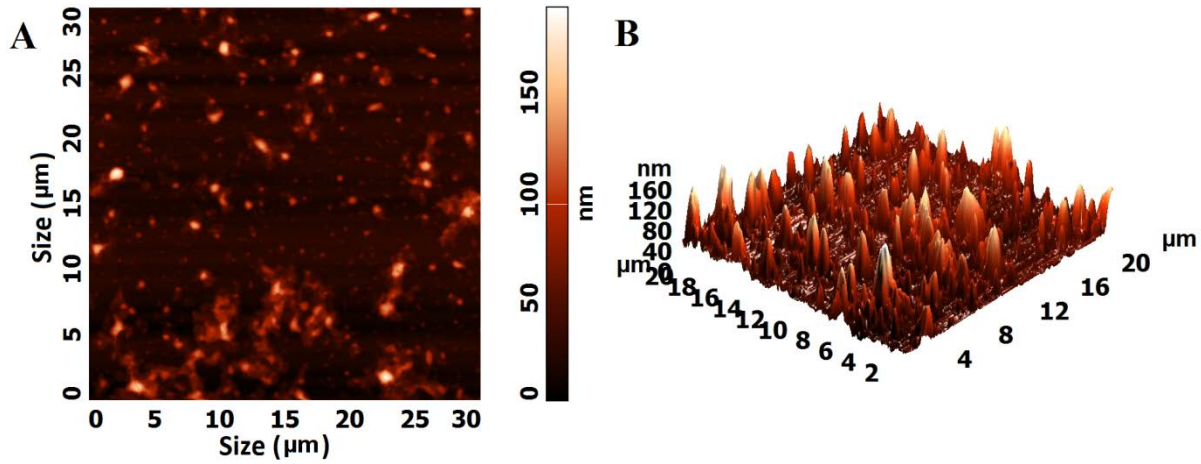

Fig. 16: 2D **(A)** and 3D **(B)** images of IBU-NLC.

5.10 Results of XRD

XRD measurements were carried out to determine the possible changes in the crystallinity of the components during the hot high-pressure homogenization procedure. Diffractograms of the pure, untreated components (IBU, Witepsol E85, and Lutrol F68) are depicted in Fig. 17.

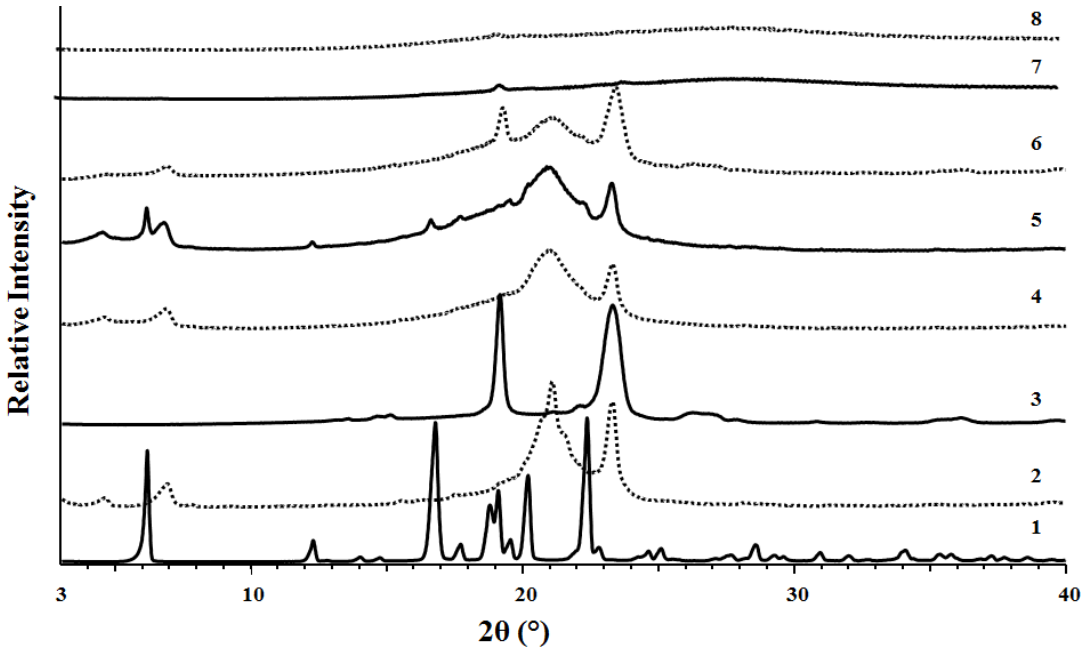

Fig. 17: XRD diffractograms of IBU **(1)**, Witepsol E85 **(2)**, Lutrol F68 **(3)**, the bulk mixture of Witepsol E85 and Miglyol 812 in a ratio of 7:3 **(4)**, the mixture of Witepsol E85, Miglyol 812 and IBU in a ratio of 7:3:1 **(5)**, the mixture of Witepsol E85, Miglyol 812, IBU and Lutrol F68 in a ratio of 7:3:1:5 **(6)**, blank NLC **(7)**, and IBU-NLC **(8)**.

Diffractograms were also recorded of the melted lipid mixture (Witepsol E85 and Miglyol 812 in a ratio of 7:3) with or without IBU, the melted total physical mixture, the blank and IBU-NLC. The crystallinity of the solid lipid (plot 2) decreased to such an extent after the addition of the excipients (plots 4 and 6) and IBU (plot 5) that the material became amorphous in the cases of the prepared blank (plot 7) and IBU-NLC (plot 8) formulations. The XRD pattern of pure racemic IBU (plot 1) exhibited characteristic diffraction peaks at various diffraction angles (6°, 12.3°, 16°, 20.4° and 22.3° 2θ), indicating the presence of crystallinity [95]. These peaks also appeared in the plot of the melted mixture of the lipid matrix and the API (plot 5), but were absent from those of the total mixture (plot 6) and IBU-NLC (plot 8).

5.11 Results of DXR Raman spectroscopy measurements

Raman spectroscopy was employed to confirm the physical state of the IBU and to study the possible physicochemical interactions between the components. The Raman spectra of dried free racemic IBU, Lutrol F68, Witepsol E85 and Miglyol 812 in the wavenumber range 2000−200 cm^{-1} are presented in Fig. 18.

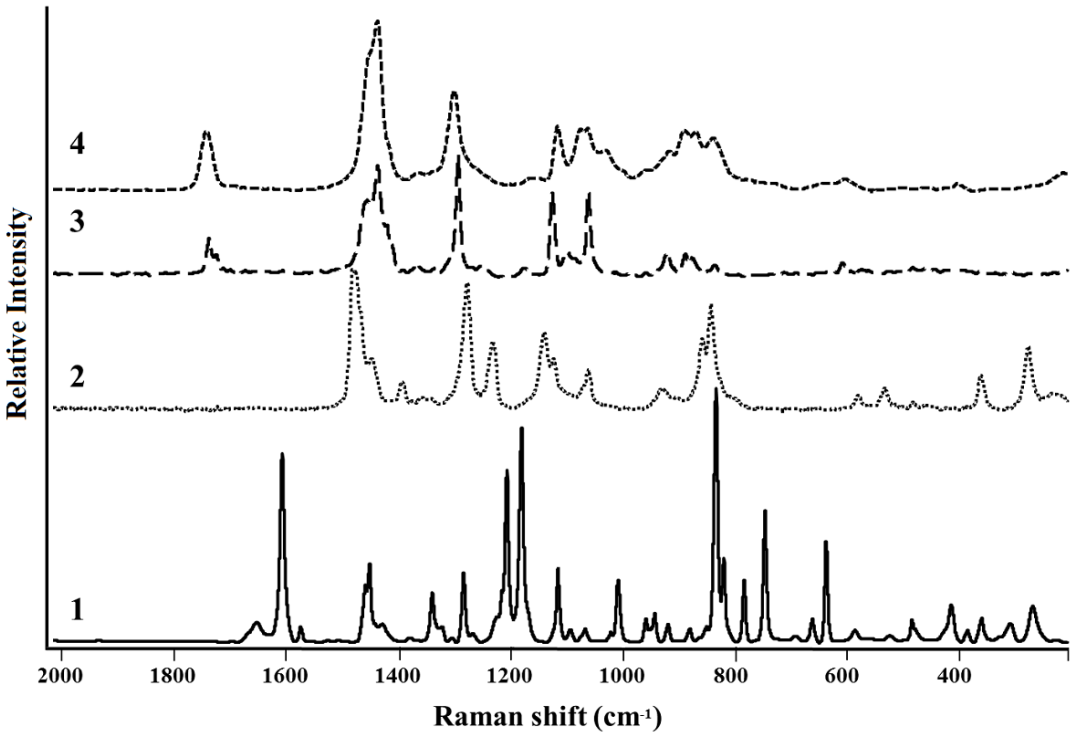

Fig. 18: Raman spectra of the individual components, IBU **(1)**, Lutrol F68 **(2)**, Witepsol E85 **(3)** and Miglyol 812 **(4)**.

As model solutions, IBU was dissolved in Miglyol 812 in two concentrations (10 and 25% w/w), to observe the principal differences in the physical state of the IBU (Fig. 19).

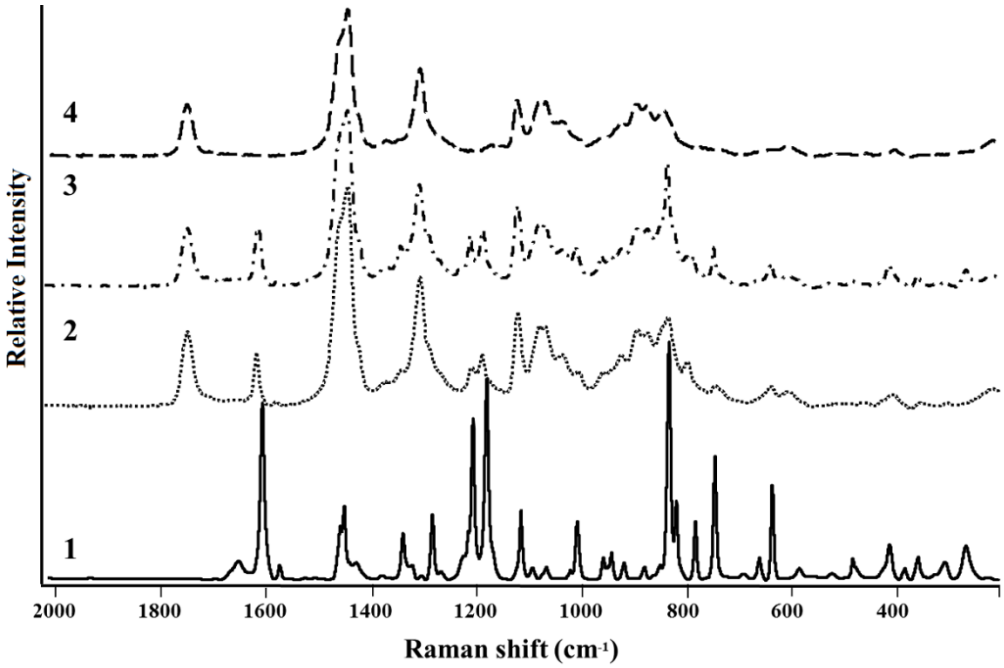

Fig. 19: Raman spectra in the range of 2000−200 $cm^{-1}$of IBU **(1)** and the model mixtures of 10% IBU **(2)**, or 25% IBU **(3)**, both dissolved in Miglyol 812 **(4)**.

The spectra of IBU, the blank NLC and IBU-NLC are presented in Fig. 20.

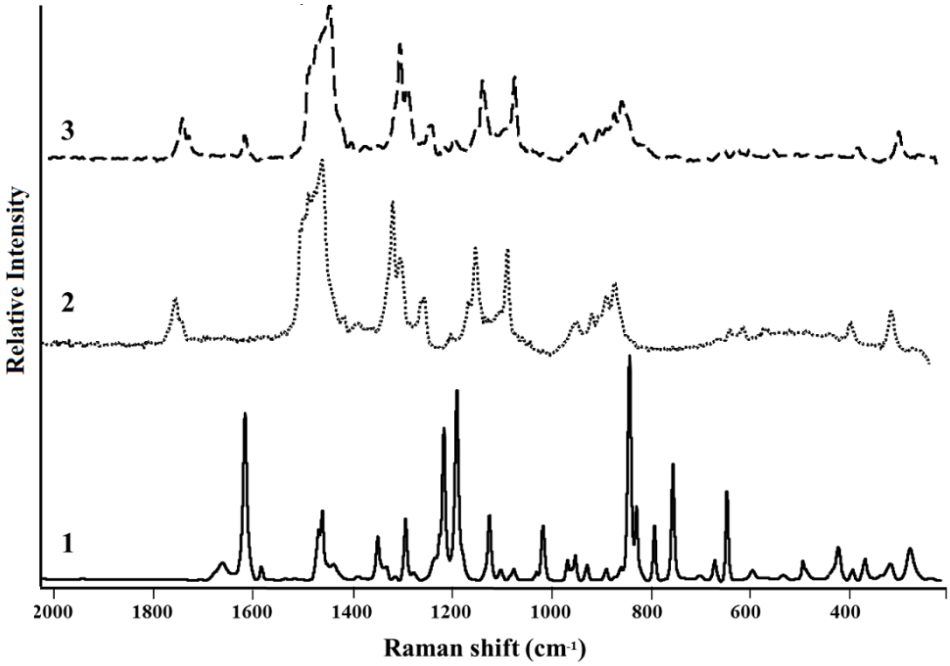

Fig 20: Raman spectra in the range 2000−200 $cm^{-1}$of IBU **(1)**, blank **(2)** and IBU-NLC **(3)**.

The selected Raman bands of IBU, the IBU-containing Miglyol model solutions and the IBU-NLC composition with the vibrational assignments (cm^{-1}) are presented in Table 9. The chemical structure of the oil is very similar to those of the other lipid components, and the bands from the IBU-NLC sample, i.e. the Raman spectrum characteristic of Miglyol 812, could therefore be overlapped by the bands characteristic of other lipids.

Table 9: Observed Raman peaks (in cm^{-1}) and peak assignments of free racemic IBU and IBU-containing model solutions and NLC compositions.

IBU	Assignment	10%	25%	IBU-NLC
1608	*s*(C-C)Ar	1613	1609	1616
1576	*s*(C-C)Ar and *v*(C=C)Ar	1574	1574	-
1208	*t*(CH_2) (C_{11}-C_{12}-C_{13})	1207	1206	1208
1182	*s*(C_6-C_{11})	1185	1182	1185
1008	*in*(CH)Ar	1004	1007	1004
959	*r*($C_{26}H_3$) and antisymmetric *s*(C_{26}-C_{24}-C_{30})	957	957	955
834	*out*(CH)Ar	832	833	-
746	*r*(CH_3) and *out*(CH)Ar	739	745	-
638	*out*(CO-H) and *in*(Ar)	637	636	-
415	*d*(C_{15}-C_{14}-C_{19})	405	412	-

(*s* = stretching, *β* = bending, *v* = vibration, Ar = aromatic, *t* = twisting, *out* = out-of-plane bending, *in* = in-plane-bending, *r* = rocking, and *d* = deformation).

The IBU spectrum exhibited characteristic peaks at 1608, 1576, 1208, 1182, 1008, 959, 834, 746, 638 and 415 cm^{-1}. These peaks are attributed mainly to aryl ring stretching and C_{24}-Ar-C_{11} conformational stretching and wagging. Medium sharp peaks are attributed to the Ar and Ar-CH in-plane and out-of-plane bending. In spite of the many free racemic IBU peaks, the Raman spectra of the model solutions and the NLC composition were characteristic of the auxiliary materials. The medium-intensity IBU peaks at 1452, 1341, 1116, 943, 820, 662, 784 and 269 cm^{-1} (C_x-H_y bending, twisting or rocking) were absent from the spectra of the IBU-containing model solutions and NLC composition. Comparison of the Raman peaks of the IBU and the model solutions (10% and 25%) revealed small shifts in the wavenumbers of the characteristic IBU peaks. Moreover, the Raman spectrum of the IBU-NLC composition (with less characteristic IBU peaks) revealed the same small shifts, indicating the occurrence of weak interactions between IBU and the lipids. A significant change in the spectrum of interacted IBU was the shift in the peak corresponding to the aryl C-C stretching from 1608 cm^{-1} to 1609-1616 cm^{-1}. This latter shift indicates that the aryl ring is affected by the interaction with the lipid molecules and not the C=O group of IBU. In Table 10, the Raman spectra of the lipid components are compared with those of IBU-NLC and the blank NLC. The lipid components used in this study have similar chemical structures and therefore similar Raman bands. The Raman spectra of the lipid components in the range 3000-200 cm^{-1} displayed characteristic peaks, which are assigned to vibrations of the fatty acid hydrocarbon chains. The sharp and intense peaks at 2881 and 2850 cm^{-1} and the medium peaks at 1128 and 1062 cm^{-1} in all the NLC compositions confirmed the ordered acyl chains in the lipid structure. The incorporation of IBU did not lead to the disappearance of the sharp bands at 2881 and 2850 cm^{-1} in the Raman spectrum of IBU-NLC.

Table 10: Observed Raman peaks (in cm^{-1}) and peak assignments of individual lipid components and NLC compositions.

Assignment	Lutrol F68	Witepsol E85	Miglyol 812	blank NLC	IBU-NLC
s(CH)	2934	2935	2931	2936	2935
s(CH_2) antisymmetric	2884	2880	-	2881	2881
s(CH_2) symmetric	-	2846	2853	2850	2850
s(CH)	-	2724	2728	2724	2725
s(C=O)	-	1739	1745	1741	1742
CH_2 scissoring and *s*(C-O)	-	1438	1439	1441	1441
t(CH_2) and *s*(C-O)	-	1295	1302	1297	1297
s(C-C) symmetric and *s*(C-O-C) asymmetric	1125	1126	-	1128	1128
s(C-C) asymmetric and *s*(C-O) symmetric	1062	1062	1063	1063	1063
r(CH_3)	-	889	889	889	892
r(CH_3)	843	-	841	844	845

(*s* = stretching, *β* = bending, *v* = vibration, Ar = aromatic, *t* = twisting, *out* = out-of-plane bending, *in* = in-plane bending, *r* = rocking, and *d* = deformation).

In order to confirm the homogenity of the IBU, Raman mapping of the NLC was performed. Figure 21 shows the distribution map of IBU in the NLC composition at 10x-magnification. The characteristic bands obtained for IBU at around 1608 cm^{-1} were used to visualize the spatial distribution of IBU from Raman chemical mapping. The IBU was found homogenously in the dried, round areas. The purpose of this analysis was to estimate the distribution of the individual ingredients in the scanned area.

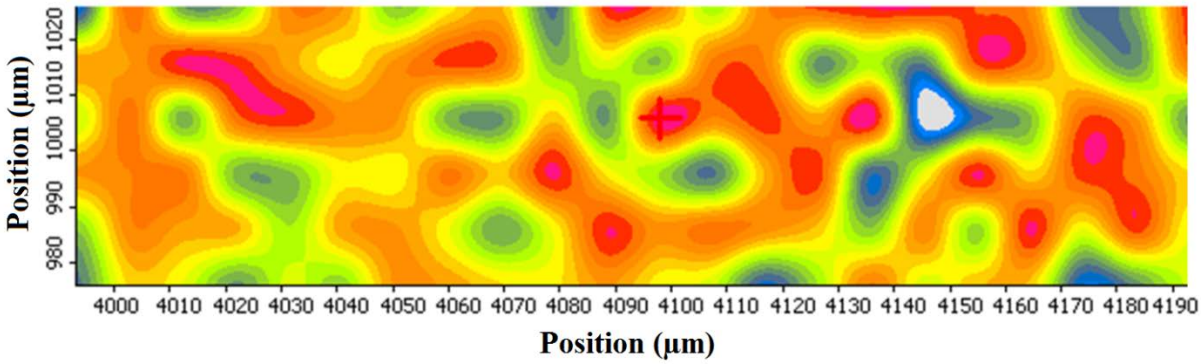

Fig. 21: Raman distribution map of IBU (yellow to red colors) in the IBU-NLC composition (10x magnification).

The spectra of the estimated 'Components' were compared with the reference ingredient spectra (Fig. 22). The spectra of Components 1 and 4 were identified as the Raman spectrum of Lutrol F68, with characteristic Raman band regions of 1750-1150, 900-750 and 400-200 cm^{-1}. The resolved spectrum of Component 2 does not correspond to the reference spectra, but contains similar Raman bands to those of Miglyol 812. The spectrum of Component 2 displays several other peaks; the reason may be the low signal-to-noise ratio. Component 3 corresponds to Witepsol E85, with very characteristic Raman band regions of 1500-1400 and 1150-1000 cm^{-1}. The Raman spectra of each Component contain the characteristic Raman peaks of IBU at 1614-1608 cm^{-1}.

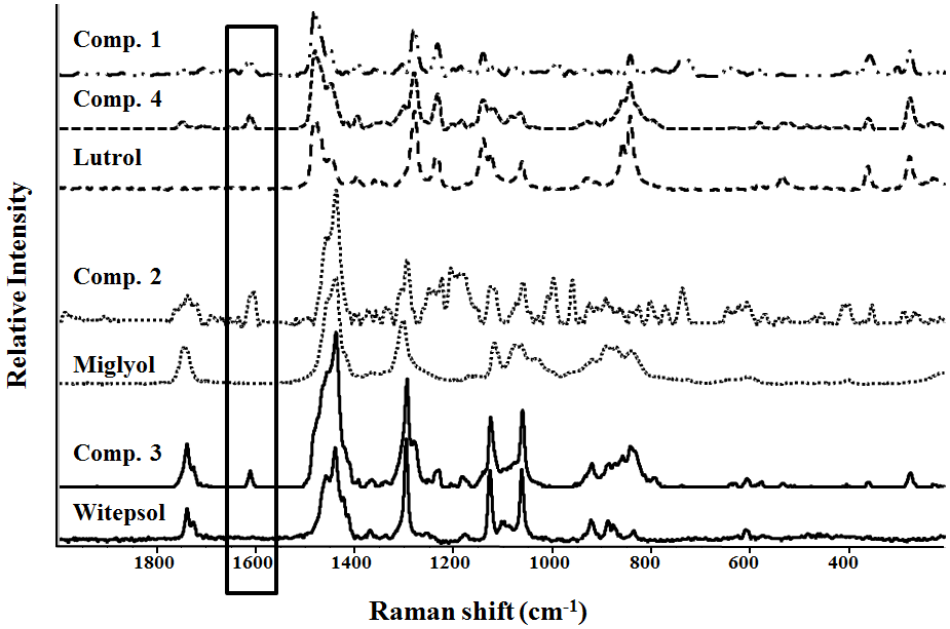

Fig. 22 Multivariate curve resolution of IBU-NLC Raman chemical mapping. The spectra of the estimated ingredients, the 'Components', are compared with the reference spectra of the individual ingredients.

5.12 Results of FT-IR

The FT-IR spectra of the excipients, blank NLC and IBU-NLC were recorded to obtain information about the possible interactions between IBU and the matrix of the nanoparticles. Analysis of the spectrum of IBU-NLC clearly indicates that there are no strong interactions between the drug and the excipients (Fig. 23). Comparison of the FT-IR spectra of the blank NLC and the drug-loaded IBU-NLC at 1700 cm^{-1} and 1550 cm^{-1} revealed two peaks (which are characteristic of the drug) as shoulders in the spectrum of IBU-NLC (Fig. 23, marked peaks).

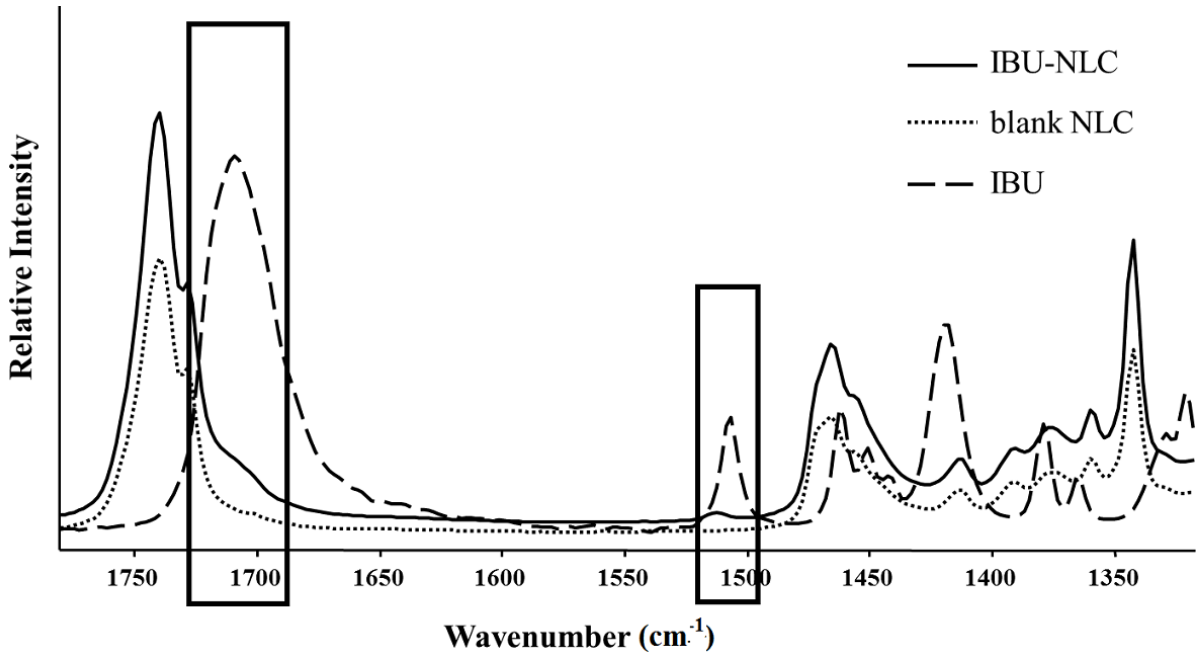

Fig. 23: FT-IR spectra of IBU-NLC, blank NLC and IBU.

After the deconvolution of the wavelength range 1800-1660 cm^{-1}, the characteristic peak of IBU at 1721 cm^{-1}, described as the vibration of the C=O bond [89], could be characterized (Fig. 24). The intensity of this peak is low, which means that non-dissolved IBU is present in low concentrations. The presence of drug crystals could be due to the pretreatment of the samples prior to the measurement (the NLC dispersions were dried in air).

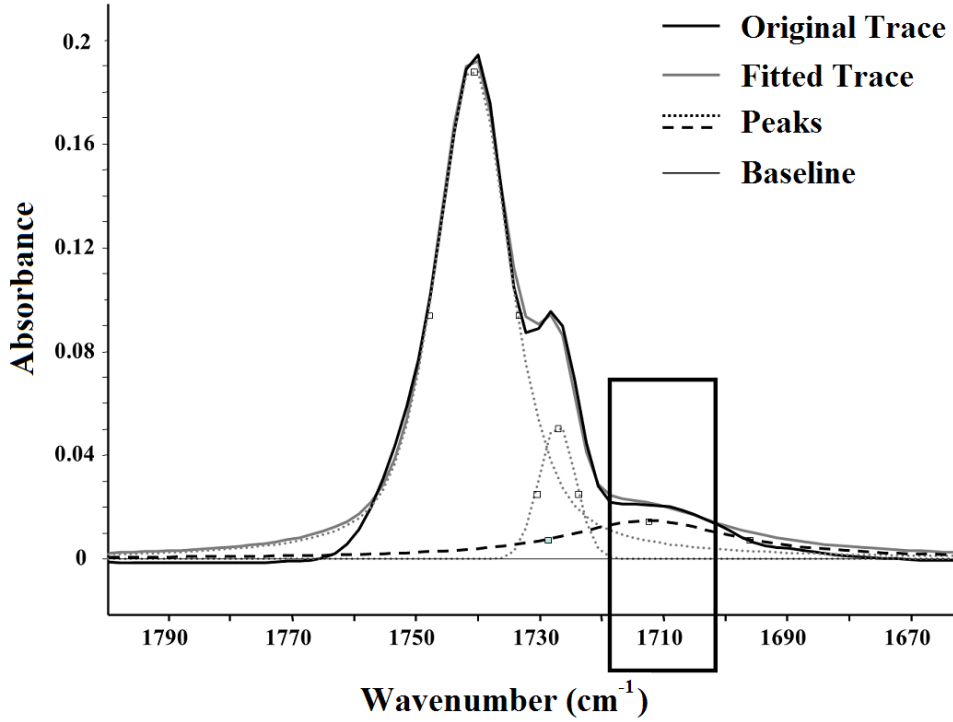

Fig. 24: Deconvolution of the IBU-NLC spectrum in the range 1800−1665 cm^{-1}.

5.13 Results of drug loading and entrapment efficiency

From the results of the applied HPLC method, DL% was found to be 9.85 ± 4.10% and EE% 98.51±4.10% for the prepared IBU-NLC composition, since 1.49 ± 4.10% of the IBU was measured in the outer aqueous phase.

5.14 Results of drug penetration studies

5.14.1. *In vitro* drug diffusion

The *in vitro* diffusion of IBU through the artificial membrane from IBU-NLC and the IBU suspension was calculated in terms of the mean cumulative amount diffused at each sampling time point during a period of 6 h (Fig. 25). The amount of IBU diffused from the IBU-NLC after 6 h was significantly, 2.59-fold higher ($p < 0.0001$) than that from the IBU suspension.

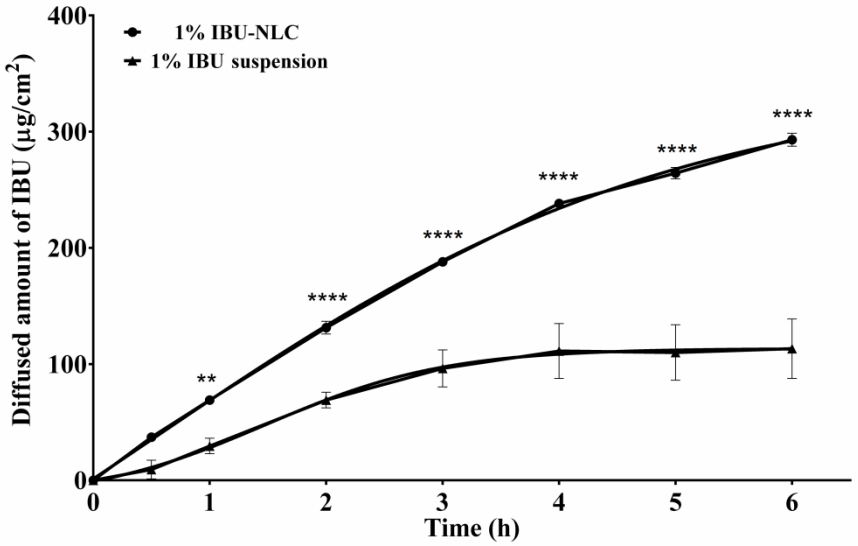

Fig. 25: *In vitro* diffusion of IBU from the IBU-NLC (●) and the IBU suspension (▲).

5.14.2. *Ex vivo* drug permeation

The *ex vivo* permeation of the drug from the prepared IBU-NLC gel and IBU gel through excised human skin was calculated in the same way as for the *in vitro* measurements (Fig. 26). The permeation of IBU through the excised human skin was 12.78-fold higher ($p < 0.001$) from the IBU-NLC gel than from the traditional IBU gel. These findings correlate with those of the *in vitro* diffusion study, since after 6 h much higher drug permeation was observed from the IBU-NLC gel than from the IBU gel.

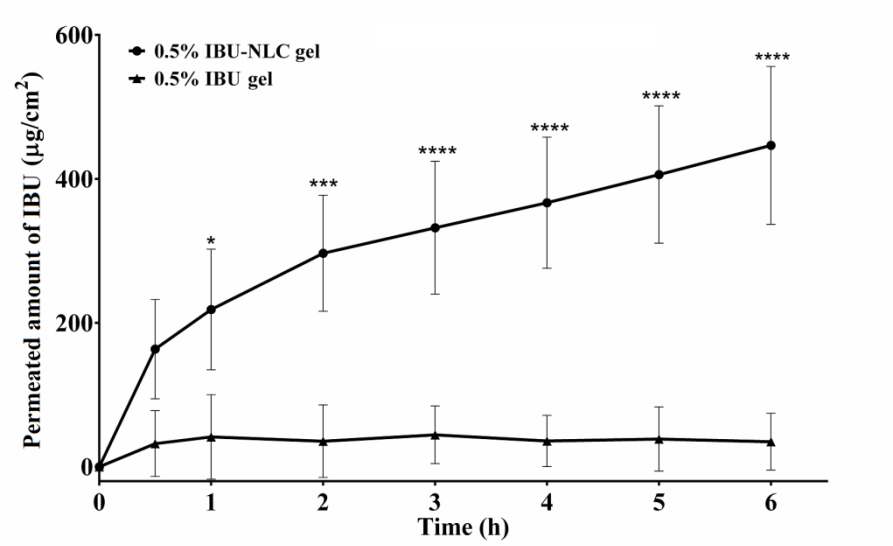

Fig. 26: *Ex vivo* permeation of IBU from the IBU-NLC gel (●) and the IBU gel (▲) through excised human epidermis.

5.14.3. *In vivo* animal studies

Finally, the *in vivo* permeation of IBU from the IBU-NLC gel and the IBU gel was determined with a murine model, using a modified dorsal skin chamber; the results are presented in Fig. 27. After 6 h, the drug penetration was significantly higher (1.87-fold, $p < 0.0001$) from the IBU-NLC gel formulation than from the IBU gel, as found in the previous *in vitro* and *ex vivo* studies.

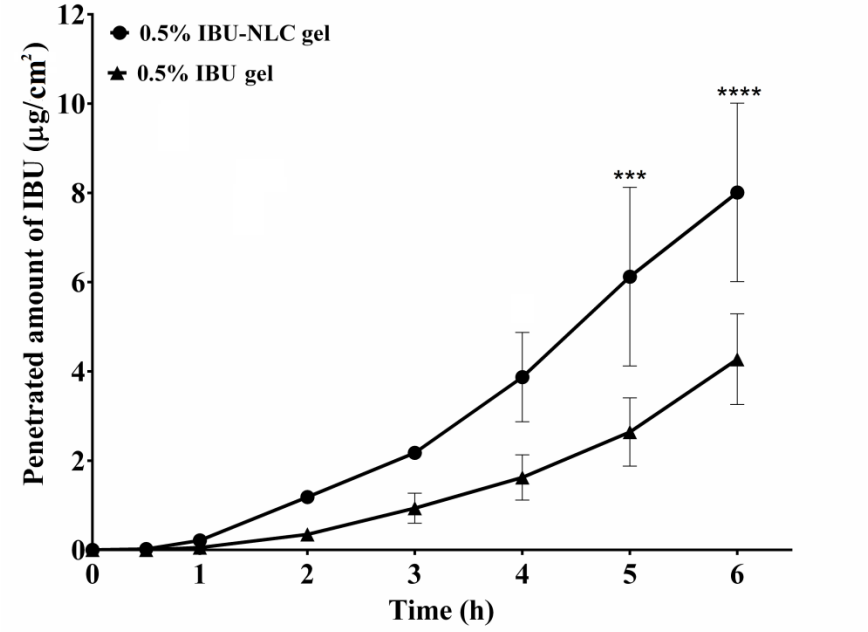

Fig. 27: *In vivo* permeation of IBU from IBU-NLC gel (●) and from the IBU gel (▲) through living animal skin.

6. SUMMARY

The aim of my Ph.D. work was to investigate IBU-NLC systems in order to optimize their compositions and to characterize their properties for musculoskeletal disorders requiring prolonged therapy. To summarize my experimental work it can be concluded that:

- the lipid screening led to Witepsol E85 being selected as the solid lipid and Miglyol 812 as the liquid lipid, which proved to be compatible with and could incorporate IBU in the highest concentration, 50% (w/w);
- on the basis of the results of contact angle measurements, Lutrol F68 was selected as a surfactant that could provide a stable NLC system;
- the drug–excipient compatibility was demonstrated by:
    - DSC measurements;
    - XRD analysis;
    - FT-IR spectroscopy measurements;
- the composition was optimized via a 2^3 full factorial design, and NLC 5 (7% Witepsol E85, 3% Miglyol 812 and 5% Lutrol F68) was selected for further investigations;
- an optimum equation was defined with consideration of the effects of the excipient concentration which could serve as a useful tool, with selection of the optimal formulation at which the surface plot has a minimum value.

In the second part, the optimized IBU-NLC formulation was characterized. It emerged that:

- the PS of the blank and IBU-NLC formulations measured by PCS, LD and AFM methods were in the nanometer range (below 205 nm) with low PDI and Span values;
- the ZP revealed that the particles were negatively charged and their stability could be predicted as sufficient;
- the lipid matrix was in the amorphous form and the formulations did not contain IBU in a crystalline form;
- FT-IR spectroscopy and Raman spectroscopy did not reveal any significant interactions between the components of the prepared samples, predicting the fast release of IBU from the NLC formulation;
- Raman mapping verified that the drug was homogenously distributed in the lipid matrix;

- drug permeability studies showed the fast initial release of IBU from the nanoparticles, and the amount released after 6 h was significantly higher relative to the prepared reference formulations *in vitro*, *ex vivo* and *in vivo*.

Novelty of this work can be summarized in the following:

- the optimum equation was first defined serving as a useful tool, to select the optimal formulation at which the surface plot has a minimum value;
- Raman mapping was used to localize an API, namely the IBU in an NLC formulation, in the lipid matrix of the IBU-NLC;
- *ex vivo* and *in vivo* drug permeation studies of the ibuprofen-loaded nanostructured lipid carrier were first compared (and found to be significantly higher after 6 h) to a reference (IBU gel) which composition mimicked the composition of those available on the market;
- the modified dorsal skin chamber was first used to prove that the IBU could permeate through the skin of SKH-1 hairless mice *in vivo*;

All of the results of the measurements performed excellently illustrated the potential of the application of the developed IBU-NLC formulation as a stable IBU delivery system, its fast release and enhanced skin permeability predicting better bioavailability with the possibility of topical therapy.

REFERENCES

1. Puglia, C., et al., *Lipid nanoparticles for prolonged topical delivery: an in vitro and in vivo investigation.* International Journal of Pharmaceutics, 2008. **357**(1-2): p. 295-304.
2. Mehnert, W. and K. Mäder, *Solid lipid nanoparticles: Production, characterization and applications.* Advanced Drug Delivery Reviews, 2001. **47**(2–3): p. 165-196.
3. zur Mühlen, A., C. Schwarz, and W. Mehnert, *Solid lipid nanoparticles (SLN) for controlled drug delivery – Drug release and release mechanism.* European Journal of Pharmaceutics and Biopharmaceutics, 1998. **45**(2): p. 149-155.
4. Müller, R.H., K. Mäder, and S. Gohla, *Solid lipid nanoparticles (SLN) for controlled drug delivery - a review of the state of the art.* European Journal of Pharmaceutics and Biopharmaceutics, 2000. **50**(1): p. 161-177.
5. Müller, R.H., M. Radtke, and S.A. Wissing, *Solid lipid nanoparticles (SLN) and nanostructured lipid carriers (NLC) in cosmetic and dermatological preparations.* Advanced Drug Delivery Reviews, 2002. **54**(0): p. S131-S155.
6. Lippacher, A., R.H. Müller, and K. Mäder, *Preparation of semisolid drug carriers for topical application based on solid lipid nanoparticles.* International Journal of Pharmaceutics, 2001. **214**(1–2): p. 9-12.
7. Kaur, I.P., et al., *Potential of solid lipid nanoparticles in brain targeting.* Journal of Controlled Release, 2008. **127**(2): p. 97-109.
8. Phatak, A.A. and P.D. Chaudhari, *Development and evaluation of Nanostructured Lipid Carrier (NLC) based topical delivery of an anti-inflammatory drug.* Journal of Pharmacy Research, 2013. **7**(8): p. 677-685.
9. Joshi, M. and V. Patravale, *Nanostructured lipid carrier (NLC) based gel of celecoxib.* International Journal of Pharmaceutics, 2008. **346**(1): p. 124-132.
10. Bhaskar, K., et al., *Lipid nanoparticles for transdermal delivery of flurbiprofen: formulation, in vitro, ex vivo and in vivo studies.* Lipids in Health and Disease, 2009. **8**(6): p. 1-15.
11. Ricci, M., et al., *Evaluation of indomethacin percutaneous absorption from nanostructured lipid carriers (NLC): in vitro and in vivo studies.* Journal of Pharmaceutical Sciences, 2005. **94**(5): p. 1149-1159.

12. Khurana, S., N.K. Jain, and P.M. Bedi, *Development and characterization of a novel controlled release drug delivery system based on nanostructured lipid carriers gel for meloxicam.* Life Sciences, 2013. **93**(21): p. 763-772.
13. Li, X., et al., *A controlled-release ocular delivery system for ibuprofen based on nanostructured lipid carriers.* International Journal of Pharmaceutics, 2008. **363**(1–2): p. 177-182.
14. Müller, R.H., et al., *Nanostructured lipid carriers (NLC) in cosmetic dermal products.* Advanced Drug Delivery Reviews, 2007. **59**(6): p. 522-530.
15. Schäfer-Korting, M., W. Mehnert, and H.-C. Korting, *Lipid nanoparticles for improved topical application of drugs for skin diseases.* Advanced Drug Delivery Reviews, 2007. **59**(6): p. 427-443.
16. Baroli, B., *Penetration of nanoparticles and nanomaterials in the skin: fiction or reality?* Journal of Pharmaceutical Sciences, 2010. **99**(1): p. 21-50.
17. de Carvalho, S.M., et al., *Optimization of α-tocopherol loaded solid lipid nanoparticles by central composite design.* Industrial Crops and Products, 2013. **49**(0): p. 278-285.
18. Baş, D. and İ.H. Boyacı, *Modeling and optimization I: Usability of response surface methodology.* Journal of Food Engineering, 2007. **78**(3): p. 836-845.
19. Hao, J., et al., *Development and optimization of solid lipid nanoparticle formulation for ophthalmic delivery of chloramphenicol using a Box-Behnken design.* International Journal of Nanomedicine, 2011. **6**: p. 683-692.
20. Pardeike, J., A. Hommoss, and R.H. Müller, *Lipid nanoparticles (SLN, NLC) in cosmetic and pharmaceutical dermal products.* International Journal of Pharmaceutics, 2009. **366**(1–2): p. 170-184.
21. Sütő, B., Sz. Berkó, and E. Csányi, *Nanostrukturált lipid hordozó rendszerek alkalmazása a bőrön keresztüli hatóanyag-penetráció elősegítésére.* Gyógyszerészet, 2016. **60**: p. 76-85.
22. Chen, Y., G. Dalwadi, and H. Benson, *Drug delivery across the blood-brain barrier.* Current Drug Delivery, 2004. **1**(4): p. 361-376.
23. Müller, R.H., et al., *Solid lipid nanoparticles (SLN): an alternative colloidal carrier system for controlled drug delivery.* European Journal of Pharmaceutics and Biopharmaceutics, 1995. **41**(1): p. 62-69.

24. Freitas, C. and R.H. Müller, *Effect of light and temperature on zeta potential and physical stability in solid lipid nanoparticle (SLN™) dispersions.* International Journal of Pharmaceutics, 1998. **168**(2): p. 221-229.
25. Freitas, C. and R.H. Müller, *Correlation between long-term stability of solid lipid nanoparticles (SLN™) and crystallinity of the lipid phase.* European Journal of Pharmaceutics and Biopharmaceutics, 1999. **47**(2): p. 125-132.
26. Fundaro, A., et al., *Non-stealth and stealth solid lipid nanoparticles (SLN) carrying doxorubicin: pharmacokinetics and tissue distribution after i.v. administration to rats.* Pharmacological Research, 2000. **42**(4): p. 337-343.
27. Suresh Reddy, J. and V. Venkateswarlu, *Novel delivery systems for drug targeting to the brain.* Drugs of the Future, 2004. **29**(1): p. 63-83.
28. Chen, D.B., et al., *In vitro and in vivo study of two types of long-circulating solid lipid nanoparticles containing paclitaxel.* Chemical & Pharmaceutical Bulletin (Tokyo), 2001. **49**(11): p. 1444-1447.
29. Tabatt, K., et al., *Effect of cationic lipid and matrix lipid composition on solid lipid nanoparticle-mediated gene transfer.* European Journal of Pharmaceutics and Biopharmaceutics, 2004. **57**(2): p. 155-162.
30. Yang, S., et al., *Body distribution of camptothecin solid lipid nanoparticles after oral administration.* Pharmaceutical Research, 1999. **16**(5): p. 751-757.
31. Dingler, A., *Solid lipid nanoparticles as colloidal drug carriers for dermal application*, in *Department of Biology, Chemistry and Pharmacy*. 1998, Free University of Berlin: Berlin.
32. Gohla, S.H. and A. Dingler, *Scaling up feasibility of the production of solid lipid nanoparticles (SLN).* Pharmazie, 2001. **56**(1): p. 61-63.
33. Gasco, M.R., *Method for producing solid lipid microspheres having a narrow size distribution*. 1993, Google Patents.
34. Pardeike, J., et al., *Formation of a physical stable delivery system by simply autoclaving nanostructured lipid carriers (NLC).* International Journal of Pharmaceutics, 2012. **439**(1–2): p. 22-27.
35. Swathi, G., et al., *Solid lipid nanoparticles: colloidal carrier systems for drug delivery.* International Journal of Pharmaceutical Sciences and Research 2012. **43**(2): p. 1-16.

36. Müller, R.H., M. Radtke, and S.A. Wissing, *Nanostructured lipid matrices for improved microencapsulation of drugs.* International Journal of Pharmaceutics, 2002. **242**(1): p. 121-128.
37. Shah, R., et al., *Lipid Nanoparticles: Production, Characterization and Stability.* 2015: Springer.
38. Amman, H., *Nanostructured lipid carriers (NLC) in dermal and personal care formulations*, in *Department of Biology, Chemistry and Pharmacy*. 2009, Free University Berlin: Berlin. p. 202.
39. Pardeike, J., *Nanosuspensions and nanostructured lipid carriers for dermal application*, in *Department of Biology, Chemistry and Pharmacy*. 2009, Free university of Berlin: Berlin. p. 258.
40. zur Mühlen, A. and W. Mehnert, *Drug release and release mechanism of prednisolone loaded solid lipid nanoparticles.* Pharmazie, 1998. **53**(8): p. 552-555.
41. Souto, E.B. and R.H. Müller, *Lipid nanoparticles: effect on bioavailability and pharmacokinetic changes*, in *Drug Delivery*. 2010, Springer. p. 115-141.
42. McGrath, J.A. and J. Uitto, *Anatomy and Organization of Human Skin*, in *Rook's Textbook of Dermatology*. 2010, Wiley-Blackwell. p. 1-53.
43. Prow, T.W., et al., *Nanoparticles and microparticles for skin drug delivery.* Advanced drug delivery reviews, 2011. **63**(6): p. 470-491.
44. Cevc, G. and U. Vierl, *Nanotechnology and the transdermal route: A state of the art review and critical appraisal.* Journal of Controlled Release, 2010. **141**(3): p. 277-299.
45. Müller, R.H., et al., *Cytotoxicity of Solid Lipid Nanoparticles as a Function of the Lipid Matrix and the Surfactant.* Pharmaceutical Research, 1997. **14**(4): p. 458-462.
46. Müller, R.H., S. Staufenbiel, and C.M. Keck, *Lipid Nanoparticles (SLN, NLC) for innovative consumer care & household products.* Chemistry, 2014. **9**(2): p. 18-25.
47. Yang, X., et al., *Preparation and characterization of 4-dedimethylamino sancycline (CMT-3) loaded nanostructured lipid carrier (CMT-3/NLC) formulations.* International Journal of Pharmaceutics, 2013. **450**(1–2): p. 225-234.
48. Wissing, S.A. and R.H. Müler, *Solid lipid nanoparticles as carrier for sunscreens: in vitro release and in vivo skin penetration.* Journal of Controlled Release, 2002. **81**(3): p. 225-233.

49. Wissing, S.A. and R.H. Müller, *The influence of the crystallinity of lipid nanoparticles on their occlusive properties.* International Journal of Pharmaceutics, 2002. **242**(1–2): p. 377-379.
50. Lacatusu, I., et al., *The encapsulation effect of UV molecular absorbers into biocompatible lipid nanoparticles.* Nanoscale research letters, 2011. **6**(1): p. 73.
51. Potthast, H., et al., *Biowaiver monographs for immediate release solid oral dosage forms: Ibuprofen.* Journal of Pharmaceutical Sciences, 2005. **94**(10): p. 2121-2131.
52. Rhee, Y.S., et al., *Optimization of ibuprofen gel formulations using experimental design technique for enhanced transdermal penetration.* Int J Pharm, 2008. **364**(1): p. 14-20.
53. Patel, A., et al., *Delivery of ibuprofen to the skin.* International Journal of Pharmaceutics, 2013. **457**(1): p. 9-13.
54. Chen, W., et al., *Ibuprofen nanoparticles prepared by a PGSS™-based method.* Powder Technology, 2013. **245**(0): p. 241-250.
55. Blasi, P., et al., *Lipid nanoparticles for brain targeting II. Technological characterization.* Colloids and Surfaces B: Biointerfaces, 2013. **110**: p. 130-137.
56. Blasi, P., et al., *Lipid nanoparticles for brain targeting III. Long-term stability and in vivo toxicity.* International Journal of Pharmaceutics, 2013. **454**(1): p. 316-323.
57. Doktorovova, S., et al., *Trehalose is not a universal solution for solid lipid nanoparticles freeze-drying.* Pharmaceutical Development and Technology, 2014. **19**(8): p. 922-929.
58. Durán-Lobato, M., et al., *Statistical analysis of solid lipid nanoparticles produced by high-pressure homogenization: a practical prediction approach.* Journal of Nanoparticle Research, 2013. **15**(2): p. 1-14.
59. Dwivedi, P., et al., *Preparation and characterization of solid lipid nanoparticles of antimalarial drug arteether for oral administration.* Journal of Biomaterials and Tissue Engineering, 2014. **4**(2): p. 133-137.
60. Bummer, P.M., *Physical chemical considerations of lipid-based oral drug delivery--solid lipid nanoparticles.* Critical Reviews in Therapeutic Drug Carrier Systems, 2004. **21**(1): p. 1-20.
61. Kasongo, K.W., et al., *Selection and characterization of suitable lipid excipients for use in the manufacture of didanosine-loaded solid lipid nanoparticles and nanostructured lipid carriers.* Journal of Pharmaceutical Sciences, 2011. **100**(12): p. 5185-5196.

62. Chapman, D., *The Polymorphism of Glycerides.* Chemical Reviews, 1962. **62**(5): p. 433-456.
63. Ho Lun, W., et al., *Solid Lipid Nanoparticles for Anti-Tumor Drug Delivery*, in *Nanotechnology for Cancer Therapy*. 2006, CRC Press. p. 741-776.
64. Jenning, V. and S. Gohla, *Comparison of wax and glyceride solid lipid nanoparticles (SLN®).* International Journal of Pharmaceutics, 2000. **196**(2): p. 219-222.
65. Jenning, V., A.F. Thünemann, and S.H. Gohla, *Characterisation of a novel solid lipid nanoparticle carrier system based on binary mixtures of liquid and solid lipids.* International Journal of Pharmaceutics, 2000. **199**(2): p. 167-177.
66. Souto, E.B., et al., *Development of a controlled release formulation based on SLN and NLC for topical clotrimazole delivery.* International Journal of Pharmaceutics, 2004. **278**(1): p. 71-77.
67. Rowe, R.C., et al., *Handbook of pharmaceutical excipients*. Vol. 6. 2009: Pharmaceutical press London.
68. Owen, I.C. and H. Anne Marie, *Surfactants in Pharmaceutical Products and Systems*, in *Encyclopedia of Pharmaceutical Technology, Third Edition*. 2013, Taylor & Francis. p. 3583-3596.
69. Sütő, B., et al., *Optimization and design of an Ibuprofen-loaded nanostructured lipid carrier with a 2^3 full factorial design.* Chemical Engineering Research and Design, 2015. **104**: p. 488-496.
70. Xu, F., et al., *Thermodynamic study of ibuprofen by adiabatic calorimetry and thermal analysis.* Thermochimica Acta, 2004. **412**(1–2): p. 33-57.
71. Kumbhar, D.D. and V.B. Pokharkar, *Engineering of a nanostructured lipid carrier for the poorly water-soluble drug, bicalutamide: Physicochemical investigations.* Colloids and Surfaces A: Physicochemical and Engineering Aspects, 2013. **416**(0): p. 32-42.
72. Araújo, J., et al., *Nanostructured lipid carriers for triamcinolone acetonide delivery to the posterior segment of the eye.* Colloids and Surfaces B: Biointerfaces, 2011. **88**(1): p. 150-157.
73. Sütő, B., et al., *Development of Ibuprofen-loaded nanostructured lipid carrier based-gels: characterization and investigation of in vitro and in vivo penetration through the skin.* International Journal of Nanomedicine, 2016.

74. Kushwaha, A.K., et al., *Development and evaluation of solid lipid nanoparticles of raloxifene hydrochloride for enhanced bioavailability.* BioMed Research International, 2013. **2013**.
75. How, C.W., et al., *Tamoxifen-loaded nanostructured lipid carrier as a drug delivery system: Characterization, stability assessment and cytotoxicity.* Colloids and Surfaces B: Biointerfaces, 2013. **112**(0): p. 393-399.
76. Araujo, J., et al., *Release profile and transscleral permeation of triamcinolone acetonide loaded nanostructured lipid carriers (TA-NLC): in vitro and ex vivo studies.* Nanomedicine, 2012. **8**(6): p. 1034-1041.
77. Kheradmandnia, S., et al., *Preparation and characterization of ketoprofen-loaded solid lipid nanoparticles made from beeswax and carnauba wax.* Nanomedicine, 2010. **6**(6): p. 753-759.
78. Csizmazia, E., et al., *Penetration enhancer effect of sucrose laurate and Transcutol on ibuprofen.* Journal of Drug Delivery Science and Technology, 2011. **21**(5): p. 411-415.
79. Kligman, A.M. and E. Christophers, *Preparation of isolated sheets of human stratum corneum.* Archives of Dermatology, 1963. **88**(6): p. 702-705.
80. Erős, G., et al., *A Novel Murine Model for the In Vivo Study of Transdermal Drug Penetration.* Scientific World Journal, 2012. **2012**: p. 543536.
81. Berkó, Sz., B., Balázs, B. Sütő, et al., *Monitoring of Skin Penetration and Absorption with a new in vivo Experimental Model.* Farmacia, 2014. **62**(6): p. 1157-1163.
82. Pardeike, J., et al., *Development of an itraconazole-loaded nanostructured lipid carrier (NLC) formulation for pulmonary application.* Int J Pharm, 2011. **419**(1-2): p. 329-38.
83. Üner, M., et al., *Influence of surfactants on the physical stability of solid lipid nanoparticle (SLN) formulations.* Pharmazie, 2004. **59**(4): p. 331-332.
84. Han, F., et al., *Effect of surfactants on the formation and characterization of a new type of colloidal drug delivery system: Nanostructured lipid carriers.* Colloids and Surfaces A: Physicochemical and Engineering Aspects, 2008. **315**(1–3): p. 210-216.
85. Schöler, N., et al., *Surfactant, but not the size of solid lipid nanoparticles (SLN) influences viability and cytokine production of macrophages.* International Journal of Pharmaceutics, 2001. **221**(1-2): p. 57-67.

86. Tian, B.-C., et al., *Further investigation of nanostructured lipid carriers as an ocular delivery system: In vivo transcorneal mechanism and in vitro release study.* Colloids and Surfaces B: Biointerfaces, 2013. **102**(0): p. 251-256.
87. Vivek, K., H. Reddy, and R.S.R. Murthy, *Investigations of the effect of the lipid matrix on drug entrapment, in vitro release, and physical stability of olanzapine-loaded solid lipid nanoparticles.* AAPS PharmSciTech, 2007. **8**(4): p. 16-24.
88. McConnell, J.F., *2-(4-Isobutylphenyl)propionic acid. C13H18O2 ibuprofen or brufen.* Crystal Structure Communications, 1974. **3**: p. 73-75.
89. Matkovic, S.R., G.M. Valle, and L.E. Briand, *Quantitative analysis of ibuprofen in pharmaceutical formulations through FTIR spectroscopy.* Latin American Applied Research, 2005. **35**: p. 189-195.
90. Nokhodchi, A., O. Amire, and M. Jelvehgari, *Physico-mechanical and dissolution behaviours of ibuprofen crystals crystallized in the presence of various additives.* Daru, 2010. **18**(2): p. 74-83.
91. Ray, R., et al., *Development and Evaluation of a New Interpenetrating Network Bead of Sodium Carboxymethyl Xanthan and Sodium Alginate.* Pharmacology & Pharmacy, 2010. **1**: p. 9-17.
92. Natarajan, S., S.A.M. Britto, and E. Ramachandran, *Growth, Thermal, Spectroscopic, and Optical Studies of l-Alaninium Maleate, a New Organic Nonlinear Optical Material.* Crystal Growth & Design, 2005. **6**(1): p. 137-140.
93. Ramukutty, S. and E. Ramachandran, *Growth, spectral and thermal studies of ibuprofen crystals.* Crystal Research and Technology, 2012. **47**(1): p. 31-38.
94. Neupane, Y.R., et al., *Lipid based nanocarrier system for the potential oral delivery of decitabine: Formulation design, characterization, ex vivo, and in vivo assessment.* International Journal of Pharmaceutics, 2014. **477**(1–2): p. 601-612.
95. de Villiers, M.M., et al., *The dissolution and complexing properties of ibuprofen and ketoprofen when mixed with N-methylglucamine.* Drug Dev Ind Pharm, 1999. **25**(8): p. 967-72.

ACKNOWLEDGMENTS

I am extremely grateful to **Prof. Dr. habil. Piroska Szabó-Révész D.Sc.**, head of the Department of Pharmaceutical Technology, University of Szeged, for providing me with the opportunity to work in her department.

I am also enormously grateful to my supervisors **Dr. habil. Erzsébet Csányi,** Associate Professor, and **Dr. Szilvia Berkó Ph.D.,** Assistant Professor, for their valuable help in my practical work and for their useful advice.

I am likewise greatly indebted to **Prof. Dr. Andreas Zimmer Ph.D.** for providing me with the possibility to work in his department, and to **Dr. Sabrina Weber Ph.D.** for her help in the practical work.

I express my kindest thanks to **Gabriella Farkas** for her huge help in the measurement and evaluation of the FT-IR spectra and to **Dr. Péter Sipos Ph.D.** for his tremendous work in measuring and evaluating the Raman spectra.

I would like to express my kindest thanks to my co-authors and especially my colleagues at the Department of Pharmaceutical Technology for their co-operation and help.

Finally, I would like to thank my family and friends for their endless support, infinite patience and unconditional love. Without them this work could not be completed.

Annex

I.

MONITORING OF SKIN PENETRATION AND ABSORPTION WITH A NEW *IN VIVO* EXPERIMENTAL MODEL

SZILVIA BERKÓ[1], BOGLÁRKA BALÁZS[1], BLANKA SÜTŐ[1], GÁBOR ERŐS[2], BRIGITTA GÁL[2], ANITA SZTOJKOV-IVANOV[3], CODRUȚA SOICA[4], PIROSKA SZABÓ-RÉVÉSZ[1], LAJOS KEMÉNY[2], ISTVÁN ZUPKÓ[3], ERZSÉBET CSÁNYI[1*]

[1]*Department of Pharmaceutical Technology, University of Szeged, 6720 Szeged, Eötvös street 6., Hungary*
[2]*Department of Dermatology and Allergology, University of Szeged, 6720 Szeged, Korányi street 6-8., Hungary*
[3]*Department of Pharmacodynamics and Biopharmacy, University of Szeged, 6720 Szeged, Eötvös street 6., Hungary*
[4]*Department of Pharmaceutical Chemistry, University of Medicine and Pharmacy "Victor Babes" Timisoara, 300041 Timisoara, 2 Eftimie Murgu Str., Romania*

**corresponding author: csanyi@pharm.u-szeged.hu*

Abstract

The purpose of the study was to use a new type of *in vivo* animal model developed by our research group for the investigation of skin penetration, compared to the results of Franz cell measurements. The new *in vivo* experimental model provides possibility for the exact measurement of the quantity of the penetrated drug through the living mouse skin. Two gel formulations containing ibuprofen were investigated with or without penetration enhancer. The applied penetration enhancer was Transcutol®. The effect of the penetration enhancer was clearly detected in both models. The *in vitro* diffused amount of ibuprofen was significantly higher than the one permeated through the living skin. The presence of the active agent in the plasma was also determined after the observation period. It was possible to monitor the penetration and absorption of topical formulations simultaneously.

Rezumat

Obiectivul studiului a fost utilizarea unui nou tip de model animal *in vivo* realizat de grupul nostru de cercetare în scopul investigării penetrării prin piele, în comparaţie cu rezultatele măsurătorilor prin celula Franz. Noul model experimental *in vivo* oferă posibilitatea unei măsurări exacte a cantităţii de substanţă medicamentoasă care penetrează prin pielea de şoarece. Au fost investigate două formulări de tip gel cu ibuprofen, cu sau fără promotor de absorbţie. Promotorul de absorbţie utilizat a fost Transcutol®. Efectul promotorului de absorbţie a fost clar detectat în ambele modele. Cantitatea de ibuprofen difuzată *in vitro* a fost semnificativ mai mare decât cea difuzată prin pielea de şoarece. Prezenţa agentului terapeutic în plasmă a fost de asemenea determinată după perioada de observaţie. A fost posibilă monitorizarea simultană a penetrării şi absorbţiei ambelor formulări topice.

Keywords: skinfold model, Franz-cell, skin permeation, ibuprofen, Transcutol®

Introduction

There are several methods for modelling drug permeation through the skin. The Franz-type diffusion cell is an accepted and widely applied model for dermal and transdermal delivery. Basically, a donor and an acceptor compartment are separated by a synthetic membrane [1-2]. Generally, these membranes are more permeable than biological membranes and are non-discriminatory to the characteristics of the diffusant molecule and not suitable for the investigation of the effect of the penetration enhancer modifying the structure of *stratum corneum*. Nowadays, various biological membranes are used more extensively such as animal skin [3] or human epidermis [4] to study the drug interaction with the skin and the incidental reservoir function of the *stratum corneum*. The *in vivo* animal studies are based on monitoring of the effect and blood level of penetrating agents. Other models show the presence of the drug in the skin or demonstrate its impact on the structure or certain functions of the skin [5].

In our previous work a novel animal model was developed successfully [6]. Dorsal skin fold chamber was used, which has been an accepted experimental model to study the microcirculation, angiogenesis and wound healing for more than twenty years [7-8]. The modified version of this experimental setup seemed to provide effective means for the *in vivo* examination of transdermal permeation. In this modified skinfold model we can determine drug permeation kinetics through living mouse skin on the same animal in time to get information on the permeation of the studied agent. Moreover, the detection of local side effects, skin irritation or any other type of alteration in the skin becomes possible.

The aim of our work was to compare diffusion (Franz cell method, with synthetic membrane) and permeation (modified skinfold method) parameters using ibuprofen gels with or without penetration enhancer.

Materials and Methods

Materials

Ibuprofen (IBU) was obtained from Sigma, St Louis, USA. Transcutol® (Diethylene glycol monoethylether, (TR)) was from S & D Chemicals Ltd. Hungary, and Carbopol 971 was from BF Goodrich Co., USA. Polyethylene glycol 400 and trolamine were purchased from Molar Chemicals Kft, Hungary.

Preparation of the gels

First 3% w/w Carbopol 971 hydrogel was prepared. The pH was adjusted with the use of trolamine. The 5 % w/w IBU was dissolved in

polyethylene glycol 400 and was added to this gel (IBU gel). Similar composition was prepared by using 10 % w/w Transcutol® added to polyethylene glycol 400 before dissolution of active agent (IBU-TR gel).

In vitro study

The rate and extent of IBU release was measured by an autosampling system containing vertical Franz diffusion cells (Hanson Microette TM Topical & Transdermal Diffusion Cell System, Hanson Research Corporation, USA). The drug release profile was determined at 37 ± 0.5 °C using phosphate buffer of pH=7.4, porafil membrane filter (cellulose acetate, the pore diameter was 0.45 μm, Macherey-Nagel GmbH & Co. KG, Germany) was used. The effective diffusion surface area was 1.767 cm^2. Experiments were performed for 6 hours. Samples were taken from the acceptor phase every hour and replaced with fresh receiving medium. The drug content of the samples was tested using an HPLC method.

In vivo study

The *in vivo* studies were carried out using a modified skinfold model developed by our research group. In our previous article the modified skinfold chamber has been described for investigation of drug penetration through living animal skin [6]. In the schematic picture (Figure 1) it can be seen that the drug penetrates through the complete living skin to reach the acceptor phase (phosphate buffer of pH=7.4), where the presence of the drug can be detected.

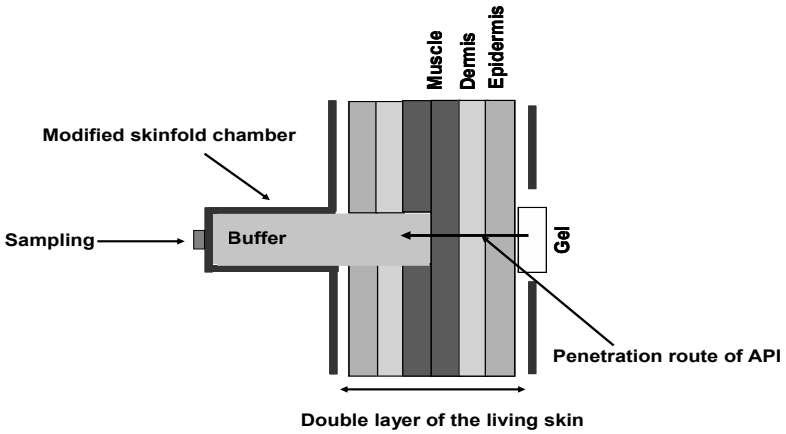

Figure 1.
Schematic picture of the model

The effective diffusion surface area was 1.539 cm^2. Experiments were performed for 6 hours. The total acceptor phase was changed every hour and the concentration of the drug was determined by an HPLC method.

At the end of the observation period a blood sample was taken from the inferior cava vein with a needle and syringe containing 250 IU of heparin. The blood was then centrifuged at 3500 g for 5 min in order to separate the cellular components. The plasma was collected and analysed by HPLC.

Data analysis

The diffusion and permeation parameters were calculated by the method described by Wagner et al. [9]. These parameters enable the comparison between different formulations of the same drug, though the influence of the vehicle can change the diffusion of the drug. The cumulative amount of IBU per area versus square time was plotted (Q). The steady state flux (J) was obtained as the slope of the plots. The lag-time (T_{lag}) was determined from the intercept of the plots with x-axis – symbolising the time of delay which describes the first contact of the drug with the skin surface until a steady state flux. The permeability coefficient (Kp) can be calculated dividing the flux by the initial concentration (Cd) of the donor phase.

$$Kp = J/Cd. \qquad \text{Eq. (1)}$$

Statistical analysis

Student's t-test was performed to see any significant difference in the diffused and permeated amount of IBU (Q) between the IBU and IBU-TR gel. Differences were regarded as significant, with $p < 0.05$.

HPLC method

Ibuprofen concentrations from buffer and plasma samples were determined by the method previously described by Eros et al. [6]. Based on the analysis of drug free serum, no interfering peaks of endogenous substances at the retention time of ibuprofen and I.S. indicated specificity of the method. The assay was linear in the range of 0.1 to 20 μg/mL and 0.5 to 15 μg/mL for buffer and plasma samples, respectively, with correlation coefficients of r=0.9993 ± 0.0031 (n=3) for buffer samples and r=0.9984 ± 0.0025 (n=3) for plasma samples. The limit of quantification was 0.2 and 0.5 μg/mL for buffer and plasma samples, respectively. The limit of detection was 0.06 μg/mL for buffer samples and 0.15 μg/mL for plasma samples. The intra- and inter-day accuracies for ibuprofen fell in the ranges 94.30–106.9% and 95.1–101.24%, and the intra- and inter-day precisions (CV%) were in the ranges 4.6–9.3% and 7.1–8.9%, respectively. Using this method the average recovery of ibuprofen from mice plasma was 98.2 ± 2.0%.

Results and Discussion

A modified skinfold animal model was studied for the investigation of skin penetration, compared to the result of Franz cell measurements. Two

gel formulations containing ibuprofen were investigated with or without penetration enhancer. The applied penetration enhancer was Transcutol®, which acts by increasing the solubility of the penetrant in the barrier. It works as a humectant, absorbing water, thus increasing the water content of the skin and the donor compartment. The change in the donor composition can influence the solubility and the thermodynamic activity of active pharmaceutical ingredient (API) [10]. However, Transcutol® has also been reported to increase the skin accumulation of topically applied compounds without a concomitant increase in transdermal permeation [11]. The results of diffusion and permeation studies are shown in Table I.

Table I.

The diffusion and permeation parameters of IBU. The table contains the means of six parallel measurements ± SD

		release time (h)	Cumulative amount of IBU (%)	Q (µg/cm^2)	J (µg/cm^2/h)	Kp*10^{-3} (cm/h)	T_{lag} (h)
IBU gel	synth. membr.	6	73.31±6.74	6276.33±291.95	2884.7	57.69	0.048
IBU-TR gel	synth. membr.	6	88.28±5.88	7504.85±249.66	3680.6	73.61	0.194
IBU gel	mouse model	6	2.13±0.09	68.17±3.1	73.577	1.47	1.548
IBU-TR gel	mouse model	6	5.81±0.85	189.03±27.74	172.82	3.45	1.369

The diffused amount of ibuprofen through the synthetic membrane was significantly higher than the one permeating through the living skin. The smaller quantity of the permeated drug, lower absorption rate and permeability coefficient and the longer lag time can be explained in terms of different factors in the present experiments. The drug has to cross the epidermis in order to enter the dermis, where ibuprofen is exposed to the barrier effect of the skin. Furthermore, ibuprofen can be taken up by the circulation. Only the proportion of the drug not eliminated by degradation or removal in the circulation can be delivered towards the deeper layer and the acceptor phase.

However, the effect of the penetration enhancer was clearly detected in both models. The cumulative amount of ibuprofen, the absorption rate and the permeability coefficient were significantly higher when applying the penetration enhancer containing IBU-TR gel. The effect of the penetration enhancer was more expressive in the animal model case. The changes of permeation parameters (Q, J, Kp) were more than twice higher. The lag time was shorter given the better permeation parameters.

In this study the presence of the active agent in the plasma was also determined after the observation period (Figure 2).

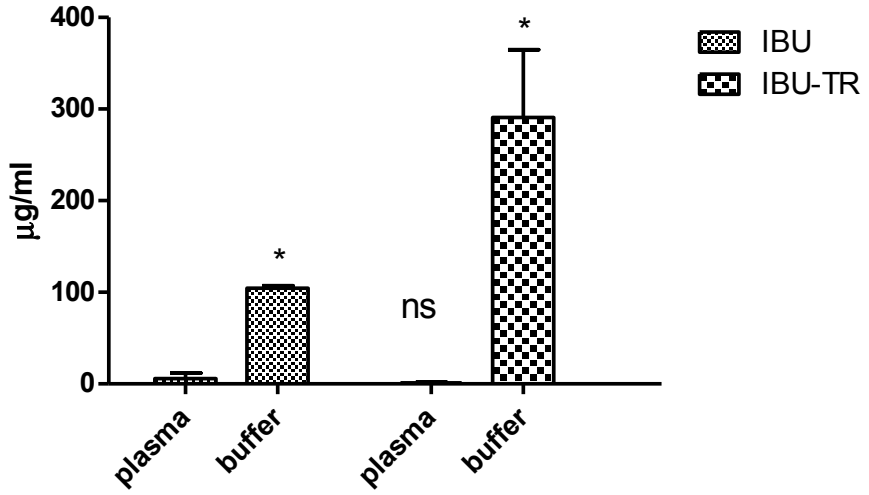

Figure 2.
Comparison of plasma and buffer concentration after 6 hours. The figure contains the means of six parallel measurements ± SD

The plasma and buffer concentrations were compared in case of IBU gel and IBU-TR gel. The buffer concentrations were significantly higher than plasma levels. The plasma levels were very low, 5.71 µg/mL in case of IBU gel and 1.03 µg/mL in case of IBU-TR gel. There was no significant difference in plasma levels when applying IBU gel or IBU-TR gel.

Conclusions

In this study it was possible to monitor the permeation of hydrogel containing ibuprofen through living skin compared to drug diffusion through synthetic membrane. The effect of penetration enhancer for diffusion and permeation could be detected in case of *in vitro* and new *in vivo* model too. Comparing the buffer and plasma levels, the buffer concentrations were significantly higher than plasma levels, which proves that the model is suitable and up-to-date for determining the quantity of drug permeation through living full-thickness skin.

Acknowledgements

The authors are grateful to S&D Chemicals Ltd, Hungary for providing samples Transcutol® and Labrasol®.

The study was supported by NKTH—A*STAR (Hungarian-Singaporean) Bilateral S&T International Co-operation (BIOSPONA) and the European Union and co-funded by the European Social Fund. Project title: "Broadening the knowledge base and supporting the long term professional sustainability of the Research University Centre of Excellence at the University of Szeged by ensuring the rising generation of excellent scientists." Project number: TÁMOP-4.2.2/B-10/1-2010-0012.

References

1. Corlan G., Pahomi G., Sandulovici R., Prasacu I., Ionescu M., Anuta V., Modelling of transfer kinetics of trichlorphon pesticid across cuprophane dialysis membrane in presence and absence of antidote powders. *Farmacia*, 2012; 60(6): 915-924.
2. Gavriloaia M.R., Budura E.A., Toma C.T., Mitu M.A., Karampelas O., Arama C.A., Lupuleasa D., *In vitro* evaluation of diffusion and rheological profiles for dexamethasone inclusion complexes with β-cyclodextrin, or hydroxypropyl β-cyclodextrin. *Farmacia*, 2012; 60(6): 895-904.
3. Jensen L.B., Petersson K., Nielsen H.M., *In vitro* penetration properties of solid lipid nanoparticles in intact and barrier-impaired skin. *Eur. J. Pharm. Biopharm*., 2011; 79: 68-75.
4. Schreiber S., Mahmoud A., Vuia A., Rübbelke M.K., Schmidt E., Schaller M., Kandárová H., Haberland A., Schäfer U.F., Bock U., Korting H.C., Liebsch M., Schäfer-Korting M., Reconstructed epidermis *versus* human and animal skin in skin absorption studies. *Toxicology in vitro*, 2005; 19: 813-822.
5. Csizmazia E., Erös G., Berkesi O., Berkó Sz., Szabó-Révész P., Csányi E., Ibuprofen penetration enhance by sucrose ester examined by ATR-FTIR *in vivo*. *Pharm. Dev. Technol*., 2012; 17: 125-128.
6. Erős G., Hartmann P., Berkó Sz., Csizmazia E., Csányi E., Sztojkov-Ivanov A., Németh I., Szabó-Révész P., Zupkó I., Kemény L., A Novel murine model for the *in vivo* study of transdermal drug penetration. *Scientific World Journal*, 2012 (2012), 1-9.
7. Laschke M.W., Strohe A., Scheuer C., Eglin D., Verrier S., Alini M., Pohlemann T., Menger M.D., *In vivo* biocompatibility and vascularization of biodegradable porous polyurethane scaffolds for tissue engineering. *Acta Biomater*., 2009; 5: 1991-2001.
8. Sckell A., Leunig M., The Dorsal Skinfold Chamber: Studying Angiogenesis by Intravital Microscopy. *Methods Mol. Biol*., 2009; 467: 305-317.
9. Wagner H., Kostka K.H., Lehr C.M., Schaefer U.F., Interrelation of permeation and penetration parameters obtained from *in vitro* experiments with human skin and skin equivalents. *J. Control. Release*, 2001; 75: 283-295.
10. Mura P., Faucci M.T., Bramanti G., Corti P., Evaluation of transcutol as a clonazepam transdermal permeation enhancer from hydrophilic gel formulations. *Eur. J. Pharm. Sci*., 2000; 9: 365-372.
11. Godwin D.A., Kim N., Felton L.A., Influence of Transcutol CG on the skin accumlation and transdermal permeation of ultraviolet absorbers. *Eur. J. Pharm. Biopharm*., 2002; 53: 23-27.

Manuscript received: April 2014

II.

Contents lists available at ScienceDirect

Chemical Engineering Research and Design

journal homepage: www.elsevier.com/locate/cherd

Optimization and design of an ibuprofen-loaded nanostructured lipid carrier with a 2^3 full factorial design

Blanka Sütő[a], *Sabrina Weber*[b], *Andreas Zimmer*[b], *Gabriella Farkas*[a], *András Kelemen*[a,c], *Mária Budai-Szűcs*[a], *Szilvia Berkó*[a], *Piroska Szabó-Révész*[a], *Erzsébet Csányi*[a,*]

[a] *Department of Pharmaceutical Technology, Faculty of Pharmacy, University of Szeged, Eötvös u. 6, H-6720 Szeged, Hungary*

[b] *Department of Pharmaceutical Technology, Institute of Pharmaceutical Sciences, Karl-Franzens Universität Graz, Universitätsplatz 1, A-8010 Graz, Austria*

[c] *Department of Applied Informatics, University of Szeged, Boldogasszony sgt. 6-8, H-6722 Szeged, Hungary*

ARTICLE INFO

Article history:
Received 9 January 2015
Received in revised form 2 July 2015
Accepted 16 September 2015
Available online 26 September 2015

Keywords:
Nanostructured lipid carriers
Ibuprofen
Factorial design
Preformulation
Particle size
Zeta potential

ABSTRACT

With the aim of the development an ibuprofen (IBU)-loaded NLC with a 2^3 full factorial design, lipid screening and contact angle measurements were applied to choose the most suitable excipients for the formulation of the system. The results of DSC, XRD and FT-IR studies demonstrated the compatibility between the drug and the components. The factorial design was utilized to investigate the effects of the excipients on the zeta potential (ZP) and the mean particle size. The addition of a liquid lipid to the solid lipid decreased both the melting point and the crystallinity index, which also occurred after the dissolution of IBU in the lipid mixture. The XRD diffractograms confirmed the reduction in the crystallinity of the components, but despite this decrease they still retained a crystalline structure. FT-IR did not reveal any interaction between the drug and the excipients. The particle sizes were 129–160 nm, the PDIs ranged between 0.065 and 0.237, and their ZPs varied from −15.40 to −7.54 mV. Random samples (picked out from the design space) were also prepared. Analysis of their particle sizes and ZPs led to an optimum equation which demonstrated the appropriateness of the analysis and allowed the shortening of further experimental planning.

1. Introduction

The topical application of drugs is a favourable administration route in the treatment of skin diseases and musculoskeletal disorders. The advantage of dermal preparations is their administration at the site where the effect is needed (Puglia et al., 2008).

Ibuprofen (IBU) is a potent nonsteroidal anti-inflammatory drug (NSAID) often used for the treatment of acute and chronic arthritic conditions and for the relief of acute pain. It is considered one of the safest NSAIDs available on the market. Although IBU is not the most potent active pharmaceutical ingredient (API) in this group, it offers the best balance between safety and therapeutic effect (Potthast et al., 2005). Its low water-solubility (Nanau and Neuman, 2010) and low bioavailability (Chen et al., 2013) pose a great challenge in the development of dermal delivery. Moreover, the oral administration of IBU can cause gastric mucosal damage, which can

* *Corresponding author*. Tel.: +36 62545573.
E-mail address: csanyi@pharm.u-szeged.hu (E. Csányi).
http://dx.doi.org/10.1016/j.cherd.2015.09.010

lead to bleeding and ulceration. Because of its valuable properties, there is great interest in the development of suitable topical dosage forms of IBU, thereby avoiding the oral side-effects and with the facile application of the API to reach the inflamed joint or muscle in high concentration. Effective permeation of the drug is difficult to achieve by transdermal delivery, however, because of its intrinsically poor skin permeability, even though this is good relative compared to other NSAIDs in common use (Rhee et al., 2008).

Lipid nanoparticles are intensively studied drug delivery systems derived from o/w emulsions. The liquid lipid (oil) phase is replaced by a lipid (or a mixture of lipids) which is solid at both room and body temperature. There are two generations of lipid nanoparticles: solid lipid nanoparticles (SLNs) and nanostructured lipid carriers (NLCs). The lipid matrix of SLNs is produced only from solid lipid(s), while the matrix of NLCs consists of a blend of solid lipid(s) and liquid lipid(s). These particles are stabilized by surfactants in an aqueous solution. NLC systems possess certain advantages as compared with SLNs, such as a higher drug loading capacity and steady drug entrapment during storage. The use of only one lipid as matrix for an SLN tends to lead to the formation of a relatively perfect crystal lattice, which will result in drug expulsion. In contrast, the matrix of an NLC consists of a mixture of lipids with differently structured molecules, so that the formation of a perfect crystal is limited (Müller et al., 2007).

The dermal use of NLC systems offers a number of advantage, such as physical stability of the applied topical formulations, enhancement of the chemical stability of the incorporated APIs, improved dermal bioavailability, the skin targeting of the APIs, and film formation on the skin, accompanied by controlled occlusion and skin hydration *in vivo* (Müller et al., 2007; Schäfer-Korting et al., 2007). UV-reflecting properties (e.g. the possibility of using these carriers in sunscreens to help increase their protective effect against UV light) and the possibility of modulating API release into the skin have also been reported (Mehnert and Mäder, 2001).

Formulation of an NLC-based drug delivery system is a complex and long-lasting procedure, since the physicochemical properties of NLCs are altered by many factors, such as the quality and quantity of the selected lipids and surfactants or the ratio of lipids to API in the formulation. On view of their significant effects on the physicochemical properties of the nanoparticles, the selection of the proper ingredients is a crucial step in the formulation of NLCs. Optimization of the formulation via a factorial design could facilitate this process (de Carvalho et al., 2013; Mehnert and Mäder, 2001). The effects of three factors, the concentrations of the solid lipid, the liquid lipid and the surfactant, on the particle size ($d(0.5)$) and the zeta potential (ZP) of the prepared nanoparticles have been examined on two levels. The results of the factorial design have been depicted as plot surfaces.

Response surface methodology (RSM) is an appropriate tool with which to evaluate the correspondence between the response and independent variables and to optimize the processes or products (Baş and Boyacı, 2007). RSM requires less experimentation and provides estimates of the relative significance of the different variables (Hao et al., 2011).

The aim of this study was to develop IBU-loaded NLC for dermal drug delivery from the results of a 2^3 full factorial design. In order to evaluate the drug–excipient compatibility, differential scanning calorimetry (DSC) measurements, X-ray diffraction (XRD) analysis and Fourier transformation-infrared (FT-IR) spectroscopy measurements were carried out. The effects of the solid lipid:liquid lipid ratio and the lipid mixture:drug ratio were quantified via the factorial design and an optimum equation, which could serve as a useful tool in the choice of the optimum formulation of IBU-NLC systems.

2. Materials and methods

2.1. Materials

NLC formulations were loaded with IBU, which was provided by PannonPharma Ltd (Hungary). Precirol ATO 5 (glycerol palmitostearate; melting point (m.p.): 52–55 °C), Compritol 888 ATO (glyceryl behenate/dibehenate; m.p.: 70 °C) and Tego Care 450 (polyglyceryl-3 methylglucose distearate; HLB value: 12) were kindly supplied by Azelis Hungary Ltd (Hungary). Witepsol E85 (hard fat – hydrogenated vegetable glycerides; m.p.: 42–44 °C) and Miglyol 812 (caprylic/capric triglyceride) were provided by Sasol GmbH (Germany). Cutina CP (cetyl palmitate; m.p.: 55–56 °C), Cremophor EL (macrogolglycerol ricinoleate; HLB value: 12–14), Cremophor RH 60 (PEG-60 hydrogenated castor oil; HLB value: 15–17) and Lutrol F68 (Poloxamer 188; HLB value: 29) were kindly supplied by BASF SE Chemtrade GmbH (Germany). Oleic acid, Tween 20 (Polysorbate 20; HLB value: 16.7) and Tween 80 (Polysorbate 80; HLB value: 15) were purchased from Sigma–Aldrich (USA). Walcer (special sunflower-seed oil) was provided by Cereal Research Non-profit Ltd (Hungary).

2.2. Lipid screening

To determine the most suitable solid lipid and liquid lipid (oil) which dissolve IBU in the highest concentration, increasing concentrations of IBU were added to the solid and liquid lipids and the mixture was stirred with a Thermomixer Comfort (Eppendorf, Germany) for 90 min at 500 rpm at least 5 °C above the melting point of the examined lipids. The solubility of IBU in the examined lipids was analysed visually. The following step was to evaluate the miscibility of the chosen solid lipid and liquid lipid, and the solubility of IBU in the lipid mixture under the previously mentioned conditions. Briefly, solid and liquid lipids with the best solubilizing potential for IBU were mixed together in different proportions according to the 2^3 factorial design (ratios 10:3, 10:5, 7:3 and 7:5). After agitation, the lipid mixtures were left to cool to room temperature. After 24 h the lipid mixtures were smeared onto filter paper, and observed visually to verify the existence of oil droplets on the filter paper, which would indicate immiscibility between the lipids (Kasongo et al., 2011).

2.3. Contact angle measurements

Contact angles were measured with an Easy Drop G1 (A.Krüss Optronic, Germany). Cover slides were coated with a thin film of one or other of the four different bulk lipid mixtures (ratios 10:3, 10:5, 7:3 and 7:5). 10 μl of purified water (as reference) or 0.5% (w/v) surfactant solution (in purified water) was applied to the lipid film and the contact angle of the droplet was assessed.

2.4. DSC measurements

To obtain information on the melting behaviour of the chosen solid lipid, the lipid mixture and the bulk mixture of IBU dissolved in the lipid mixture, DSC measurements were

performed with a DSC 204 F1 Phoenix instrument (Netzsch, Germany). 2–5 mg samples were measured into aluminium pans which were than sealed; an empty aluminium pan was used as reference. The samples were heated from 20 °C to 65 °C at a heating rate of 5 K/min under constant nitrogen flushing (80 ml/min). The melting point of IBU has been reported to be between 75 and 77 °C, and it immediately starts to decompose after further heating (Xu et al., 2004). The lipids and drug compatibilities were therefore monitored up to 65 °C. The crystallinity index (CI (%)) was calculated from the obtained DSC thermograms via Eq. (1) (Araújo et al., 2011; Kumbhar and Pokharkar, 2013). Before the measurements, lipid mixtures and lipid–drug mixtures were melted and left to cool to room temperature. The solid lipid was examined as received, without any treatment.

$$\mathrm{CI}\,(\%) = \left(\frac{\Delta H_{\text{bulk material}} \times \text{solid lipid ratio}}{\Delta H_{\text{solid lipid}}} \right) \times 100 \quad (1)$$

where ΔH is the enthalpy of the examined material.

2.5. XRD analysis

XRD analysis was performed with a Bruker D8 Advance diffractometer (Bruker AXS GmbH, Karlsruhe, Germany) system with Cu K λI radiation (λ = 1.5406 Å). The samples were scanned at 40 kV and 40 mA from 3° to 40° 2θ, at a scanning speed of 0.1°/s and a step size of 0.010°. Samples were prepared in the same way as prior to the DSC measurements.

2.6. FT-IR spectroscopy

FT-IR spectra were recorded with a Bio-Rad Digilab Division FTS-65A/896 FTIR spectrometer (Bio-Rad Digilab Division FTS-65A/869, Philadelphia, PA, USA) between 4000 and 400 cm^{-1}, with 128 scan size, at an optical resolution of 4 cm^{-1}; operating conditions: Harrick's Meridian SplitPea single reflection, diamond, ATR accessory. Thermo Scientific GRAMS/AI Suite software (Thermo Fisher Scientific Inc., Waltham, MA, USA) was used for the spectral analysis. The same samples were used as in the XRD analysis.

2.7. Preparation of IBU-NLC

IBU-NLCs were prepared by a hot high-pressure homogenization method, using a Panda K2 NS1001L Spezial modified for NLC production (GEA Niro Soavi, Germany). Briefly, 5% drug was dissolved in the mixture of the chosen solid and liquid lipid at 65 °C. The surfactant was dissolved in purified water at the same temperature. The aqueous phase was added to the lipid phase and was stirred with an Ultra Turrax T25 (IKA-Werke, Germany) for 30 s at 12,500 rpm. The pre-emulsion obtained was subjected to high-pressure homogenization, applying five cycles at 600 bar and 65 °C. Blank NLC samples were prepared by the same procedure.

2.8. Size measurements and zeta potential (ZP) analysis

2.8.1. Photon correlation spectroscopy (PCS)

Particle size (Z_{ave}) and polydispersity index (PDI) of the prepared NLC samples were analysed by PCS with a Zetasizer Nano ZS instrument (Malvern Instruments, UK) equipped with a green laser beam. The PDI refers to the width of the particle size distribution.

2.8.2. Laser diffraction (LD)

Particles in the micrometre range were excluded by LD with a Mastersizer 2000 instrument (Malvern Instruments, UK). The $d(0.1)$, $d(0.5)$, $d(0.9)$, $d(0.95)$ and $d(0.99)$ values were evaluated. These show the sizes below which 10%, 50%, 90%, 95% and 99% of the analysed particles are to be found (volume distribution). The Span value, which relates to the width of the particle size distribution curve $((d(0.99)–d(0.1))/d(0.5))$, was also calculated. The measurement medium was purified water, with a refractive index of 1.33. The real refractive index was set to 1.456, and the imaginary refractive index to 0.01.

2.8.3. Zeta potential (ZP)

To acquire information about the stability of the prepared samples, ZP was determined with a Zetasizer Nano ZS instrument (Malvern Instruments, UK) via electrophoretic mobility measurements. The applied medium was bidistilled water adjusted with 0.9% NaCl solution to achieve a conductivity of 50 μS/cm and a pH value between 5.5 and 6.0. The Helmholtz–Smoluchowski method was used to calculate the ZP ($n = 3$).

2.9. Experimental design

During the experimental design, eight different NLC samples (NLC 1–8) were prepared by the hot high-pressure homogenization method according to the 2^3 full factorial design to evaluate the effects of the three IBU-NLC formulation factors. These factors were A (the solid lipid concentration), B (the liquid lipid concentration) and C (the surfactant concentration). The optimization parameters (dependent factors) were the measured ZP and mean $d(0.5)$ value of the prepared nanoparticles. The effects of the chosen factors were examined at two levels (+1 and −1). Table 1 shows the applied factorial table with the values of the independent and dependent factors. Statistical data analysis was performed using Statistica for Windows software version 10. Besides these eight samples, eight other formulations, belonging in the same parameter space were prepared (Table 1) to check whether there was a possibility of a simpler model with which to optimize these formulations.

3. Results and discussion

3.1. Lipid screening

A large variety of solid and liquid lipids (natural, semi-synthetic and synthetic lipids with various structures, e.g. triglycerides, partial glycerides, fatty acids, waxes and steroids) which could be suitable as matrices for NLC production are accessible on the market (Mehnert and Mäder, 2001; Müller et al., 2002). However, the lipids used as matrix lipids must be carefully selected as they will directly influence the performance of the carrier system (Pardeike et al., 2011). The properties to be considered: the toxicity and biocompatibility through the selection of well tolerated physiological and biodegradable lipids; the drug payload and entrapment efficiency through the choice of lipids which can solubilize high amounts of the drug; drug expulsion during storage, which can be minimized or avoided through the use of lipid matrices with a low tendency to crystallize or a less-ordered structure;

Table 1 – Values of the examined independent factors (A, B and C) and dependent factors (ZP and *d*(0.5)) and compositions of the NLC systems.

	Sample name	Solid lipid concentration % (w/w)	Liquid lipid concentration % (w/w)	Surfactant concentration % (w/w)	Zeta potential (mV)	Particle size (nm)
Formulations used in the factorial design	NLC 1	7 (−1)	3 (−1)	4 (−1)	−14.2	135
	NLC 2	10 (+1)	3 (−1)	4 (−1)	−9.5	160
	NLC 3	7 (−1)	5 (+1)	4 (−1)	−11.2	143
	NLC 4	10 (+1)	5 (+1)	4 (−1)	−11.7	140
	NLC 5	7 (−1)	3 (−1)	5 (+1)	−14.2	129
	NLC 6	10 (+1)	3 (−1)	5 (+1)	−10.9	152
	NLC 7	7 (−1)	5 (+1)	5 (+1)	−11.4	147
	NLC 8	10 (+1)	5 (+1)	5 (+1)	−12.1	150
NLC systems randomly picked out from the parameter space	Blank NLC	10	5	5	−7.54	149
	NLC 9	7	3.5	4	−12.4	131
	NLC 10	10	4	4	−12.3	137
	NLC 11	10	4	5	−15.4	143
	NLC 12	7	4.5	5	−9.64	130
	NLC 13	10	4.5	4	−12.0	136
	NLC 14	10	4.5	5	−12.3	141
	NLC 15	7	4	4	−9.97	158

controlled drug release properties through incorporation of the drug into the lipid matrix (i.e. a drug-enriched core, a drug-enriched shell or homogeneous drug distribution in the matrix); and increased chemical drug stability if photosensitive drugs or drugs sensitive to hydrolysis or oxidation are incorporated in the matrix (Mehnert and Mäder, 2001; Müller et al., 2002; Pardeike et al., 2009).

Apart from oleic acid, all of the investigated lipid melts dissolved IBU in a very high amount (50% w/w). The samples were cooled to room temperature and analysed visually after 24 h. With most of the examined lipids, the IBU underwent recrystallization (Table 2). No IBU crystals were found in Witepsol E85 and Miglyol 812, and these materials were therefore chosen as lipid matrix for NLC formulation. The solid lipid and liquid lipid mixtures were tested in ratios of 10:3, 7:3, 10:5 and 7:5. No oil droplets were observed on the filter paper. No recrystallization was observed visually after the addition of the drug.

3.2. *Contact angle measurements and determination of surfactant concentration*

The nature and the concentration of the surfactant have a great influence on the fineness and physical stability of the NLCs, as the surfactant can reduce the interfacial tension (IFT) between the lipid particles and the aqueous phase (Pardeike et al., 2011; Üner et al., 2004). The IFT can be determined via contact angle measurements. The IFT is directly proportional to the contact angle: the lower the IFT between the lipid matrix and the water phase, the smaller the contact angle. Contact angle measurements were performed to evaluate the surfactant displaying the best wetting with the Witepsol E85 and Miglyol 812 mixture. Contact angle measurements were performed for each of the solid lipid:liquid lipid ratios used in the factorial design (10:3, 7:3, 10:5 and 7:5). Since there was no significant difference between the results, the contact angles measured for films with a solid lipid:liquid lipid ratio of 10:5 are shown in Fig. 1. For all of the examined surfactant solutions, smaller contact angles could be reached than with distilled water (which was used as reference). These results correspond

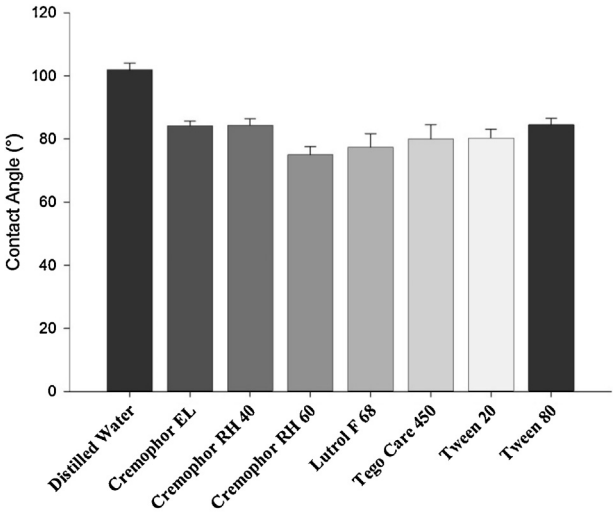

Fig. 1 – Contact angles of 0.5% (w/v) surfactant solutions applied to the 10:5 Witepsol E85:Miglyol 812 mixture.

Table 2 – Results of lipid screening.

Lipid type	Examined lipids	Solubility of 50% (w/w) IBU in the melted lipid	Recrystallization at room temperature after 24 h
Solid lipid	Compritol 888 ATO	Soluble	Yes
Solid lipid	Cutina CP	Soluble	Yes
Solid lipid	Precirol ATO 5	Soluble	Yes
Solid lipid	Witepsol E85	Soluble	No
Liquid lipid	Miglyol 812	Soluble	No
Liquid lipid	Oleic acid	Insoluble	Yes
Liquid lipid	Walcer	Soluble	Yes

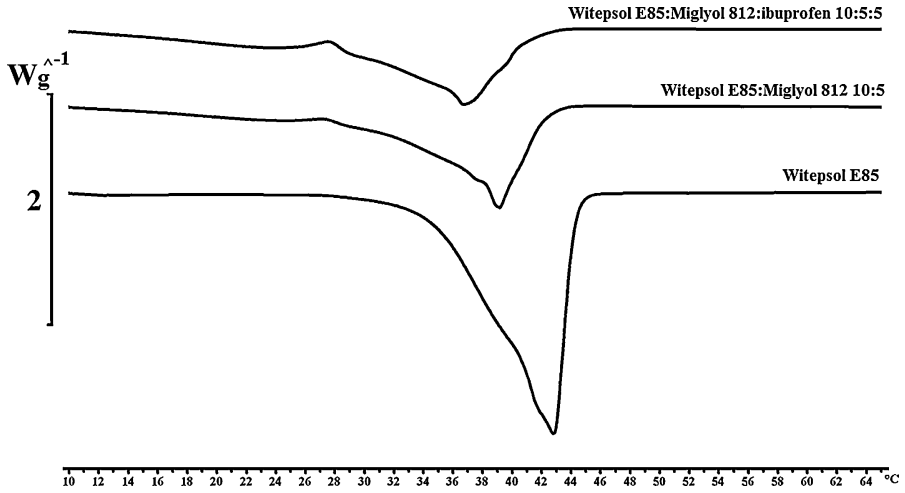

Fig. 2 – DSC curves of bulk materials: Witepsol E85, Witepsol E85:Miglyol 812 10:5, and lipid mixture:IBU 10:5:5.

with the fact that surfactant solutions exhibit a smaller surface tension than that of purified water. Cremophor RH 60 exhibited the best wetting properties with the lipid mixture (75.02 ± 2.49°), although similar results could be achieved with Lutrol F68 (77.4 ± 4.29°). NLC formulations were therefore prepared with both emulsifiers, and Lutrol F68 was chosen for further investigations on the basis of the $d(0.5)$ and ZP values (Cremophor RH 60: $d(0.5)$ = 214.4 nm, ZP = −9.17 mV; Lutrol F68: $d(0.5)$ = 112.4 nm, ZP = −12.4 mV).

The emulsifier concentration has a great influence on the particle size distribution, stability and toxicological properties of lipid nanoparticles (Han et al., 2008; Schöler et al., 2001; Üner et al., 2004). A high surfactant concentration results in a lower particle size, a narrower particle size distribution (which means a smaller PDI and a smaller Span value) and the better long-term stability of lipid nanoparticles, although it simultaneously increases the toxicological potential. Consequently, a balance is needed: the use of a sufficient amount of surfactant that ensures the desired small particle size and a proper physical stability during storage, but does not demonstrate toxicity.

3.3. *DSC measurements*

Lipid crystallization plays a very important role in the performance of NLC carriers. Other research groups have emphasized the importance of the characterization of the degree of lipid crystallinity and the modification of the lipid, because these parameters are closely correlated with the incorporation and release rates of the drug (Mehnert and Mäder, 2001; Tian et al., 2013).

Fig. 2 shows the DSC data of the different samples. Witepsol E85 is a mixture of mono-, di- and triglycerides. It has been reported that the presence of mono- and diglycerides in the matrix of the lipid can facilitate the solubilization of the drug (Müller et al., 2000; Vivek et al., 2007). Lipids which consist of a mixture of different di- and triglycerides or lipids which contain fatty acids of different chain lengths form less perfect crystals with many imperfections, offering spaces to accommodate drugs (Vivek et al., 2007). Witepsol E85 exhibited a broad endothermic event (melting range: around 42 °C), as described in the literature (Vivek et al., 2007). The bulk mixtures of the lipids, Witepsol E85 and Miglyol 812 in all investigated ratios gave a broader endothermic peak, with lower onset and peak values, as expected. The four lipid mixtures yielded similar DSC curves; the lipid mixture with a ratio of 10:5 is shown in Fig. 2. The normalized integral area under the curve, the onset, the peak, the endset and the CI (%) of the pure Witepsol E85, the 10:5 lipid mixture and the lipid mixture with IBU in a ratio of 10:5:5 have been evaluated and are listed in Table 3.

After the addition of the oil, the melting point of the solid lipid decreased from 42.78 °C to 39.16 °C, and CI (%) fell from 100% to 29.37%. A further decrease in the melting point from 42.78 °C to 36.77 °C was observed IBU was added to the lipid mixture. CI (%) also fell further from 29.37% to 15.57%. Both the addition of Miglyol 812 and the incorporation of IBU in the lipid matrix can result in an increase in the number of defects in the lipid crystal lattice, causing decreases in the CI (%) and the melting point of Witepsol E85 (Vivek et al., 2007). A less ordered crystalline structure predicts a higher loading capacity of the lipid matrix. A lipid mixture consisting of very differently structured molecules will prevent the formation of a perfect crystal, providing spaces in which to accommodate the drug in molecular form or as amorphous clusters (Müller et al., 2007).

3.4. *XRD analysis*

(*RS*)-(±)-IBU, an (*RS*)-2-(4-(2-methylpropyl)phenyl)propanoic acid, crystallizes with two molecules in the asymmetric unit to form a cyclic hydrogen-bonded dimer. Within the dimer, each molecule demonstrates subtle conformational differences via rotations about the acetic C(1)—C(2) and the C(10)—C(11) bonds.

Table 3 – Normalized integral area under curve, onset, peak, endset and CI (%) of pure Witepsol E85, the lipid mixture in a ratio of 10:5, and the lipid mixture with IBU in a ratio of 10:5:5.

Sample	Integral (normalized) (J/g)	Onset (°C)	Peak (°C)	Endset (°C)	CI (%)
Witepsol E85	−135.29	37.46	42.78	44.24	100
Witepsol E85:Miglyol 812 10:5	−59.60	36.36	39.16	41.95	29.37
Witepsol E85:Miglyol 812:IBU 10:5:5	−42.12	33.03	36.77	41.00	15.57

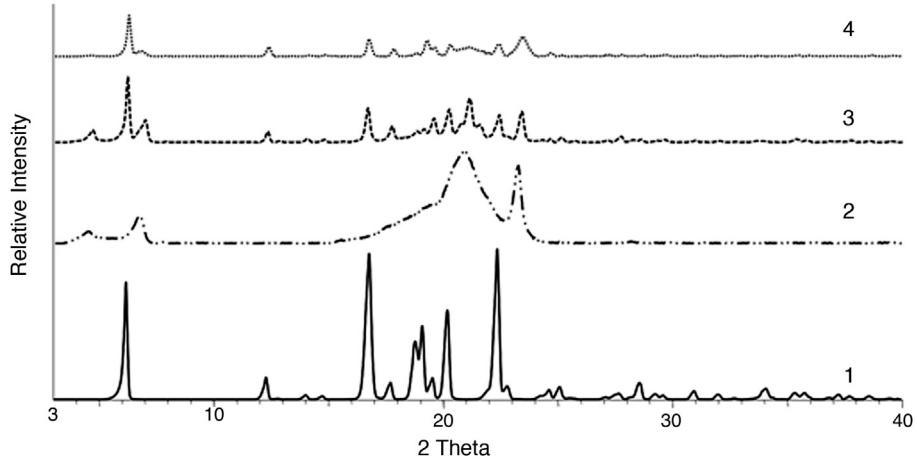

Fig. 3 – Wide-angle X-ray diffractograms of IBU (1), the 10:5 bulk mixture of Witepsol E85:Miglyol 812 (2), the 10:5:5 bulk mixture of Witepsol E85:Miglyol 812:IBU (3), and the 10:5:5:5 bulk mixture of Witepsol E85:Miglyol 812:IBU:Lutrol F68.

The bond distances and angles in (*RS*)-(±)-IBU are in close agreement with those found for the structure of the racemic compound (McConnell, 1974). For semisolid fat products (e.g. ice cream, margarine and chocolate), the solid lipids, which normally exist as a three-dimensional colloidal fat crystal network, determine the physical properties of the product. Upon crystallization, hardstock triacylglycerols aggregate to form fat crystals, which appear to aggregate, in a similar fashion as colloidal gels, to form clusters. These clusters aggregate into flocks, and finally weak links develop between the flocks in the final macroscopic network.

XRD measurements were performed to investigate the effects of the preparation temperature on the structures of the ingredients. The diffractogram of the melted bulk of the 10:5:5 physical mixture of Witepsol E85:Miglyol 812:IBU revealed the characteristic peaks of both the IBU and the lipid mixture. On the addition of Lutrol F68 to the mixture, a further reduction of the IBU peaks resulted (Fig. 3). It is clear from the diffractograms that both the IBU and the excipients retained their crystallinity, but the intensity of the IBU peaks decreased for both the lipid mixture and the physical mixture of the NLC components, which predicts the presence of the IBU in both dissolved and crystalline form.

3.5. *FT-IR analysis*

The intense band at 2955 cm^{-1} in the FT-IR spectrum of IBU is assigned to CH_3 asymmetric stretching. The very high-intensity peaks at 1721 cm^{-1} and 1231 cm^{-1} are due to C=O stretching and C—C stretching, respectively. The strong-intensity band observed at 779 cm^{-1} is due to CH_2 rocking vibration. The bands at 2955, 1721, 1231 and 668 cm^{-1} were assigned as the fingerprints of IBU in the literature (Matkovic et al., 2005; Nokhodchi et al., 2010; Ray et al., 2010). C—O stretching, CH_2 scissoring vibration and CH—CO deformation contribute to their presence. Strong-intensity CH_3 rocking of (936 cm^{-1}), CH_3 asymmetric deformation (1462 cm^{-1}), CH_2 asymmetric stretching vibration (3090 cm^{-1} and 2869 cm^{-1}) and CH_2 in-plane rocking vibration (522 cm^{-1}) are also observed. The absorption bands due to C=C stretching vibrations occur at 1507 cm^{-1} and 746 cm^{-1}. The medium-intensity O—H...O valence stretching vibration occurs at 2728 cm^{-1} and 2632 cm^{-1}. Absorption bands due to OH in-plane deformation (1321 cm^{-1}), =C—H in-plane deformation (1268 cm^{-1}, 1123 cm^{-1} and 1071 cm^{-1}), C—H in-plane deformation (1168 cm^{-1}, 1008 cm^{-1}, 636 cm^{-1} and 1092 cm^{-1}), C—H out-of-plane deformation (866 cm^{-1} and 668 cm^{-1}), in-plane ring deformation (407 cm^{-1}), C=C—C ring asymmetric bending (423 cm^{-1}), C—C deformation (588 cm^{-1}), CH_3 symmetric stretching (1380 cm^{-1}) and C—O—C stretching (970 cm^{-1}) have also been noted (Natarajan et al., 2005; Ramukutty and Ramachandran, 2012).

FT-IR analysis was used to verify whether any interaction occurred between the excipients and the drug because newly formed bonds can modify the diffusion of IBU from the nanoparticles. Fig. 4A presents the FT-IR spectra of the 10:5:5:5 physical mixture of Witepsol E85, Miglyol 812, IBU and Lutrol F68 and the individual spectra of these bulk components. A comparison of the spectra allows the conclusion that no chemical modification occurred at the temperature of NLC production. Fig. 4B depicts the lower wavelength range of the same spectra. No shifts in the major valency vibrations were detected and new peaks did not appear.

3.6. *Results of size measurements and zeta potential analysis*

The particle size and size distribution of the prepared IBU-loaded NLC were measured by PCS and LD. The particle size of the NLC systems varied in the interval 108.6–216.3 nm (Table 4). The Z_{ave} and $d(0.5)$ values appropriately correlate with each other, showing the mean particle sizes of the NLC samples. The PDI and the Span values vary in similar ways, as both relate to the size distribution of the lipid nanoparticles.

3.7. *Results of the experimental design*

3.7.1. *Effects of the dependent factors on the ZP*

The results were evaluated according to the 2^3 full factorial design. The three examined independent factors (solid lipid concentration (A), liquid lipid concentration (B) and surfactant concentration (C)) together exerted a significant effect ($p < 0.05$) on the ZP, but individually they did not do so. The coupled factors were also tested without giving a significant effect. The mathematical model is shown in the following equations (Eqs. (2)–(4)) of the response surfaces, with the ZP as the dependent factor as a function of factors A and B, factors A and C, and factors B and C, with a good correlation ($R^2 = 0.9901$):

$$ZP(A, B) = 3.61 * A + 6.99 * B - 0.77 * A * B - 43.98 \quad (2)$$

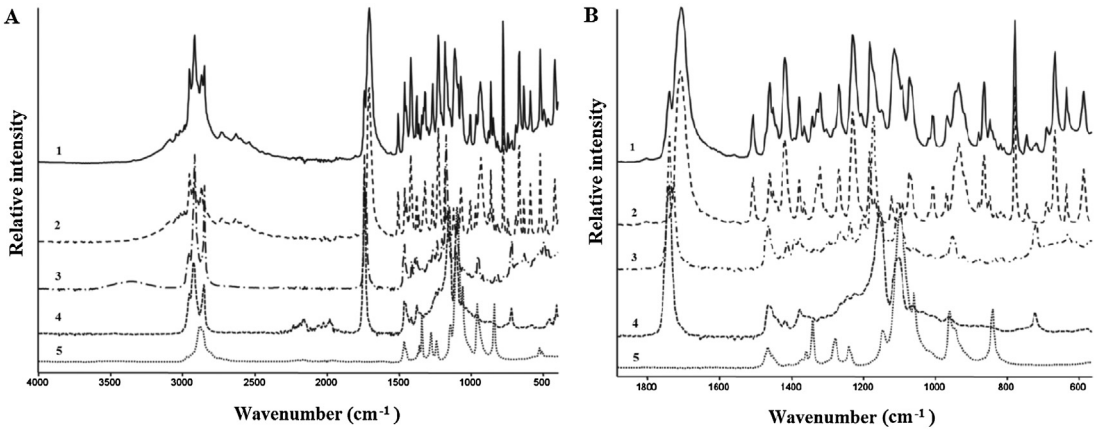

Fig. 4 – (A) FT-IR spectra of the physical mixture of the bulk components (Witepsol E85, Miglyol 812, IBU and Lutrol F68 in a ratio of 10:5:5:5) (1), IBU (2), Witepsol E85 (3), Miglyol 812 (4), Lutrol F68 (5); (B) FT-IR spectra in the lower wavenumber range of the same components.

$$ZP(A, C) = 1.75 * A + 1.77 * C - 0.27 * A * C - 24.66 \quad (3)$$

$$ZP(B, C) = -1.81 * B - 1.33 * C + 0.20 * B * C - 7.25 \quad (4)$$

A positive sign indicates a synergistic effect on the examined dependent factor, whilst a negative sign represents an antagonistic effect.

Factor A (solid lipid concentration) is directly proportional to the ZP, although this effect is not significant. The ZP becomes lower if factor A is kept on level −1 (7% Witepsol E85). The same effect was observed for factor B (liquid lipid concentration). Lower ZP values are obtained if factor B is kept at a lower level, e.g. if 3% Miglyol 812 is applied. This correspondence is clearly visible in Fig. 5A, which depicts three response surfaces where the ZP is a function of factors A and B; factor C is given on levels −1 (4% w/w), 0 (4.5% w/w) and +1 (5% w/w) (surfaces 1, 2 and 3). The ratio of factors A and B is indirectly proportional to the ZP. The response surfaces exhibit a minimum value at a solid lipid:liquid lipid ratio of 7:3; the ZP is −14.2 mV. This minimum is clearly visible and does not change if the surfactant concentration is altered from 4% to 4.5% or 5% w/w; the behaviour of the response surface remains unchanged in the examined range. Factor C is indirectly proportional to the ZP. Lower ZP values are expected if higher concentrations of the surfactant are applied; the use of 5% Lutrol F68 is therefore favourable.

3.7.2. *Effects of the dependent factors on the PS*

Similarly to the results of the statistical analysis of the ZP, the three independent factors (solid lipid concentration (A), liquid lipid concentration (B) and surfactant concentration (C)) together affected the PS significantly ($p < 0.05$), whereas their individual effects did not reach the level of significance (confidence value 95%). No significant effect was observed when the effects of the coupled factors were tested (A and B, A and C and B and C). The mathematical model of the effects of the dependent factors on the PS is shown in Eqs. (5)–(7), with a correlation of $R^2 = 0.9883$:

$$PS(A, B) = 20.02 * A + 34.50 * B - 4.00 * A * B - 27.50 \quad (5)$$

$$PS(A, C) = 1.00 * A - 5.67 * C + 0.67 * A * C + 136.00 \quad (6)$$

$$PS(B, C) = -31.00 * B - 27.97 * C + 7.00 * B * C + 268.50 \quad (7)$$

Factor A (solid lipid concentration) is directly proportional to the PS, but this effect does not reach the level of significance. PS is lower if factor A is kept on level −1 (7% Witepsol E85). The same effect is observed with factor B (liquid lipid concentration), i.e. PS of the nanoparticles is lower when 3% Miglyol 812 is used in the formulations. The ratio of factors A and B is indirectly proportional to the PS. In Fig. 5B, the response surfaces exhibit a minimum value at a solid lipid:liquid lipid ratio of 7:3; the PS is below 125 nm. The surface plot retains its

Table 4 – Results of PCS and LD measurements for all the NLC formulations.

Name	ZP (mV)	Z_{ave} (nm)	PDI	$d(0.1)$ (nm)	$d(0.5)$ (nm)	$d(0.9)$ (nm)	$d(0.95)$ (nm)	$d(0.99)$ (nm)	Span value
Blank NLC	−7.54	132.2	0.096	91	149	228	250	300	0.919
NLC 1	−14.2	216.3	0.230	97	135	249	280	330	1.126
NLC 2	−9.5	114.5	0.077	87	160	195	210	250	0.675
NLC 3	−11.2	113.1	0.067	86	143	192	210	250	0.741
NLC 4	−11.7	114.5	0.087	89	140	198	220	260	0.779
NLC 5	−14.2	108.6	0.065	86	129	192	210	250	0.822
NLC 6	−10.9	115.8	0.093	91	152	206	230	270	0.757
NLC 7	−11.4	112.7	0.089	85	147	191	210	250	0.721
NLC 8	−12.1	115.0	0.078	87	150	195	210	250	0.720
NLC 9	−12.4	112.4	0.089	87	131	195	210	250	0.824
NLC 10	−12.3	138.2	0.249	74	137	238	270	320	1.197
NLC 11	−15.4	114.7	0.108	90	143	219	240	280	0.902
NLC 12	−9.64	109.7	0.057	86	130	191	210	250	0.808
NLC 13	−12.0	116.1	0.085	90	136	200	220	260	0.809
NLC 14	−12.3	114.8	0.101	92	141	208	230	270	0.823
NLC 15	−9.97	214.4	0.237	91	158	262	300	360	1.082

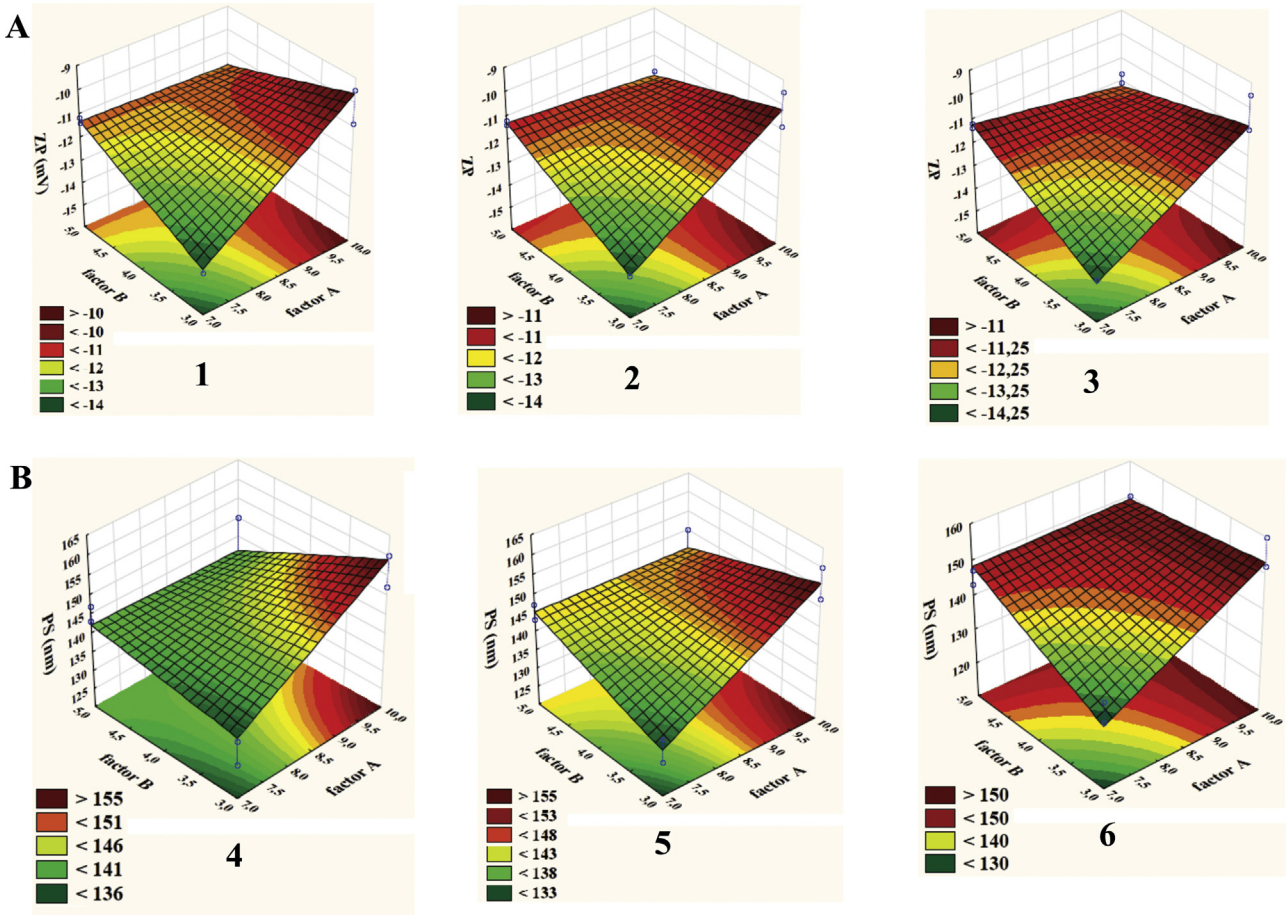

Fig. 5 – (A) Measured ZP as a function of solid lipid (factor A) and liquid lipid (factor B). The surfactant concentration was set to 4% w/w (1), 4.5% w/w (2) and 5% w/w (3); (B) measured PS as a function of solid lipid (factor A) and liquid lipid (factor B). The surfactant concentration was set to 4% w/w (4), 4.5%w/w (5) and 5%w/w (6).

minimum value regardless of the surfactant concentration. The difference between the maximum and minimum points of the surfaces becomes more explicit at higher surfactant concentrations (Fig. 5B (4), (5) and (6)) in the range of the factorial design.

Factor C (surfactant concentration) did not have an impact on the PS in this range.

The results of the applied factorial design indicate that NLC 5 was the most suitable for IBU delivery, together with 7% Witepsol E85, 3% Miglyol 812 and 5% Lutrol F68.

Table 3 gives data on NLC formulations randomly picked out from the factorial design space. By measuring the ZP, Z_{ave}, PDI and Span values of these NLC systems, a simpler function (Eq. (8)) could be defined to choose the optimum formulation. Factorial design requires a large number of samples, which may be decreased through use of the following equation if the response surface has a minimum value. The aim was to find a simpler correspondence to evaluate the optimum ratio of the compounds. The following equation gives the optimum as a non-dimensional number with a minimum value at the optimum compound.

$$\text{Optimum} = \min\left[\text{ZP} + Z_{ave} + \text{PDI} + \text{Span} + \frac{\text{SL}}{\text{LL}} + \frac{\text{SL/LL}}{\text{S}}\right], \quad (8)$$

where ZP is the zeta potential, Z_{ave} is the mean particle size measured by PCS, PDI is the polydispersity index, Span is the Span value($d(0.9)$–$d(0.1)$/$d(0.5)$), SL/LL is the solid lipid:liquid lipid ratio and SL/LL/S is the solid lipid:liquid lipid ratio proportional to the surfactant concentration.

As regards the optimum equation, NLC 5 proved optimum for the formulation of a stable IBU-loaded NLC system. This method appears suitable to design NLC formulations.

4. Conclusions

The present study highlights the importance of preformulation studies in the development of a potential NLC drug delivery system. Through the results of lipid screening and contact angle measurements, a high level of IBU loading (5% w/w) could be achieved. DSC measurements showed that the liquid lipid reduced the CI (%) of the solid lipid and slightly lowered its melting point. The incorporation of the drug caused a slight shift in the melting point and a further reduction of the CI (%). The reduced CI (%) predicts more imperfections in the crystal lattice of the solid lipid, which provides more spaces for the accommodation of the drug, thereby permitting higher drug loading capacities of the matrix. IBU was partially dissolved in the lipid matrix and was present in crystalline form, too, as revealed by the XRD diffractograms. The FT-IR data verified the drug–excipient compatibility, and there was no chemical interaction between the components, which suggests a faster release from the lipid matrix. Both PCS and LD measurements proved that the particle size of every sample was in the nanometre range, and the PDI and Span values indicated appropriate particle size distribution. It could be concluded that the 2^3 full factorial design is a useful and quick

method for the development of an IBU-NLC system prepared by hot high-pressure homogenization. The three independent factors (solid lipid concentration, liquid lipid concentration and surfactant concentration) together had a significant effect on the ZP and $d(0.5)$. The surface plot reveals a minimum value corresponding to the most suitable NLC formulation. The effects of PDI, the Span value, the solid lipid:liquid lipid ratio, and the lipid:surfactant ratio were also determined via the optimum equation, which supports the results of the factorial design and facilitates the development process. Further investigations of these nanoparticles should be performed as concerns long-term stability, entrapment efficiency and dissolution to prove their suitability for dermal application.

Acknowledgements

The authors wish to acknowledge the kindness of Azelis Hungary Ltd in supplying the lipid components.

References

Araújo, J., Nikolic, S., Egea, M.A., Souto, E.B., Garcia, M.L., 2011. Nanostructured lipid carriers for triamcinolone acetonide delivery to the posterior segment of the eye. Colloid Surf. B – Biointerfaces 88, 150–157.

Baş, D., Boyacı, İ.H., 2007. Modeling and optimization I: usability of response surface methodology. J. Food Eng. 78, 836–845.

Chen, W., Hu, X., Hong, Y., Su, Y., Wang, H., Li, J., 2013. Ibuprofen nanoparticles prepared by a PGSS^{TM}-based method. Powder Technol. 245, 241–250.

de Carvalho, S.M., Noronha, C.M., Floriani, C.L., Lino, R.C., Rocha, G., Bellettini, I.C., Ogliari, P.J., Barreto, P.L.M., 2013. Optimization of α-tocopherol loaded solid lipid nanoparticles by central composite design. Ind. Crop. Prod. 49, 278–285.

Han, F., Li, S., Yin, R., Liu, H., Xu, L., 2008. Effect of surfactants on the formation and characterization of a new type of colloidal drug delivery system: nanostructured lipid carriers. Colloid Surf. A – Physicochem. Eng. Asp. 315, 210–216.

Hao, J., Fang, X., Zhou, Y., Wang, J., Guo, F., Li, F., Peng, X., 2011. Development and optimization of solid lipid nanoparticle formulation for ophthalmic delivery of chloramphenicol using a Box-Behnken design. Int. J. Nanomed. 6, 683–692.

Kasongo, K.W., Pardeike, J., Müller, R.H., Walker, R.B., 2011. Selection and characterization of suitable lipid excipients for use in the manufacture of didanosine-loaded solid lipid nanoparticles and nanostructured lipid carriers. J. Pharm. Sci. 100, 5185–5196.

Kumbhar, D.D., Pokharkar, V.B., 2013. Engineering of a nanostructured lipid carrier for the poorly water-soluble drug, bicalutamide: physicochemical investigations. Colloid Surf. A – Physicochem. Eng. Asp. 416, 32–42.

Matkovic, S.R., Valle, G.M., Briand, L.E., 2005. Quantitative analysis of ibuprofen in pharmaceutical formulations through FTIR spectroscopy. Latin Am. Appl. Res. 35, 189–195.

McConnell, J.F., 1974. 2-(4-Isobutylphenyl)propionic acid. $C_{13}H_{18}O_2$ ibuprofen or brufen. Cryst. Struct. Commun. 3, 73–75.

Mehnert, W., Mäder, K., 2001. Solid lipid nanoparticles: production, characterization and applications. Adv. Drug Deliv. Rev. 47, 165–196.

Müller, R.H., Mäder, K., Gohla, S., 2000. Solid lipid nanoparticles (SLN) for controlled drug delivery – a review of the state of the art. Eur. J. Pharm. Biopharm. 50, 161–177.

Müller, R.H., Petersen, R.D., Hommoss, A., Pardeike, J., 2007. Nanostructured lipid carriers (NLC) in cosmetic dermal products. Adv. Drug Deliv. Rev. 59, 522–530.

Müller, R.H., Radtke, M., Wissing, S.A., 2002. Solid lipid nanoparticles (SLN) and nanostructured lipid carriers (NLC) in cosmetic and dermatological preparations. Adv. Drug Deliv. Rev. 54 (Suppl.), S131–S155.

Nanau, R.M., Neuman, M.G., 2010. Ibuprofen-induced hypersensitivity syndrome. Transl. Res. 155, 275–293.

Natarajan, S., Britto, S.A.M., Ramachandran, E., 2005. Growth, thermal, spectroscopic, and optical studies of l-alaninium maleate, a new organic nonlinear optical material. Cryst. Growth Des. 6, 137–140.

Nokhodchi, A., Amire, O., Jelvehgari, M., 2010. Physico-mechanical and dissolution behaviours of ibuprofen crystals crystallized in the presence of various additives. DARU 18, 74–83.

Pardeike, J., Hommoss, A., Müller, R.H., 2009. Lipid nanoparticles (SLN, NLC) in cosmetic and pharmaceutical dermal products. Int. J. Pharm. 366, 170–184.

Pardeike, J., Weber, S., Haber, T., Wagner, J., Zarfl, H.P., Plank, H., Zimmer, A., 2011. Development of an itraconazole-loaded nanostructured lipid carrier (NLC) formulation for pulmonary application. Int. J. Pharm. 419, 329–338.

Potthast, H., Dressman, J.B., Junginger, H.E., Midha, K.K., Oeser, H., Shah, V.P., Vogelpoel, H., Barends, D.M., 2005. Biowaiver monographs for immediate release solid oral dosage forms: ibuprofen. J. Pharm. Sci. 94, 2121–2131.

Puglia, C., Blasi, P., Rizza, L., Schoubben, A., Bonina, F., Rossi, C., Ricci, M., 2008. Lipid nanoparticles for prolonged topical delivery: an in vitro and in vivo investigation. Int. J. Pharm. 357, 295–304.

Ramukutty, S., Ramachandran, E., 2012. Growth, spectral and thermal studies of ibuprofen crystals. Cryst. Res. Technol. 47, 31–38.

Ray, R., Maity, S., Mandal, S., Chatterjee, T.K., Sa, B., 2010. Development and evaluation of a new interpenetrating network bead of sodium carboxymethyl xanthan and sodium alginate. Pharmacol. Pharm. 1, 9–17.

Rhee, Y.-S., Chang, S.-Y., Park, C.-W., Chi, S.-C., Park, E.-S., 2008. Optimization of ibuprofen gel formulations using experimental design technique for enhanced transdermal penetration. Int. J. Pharm. 364, 14–20.

Schäfer-Korting, M., Mehnert, W., Korting, H.-C., 2007. Lipid nanoparticles for improved topical application of drugs for skin diseases. Adv. Drug Deliv. Rev. 59, 427–443.

Schöler, N., Olbrich, C., Tabatt, K., Muller, R.H., Hahn, H., Liesenfeld, O., 2001. Surfactant, but not the size of solid lipid nanoparticles (SLN) influences viability and cytokine production of macrophages. Int. J. Pharm. 221, 57–67.

Tian, B.-C., Zhang, W.-J., Xu, H.-M., Hao, M.-X., Liu, Y.-B., Yang, X.-G., Pan, W.-S., Liu, X.-H., 2013. Further investigation of nanostructured lipid carriers as an ocular delivery system: in vivo transcorneal mechanism and in vitro release study. Colloid Surf. B – Biointerfaces 102, 251–256.

Üner, M., Wissing, S.A., Yener, G., Müller, R.H., 2004. Influence of surfactants on the physical stability of solid lipid nanoparticle (SLN) formulations. Pharmazie 59, 331–332.

Vivek, K., Reddy, H., Murthy, R.S.R., 2007. Investigations of the effect of the lipid matrix on drug entrapment, in vitro release, and physical stability of olanzapine-loaded solid lipid nanoparticles. AAPS PharmSciTech 8, 16–24.

Xu, F., Sun, L.-X., Tan, Z.-C., Liang, J.-G., Li, R.-L., 2004. Thermodynamic study of ibuprofen by adiabatic calorimetry and thermal analysis. Thermochim. Acta 412, 33–57.

III.

Gyógyszerészet 60. 76-85. 2016.

Nanostrukturált lipid hordozó rendszerek alkalmazása a bőrön keresztüli hatóanyag-penetráció elősegítésére

Sütő Blanka, Berkó Szilvia, Csányi Erzsébet

Bevezetés

A gyógyszertechnológia meghatározó feladatai közé tartozik a farmakonok fizikai-kémiai tulajdonságaiból eredő, a liberációt, a felszívódást, a megoszlást és a mellékhatásprofilt negatívan befolyásoló tényezők hatásának mérséklése, kiküszöbölése. A hatóanyag nanostrukturált lipid gyógyszerhordozó rendszerbe való inkorporálása egyike a lehetséges megoldásoknak. Mivel a hatóanyagok nagy része a BCS (*Biopharmaceutics Classification System*) II. (rossz vízoldékonyság és jó permeabilitás) és IV. osztályába (rossz vízoldékonyság és rossz permeabilitás) tartozik, a nanohordozók alkalmazása előnyös, hiszen mind az oldékonyság, mind a penetráció növelhető a segítségükkel, amely jobb biohasznosíthatóságot prediktál. A megfelelő mérettartományba eső részecskék könnyen átjuthatnak a barrier funkciót ellátó membránokon, és hatásukat kifejthetik egyes sejteken belül is, lehetőséget nyújtva ezzel a célzott gyógyszerleadásra. A megfelelő hordozók kialakításával depókészítmények is előállíthatók, amelyek egyszerűbb terápiát és állandó vérszintet biztosíthatnak, valamint javíthatják a betegek együttműködését is.

Más szemszögből megközelítve a gyógyszerformák ilyen irányú tervezése igen fontos lehet a generikumok, illetve a prefarmakonok fejlesztésénél és gyártásánál, hiszen új lehetőségek nyílnak a kutatók számára, kiküszöbölve ezzel a hagyományos eljárások korlátait.

Az 1990-es évek eleje óta egyre több kutatócsoport érdeklődését keltették fel a lipid nanorészecskék (*lipid nanoparticles*, LNP) világszerte. Napjainkban intenzív kutatások folynak olyan készítmények fejlesztésére, amelyek hordozójaként lipid nanorészecskéket választanak, mind a gyógyszerészet, mind a kozmetikai ipar területén [1]. Az elmúlt közel húsz évben számos vizsgálatot végeztek és ezek eredményét publikálták tudományos cikk formájában a parenterális [2-5], perorális [6-8], dermális [1, 9-12], szemészeti [13-15], valamint pulmonáris [16-18] készítményekről, amelyek formulálásakor nanostruktúrált lipid hordozó rendszerekbe inkorporálták a hatóanyagokat, illetve a biológiailag aktív anyagokat.

Célunk a nanostrukturált lipid hordozó rendszerek elméleti és gyakorlati jelentőségének bemutatása, a dermális/transzdermális terápiában való alkalmazhatóságukra fókuszálva.

Általános jellemzés, a lipid nanorészecskék típusai

A lipid nanorészecskék olyan gyógyszerhordozó rendszerek, amelyeket az emulziók, liposzómák és polimer nanorészecskék alternatívájaként fejlesztettek ki. A hatóanyag a lipid nanorészecskékben molekulárisan oldott vagy szuszpendált formában található [1, 19-21]. Elsősorban vízben rosszul oldódó hatóanyagok oldékonyságának növelésére, illetve oxidációra és fényre érzékeny anyagok stabilizálására alkalmazhatóak.

A lipid nanorészecskéknek négy típusát különböztetjük meg [22]:

1. szilárd lipid nanorészecske,
2. nanostruktúrált lipid hordozó,
3. lipid hatóanyag konjugátum,
4. polimer-lipid hibrid nanorészecske.

Szilárd lipid nanorészecske (SLN)

A szilárd lipid nanorészecskéket (***S**olid **L**ipid **N**anoparticle*, SLN) a lipid nanorészecskék első generációjaként fejlesztették ki. Előállításuk során egy o/v emulzió folyékony lipid fázisát (olaj) szilárd lipiddel, vagy azok keverékével helyettesítik. Az alkalmazott lipidek szobahőmérsékleten és testhőmérsékleten is szilárd halmazállapotúak. Az SLN szilárd zsír tartalma 0,1–30% intervallumban található, amelyet vizes közegben diszpergálnak. A rendszer stabilitásának növelése érdekében 0,5–5% közötti emulgenst vagy emulgenskeveréket alkalmazhatnak. A lipid mátrixba inkorporálják a lipofil hatóanyagot vagy farmakológiailag aktív anyagot. Az átlagos részecskeméret az SLN rendszerekben 40 és 1000 nm közötti mérettartományba esik [1]. Az alkalmazott lipidek GRAS (*generally recognized as safe*) minősítésűek, így az SLN rendszerek minimalizálják a citotoxicitást, emellett irányított hatóanyag-leadást tesznek lehetővé és jó fizikai stabilitással rendelkeznek [1, 23].

Nanostrukturált lipid hordozó (NLC)

A második generációs forma a nanostruktúrált lipid hordozó (***N**anostructured **L**ipid **C**arrier,* NLC). Az NLC lipid mátrixa a szilárd lipid(ek) mellett folyékony lipid komponens(eke)t is tartalmaz. Az NLC-t azért fejlesztették ki, hogy növeljék a lipid részecske bezárási hatékonyságát és stabilitását. Az SLN-hez viszo-

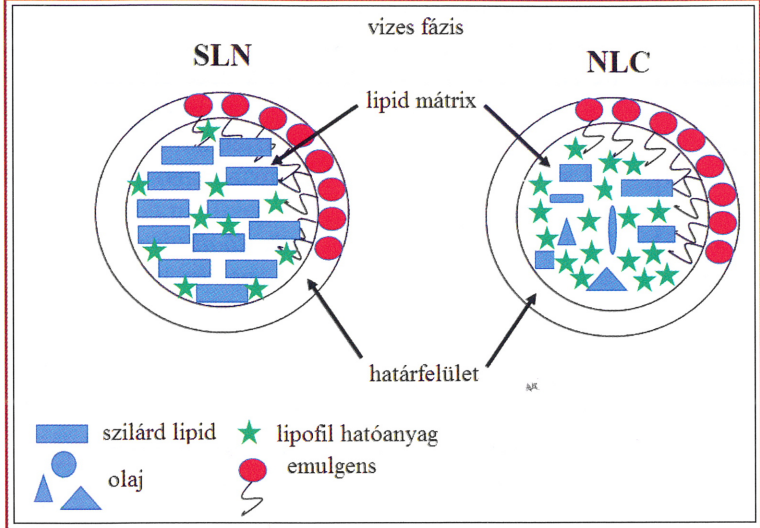

1. ábra: az SLN és az NLC szerkezete

nyítva az NLC alkotta mátrix lényegesen több hatóanyag befogadására képes, csökkenthető a hatóanyag és a mátrix szétválása a tárolás során. Ennek oka, hogy az SLN esetében egy, a szabályos kristályszerkezethez hasonló struktúra alakul ki, amelyben a szilárd lipidek szorosan, „téglafalszerűen" rendeződnek, és így a farmakon beépülése sztérikusan gátolt. Ezzel szemben az NLC mátrixa kevésbé lesz rendezett az alkalmazott folyékony lipid hatására, amelynek sokkal nagyobb a hatóanyagkötő kapacitása, mivel több a „hézag" (*1. ábra*). Ha rendezetlenebb szilárd lipid mátrixot készítünk, például szilárd lipidet folyékony lipiddel keverünk össze, több hatóanyagot inkorporálhatunk a rendszerbe. A folyékony lipid a szilárd lipidek szabályos kristályokba rendeződését is képes meggátolni, megelőzve ezzel a hatóanyag kilökődését [1, 19, 22].

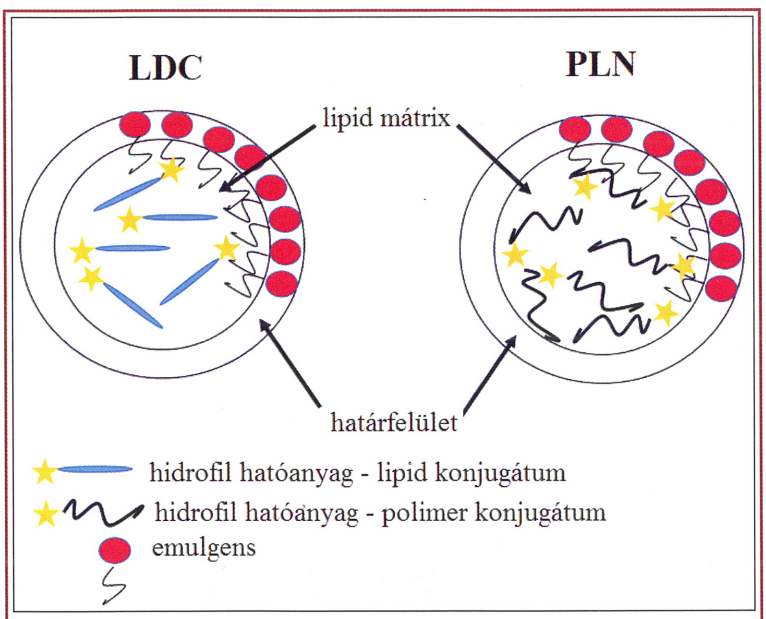

2. ábra: A lipid-hatóanyag konjugátum (LDC) és a polimer-lipid keverék (PLN) szerkezete

Lipid-hatóanyag konjugátum (LDC)

Hidrofil hatóanyagok hordozójaként fejlesztették ki a lipid-hatóanyag konjugátum típusú rendszereket (*Lipid Drug Conjugate*, LDC), amelyekbe csak nagyon kis koncentrációban, illetve szolubilizált formában lehet bevinni a hatóanyagot (*2. ábra*). Az alacsony bezárási kapacitás miatt csak olyan molekulák jöhetnek szóba, amelyek már igen kis koncentrációban is kifejtik hatásukat, mint pl. a proteinek és a peptidek. Ezek a molekulák rossz lipidoldékonyságuk miatt nehezen permeálódnak a gasztrointesztinális (GI) traktusból, így biológiai hasznosíthatóságuk is alacsony. Az LDC megnöveli a proteinek lipofilitását, ez által csökkenti a degradációt és javítja a permeációt. A konjugáció, kovalens kötés kialakításával (észter- vagy amid-képzéssel) valósítható meg.

Polimer-lipid keverék nanorészecske (PLN)

A polimer-lipid keverék nanorészecskéket (*Polimer-Lipid hybrid Nanoparticle,* PLN) olyan hidrofil hatóanyagoknál használják hordozóként, amelyek só formában is előfordulnak. Ebben az esetben is alacsony bezárási kapacitással kell számolnunk a molekulák töltöttsége miatt. Azonban egy ellentétes töltéssel rendelkező polimer alkalmazásával a hatóanyag-molekula komplexet képez, és ez a komplex már jobb eloszlást tesz lehetővé a lipid mátrixban (*2. ábra*).

A hatóanyag elhelyezkedése a lipid mátrixon belül

A hatóanyag lehetséges eloszlása a mátrixban háromféle lehet:

1. homogén,
2. kialakulhat egy lipidmag hatóanyag-tartalmú héjjal,
3. hatóanyagot tartalmazó mag lipidkéreggel (*3. ábra*).

Homogén eloszlásról beszélünk, amennyiben a hatóanyag molekulák a zsírsav láncok között, a lipid rétegek között, vagy a lipid mátrix hézagaiban helyezkednek el [1]. Ez a szerkezet általában a nagynyomású homogenizálás ún. „cold" (hideg) módszerével, vagy az ún. „hot" (meleg) módszer (lásd később) esetén nagyon lipofil hatóanyagok alkalmazásával készíthető [19]. Ha olyan szilárd lipideket választunk, amelyekben a molekulák alakja nagyon hasonló, a rendszer hatóanyag-befogadó képessége nagyon alacsony lesz, és a hatóanyag rövid időn belül kiválik a mátrixból

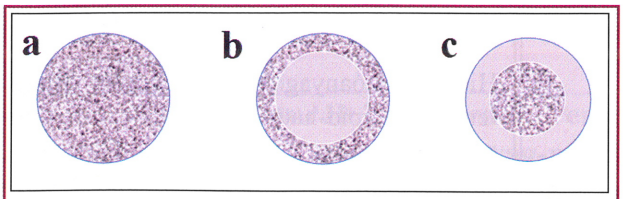

3. ábra: A hatóanyag eloszlása a lipid nanorészecskén belül: homogén hatóanyag eloszlás (a), lipidmag hatóanyagtartalmú héjjal (b), hatóanyagot tartalmazó mag lipidkéreggel (c)

a rendezettebb β módosulat kialakulása miatt. A második típusú NLC (hatóanyag felhalmozódás a héjban) akkor alakul ki, amikor a lipid kezd el megszilárdulni előbb a hűlési szakasz során, és egy hatóanyagmentes magot képez. A harmadik típusú NLC akkor alakul ki, amikor a hatóanyag kezd el precipitálódni; először és a nanorészecskék héját a később megszilárduló lipidek képezik. Ezen kívül bármelyik komponens (hatóanyag, lipidek, emulgens) kémiai tulajdonsága és koncentrációja nagyban befolyásolja az NLC szerkezetét. Az alkalmazott előállítási módszer („hot" vagy „cold" nagynyomású homogenizálás) is döntő szerepet játszik a hatóanyag nanorészecskén belüli elhelyezkedésében [24].

Formulálás

Preformulációs vizsgálatok

Az NLC rendszer előállítását az ún. „lipid screening" előzi meg, amelynek célja a hatóanyagnak (vagy biológiailag aktív komponensnek) leginkább megfelelő tulajdonságokkal rendelkező lipidek kiválasztása, koncentrációjának meghatározása. A vizsgálatok során a farmakont oldják több különböző megolvasztott szilárd lipidben, meghatározva azt a maximális koncentrációt, amely oldódik benne, majd a lipid/hatóanyag keverékeket szobahőmérsékletűre hűtik és vizsgálják, hogy kikristályosodik-e a farmakon az adott keverékből. Amennyiben az alkalmazott farmakon folyékony (pl.: olaj), a szilárd lipid/olaj elegyedését vizsgálják. Az organoleptikus vizsgálaton kívül differenciális pásztázó kalorimetriával (DSC), mikroszkópos és röntgendiffrakciós (XRD) vizsgálatok segítségével kimutathatók azok a hatóanyag-kristályok, amelyek nem oldódtak fel a közegben, illetve a nem inkorporálódott hatóanyagok a lipid mátrixban (pl. olaj alkalmazásakor) [10].

A megfelelő emulgens kiválasztása nedvesedési peremszög meghatározással történik. A nedvesedési peremszög egyenesen arányos a lipid-emulgens mátrix és a víz közötti határfelületi feszültséggel. Minél kisebb a két felület közötti határfelületi feszültség, annál nagyobb stabilitás várható a nanorészecskéktől [16, 25].

Az NLC rendszerek előállítása

Az NLC rendszerek előállítására számos módszer található az irodalomban [1, 26]:
- nagynyomású homogenizálás,
- mikroemulziós technológia,
- emulziós – oldószer elpárologtatásos módszer,
- emulziós – oldószer diffúziós módszer,

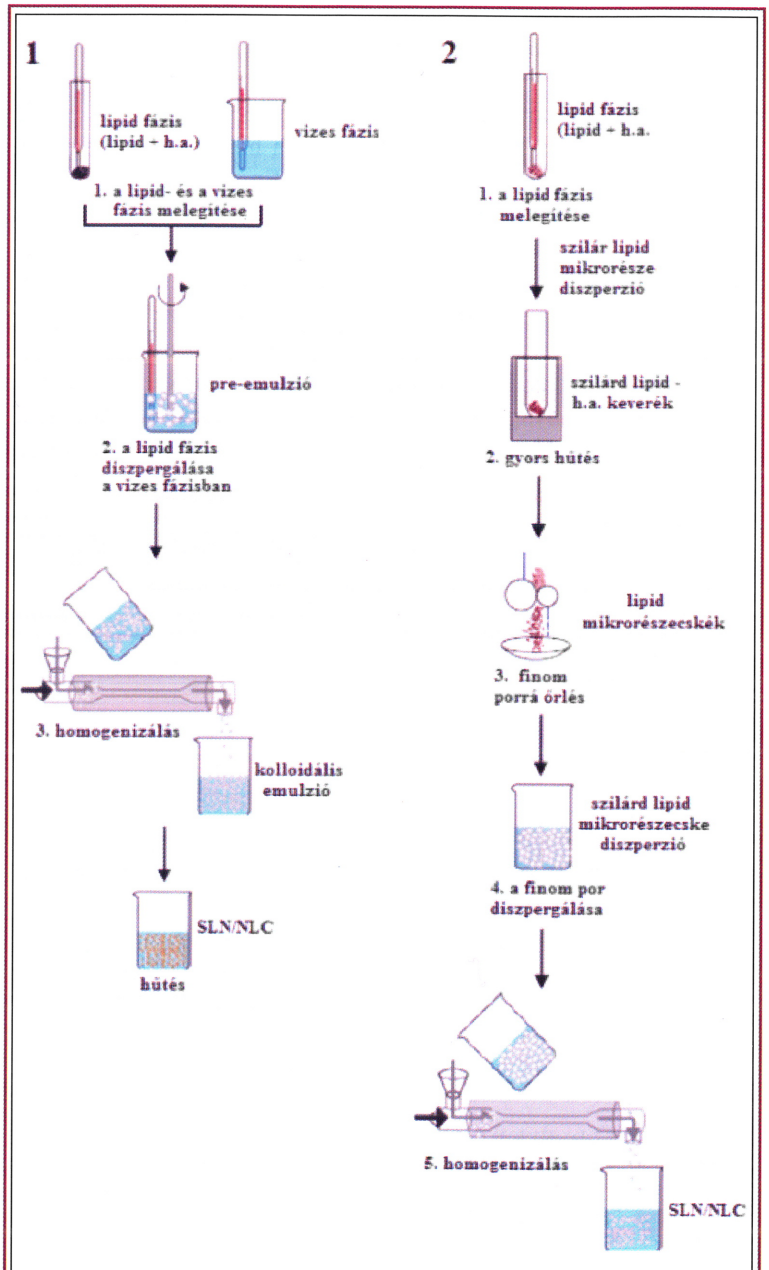

4. ábra: A nagynyomású homogenizálás lépései: „hot" módszer (1), „cold" módszer (2)

– oldószer injektálásos módszer (oldószer helyettesítő módszer),
– fázis inverziós technológia,
– összetett emulziós módszer,
– ultrahangos módszer, valamint
– membrán-összehúzó módszer.

A felsorolt módszerek közül a nagynyomású homogenizálást, illetve az ultrahangos módszert alkalmazzák a leggyakrabban, mivel egyszerűen léptéknövelhető, az előállítási idő rövid és nem igényli szerves oldószerek alkalmazását. Az alábbiakban a nagynyomású homogenizálásról lesz szó részletesebben.

Az ipar számos területén alkalmazzák a nagynyomású homogenizátorokat, így a gyógyszeriparban is, például parenterális emulziók előállítására. Az NLC rendszerek előállításának két lehetséges változata ismert: a már említett „hot" és „cold" technológia. Első lépésként mindkét esetben a hatóanyagot feloldják vagy diszpergálják a folyékony lipidek (olajok) és megolvasztott szilárd lipid keverékében.

A *forró módszer* esetében ezt a keveréket azonos hőmérsékletű emulgens tartalmú oldatban diszpergálják magas fordulatszámú keverés mellett. Fontos, hogy a kiválasztott hőmérséklet legalább 5-10 °C-kal az alkalmazott szilárd lipidek olvadáspontja felett legyen, hogy megakadályozzák ezen anyagok kifagyását a különböző felületeken (edény fala, keverő szára stb.). Az így készült emulzió a pre-emulzió, amelyet nagynyomású homogenizátorban keringetnek, általában ugyanezen a hőmérsékleten, több cikluson keresztül, megfelelő nyomást alkalmazva [1]. Ezt követően a rendszert lehűtik, melynek során a folyékony lipofil fázis megszilárdul, és kialakulnak a lipid nanorészecskék.

A *hideg módszer* alkalmazásakor második lépésként a hatóanyag és a megolvasztott lipid keverékét szobahőmérsékletűre hűtik. A megszilárdult keveréket őrlik, így lipid mikrorészecskéket kapnak. Ezeket a lipid mikrorészecskéket a hideg emulgens oldatával diszpergálják, és megkapják a hideg pre-szuszpenziót. Ezt a szuszpenziót nagynyomású homogenizátorban cirkuláltatják általában 5 – 10 cikluson keresztül, 1500 bar nyomáson. A két módszer lépéseit szemlélteti a ***4. ábra***.

NLC rendszerek jellemzése

Részecskeméret meghatározása

A stabilitás nyomon követése történhet a részecskeméret megoszlás időnkénti meghatározásával, hiszen az idő előrehaladtával a részecskék aggregálódhatnak, oldódhatnak, ami komoly problémát okozhat a tárolás során. A részecskeméret meghatározás az alábbi módszerek segítségével történhet:

– A *mikroszkópos vizsgálatok* legfőbb előnye a többi részecskeméretet vizsgáló módszerrel szemben az, hogy itt ténylegesen a részecske méretét határozzák meg (direkt technika), és nem egy olyan tulajdonságot vizsgálnak, amely függ a részecskemérettől (indirekt technika). E mellett a mikroszkóppal végzett vizsgálatok esetében nincsenek olyan faktorok, amelyek befolyásolhatnák a mérést (például hőmérséklet, refraktív index) [10]. Ezen kívül vizsgálható, hogy a diszperzió tartalmaz-e aggregátumokat, agglomerátumokat, amelyek jelenléte előállítási és/vagy stabilitási problémákra utalhat, valamint az esetleges kristályképződés folyamata is megfigyelhető.
– A *lézer diffraktometria* segítségével 10 nm és a 2000 μm tartományba eső részecskék méretét tudjuk detektálni [10]. A módszer segítségével meghatározhatóak a $d(0.1)$, $d(0.5)$, $d(0.9)$, és $d(0.99)$, valamint a Span értékek ***(1. egyenlet)***. A Span érték a részecskeméret eloszlás szélességét, vagyis a rendszer monodiszperzitását jellemzi, amely az alábbi képlettel számolható ki:

$$Span = \frac{d(0.9) - d(0.1)}{d(0.5)} \quad (1)$$

A $d(0.1)$, $d(0.5)$ és $d(0.9)$ értékek azok a mért részecskeméretek, amelyektől a vizsgált részecskék 10%, 50% és 90%-a kisebb.
– A *foton korrelációs spektroszkópia* egy széleskörűen alkalmazott módszer a részecskeméret meghatározására a szubmikronos tartományban. Segítségével meghatározható a részecskék átlagos mérete (Z-ave) és a polidiszperzitási index (PI) [11].
– A *zéta potenciál analízis* segítségével meghatározható a kolloid rendszerek elektrokinetikai potenciálja. Ez az érték összefüggésben áll a rendszer stabilitásával, ezért segítségével megjósolható annak fizikai stabilitása tárolás során [27]. Minél kisebb a rendszer zéta-potenciálja, az annál stabilabb. A –30 mV feletti értékek jó fizikai stabilitást jelentenek, az optimális a –60 mV elérése, amely az eltarthatóság szempontjából nagyon jó fizikai stabilitásra utal [11].

Kristályosság meghatározása

A kristályosság meghatározása alkalmas a hatóanyag mátrixon belüli elhelyezkedésének vizsgálatára (homogén, koncentrálódás a kéregben vagy a magban), a hatóanyag olvasztás során esetlegesen képződő amorf formáinak vizsgálatára, a bezárási hatékonyság, illetve annak a tárolás során történő ellenőrzésére. A kristályosság meghatározása történhet DSC, illetve XRD vizsgálatokkal.

Reológiai tulajdonságok

A diszperz rendszerek, így az NLC esetében is, a stabilitás vizsgálata fontos, amire a reológiai tulajdonságok változásaiból is lehet következtetni, mivel tárolás során az instabil rendszerekben történő részecskeaggregáció a reológiai paraméterek változásában nyilvánul meg.

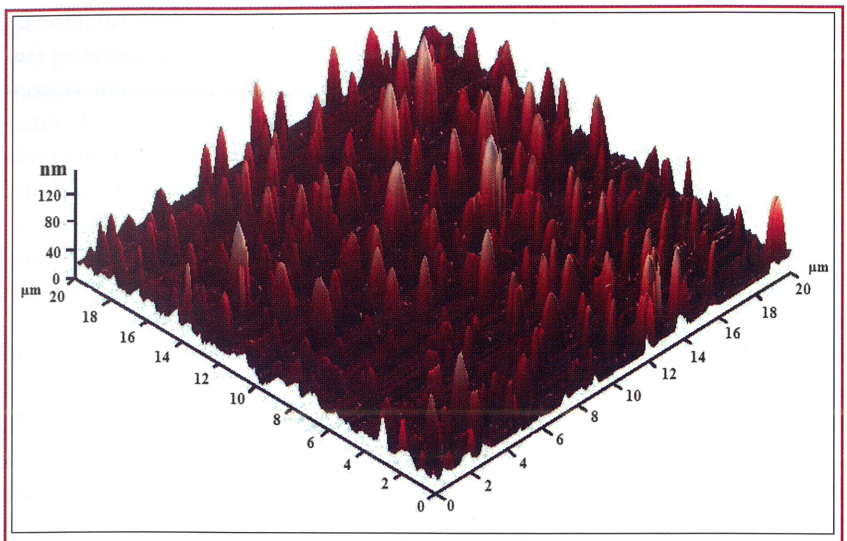

5. ábra: Ibuprofén tartalmú NLC minta 3D-s AFM felvétele

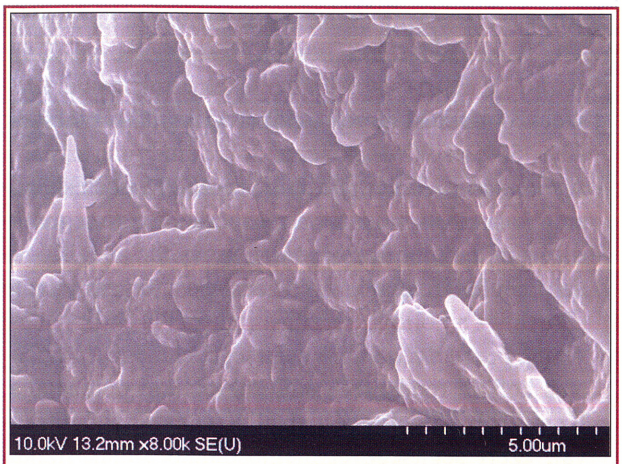

6. ábra: Beszárított ibuprofén tartalmú NLC minta SEM felvétele

Részecske morfológia

A morfológiai paraméterek meghatározása történhet atomerő mikroszkóp (AFM), pásztázó elektronmikroszkóp (SEM), vagy transzmissziós elektronmikroszkóp (TEM) segítségével.

– Az *atomerő mikroszkópos (AFM)* módszer segítségével információ nyerhető a részecskék méretéről és alakjáról. Nagy előnye, hogy a minták natív állapotukban, hidratáltan vizsgálhatóak, hiszen nincs szükség előkezelésre. A kontakt módban történő mérés alatt interakció alakulhat ki a tű és a minta között, ami a kép torzulásához vezethet. A nem-kontakt módban történő mérés felbontása körülbelül 2 nm méretig terjed. Az ***5. ábrán*** egy ibuprofén tartalmú NLC minta nem-kontakt módban készült 3D-s AFM-es képe látható. A felvétel egy 20x20 µm-es négyzetnyi területen készült (x és z tengely), a részecskeméretet a részecskék magasságából (y tengely) határozhatjuk meg [28].

– A *pásztázó elektronmikroszkópos (SEM) eljárást* alkalmazzák abban az esetben, ha információt szeretnének nyerni a részecskék alakjáról és méretéről (***6. ábra***). Vizes NLC diszperziók vizsgálata történhet olyan módon, hogy a minta egy részletét vékony karbon film mintatartóra viszik fel, 30 percig száradni hagyják, majd a mikroszkóp vákuumoszlopába helyezik, onnan pedig kiszívják a levegőt [10].

– A *transzmissziós elektronmikroszkópos (TEM)* mérések során a kolloid rendszerek mikrostruktúrái megfigyelhetőek az elektronmikroszkóp nagy nagyításának köszönhetően. A vizes alapú minták az elektronmikroszkóp erős vákuumjában elveszítik víztartalmukat, és mikrostruktúrájuk megváltozik. Ezért ebben az esetben egy speciális minta-előkészítést kell végezni. Ez az ún. fagyasztva töréses módszer, amelynek során a minta lenyomata látható a TEM felvételen [23, 29].

Bezárási hatékonyság meghatározása

Az SLN rendszerek esetében az egyik lehetséges probléma, hogy a tárolás során rendezett kristályszerkezet alakul ki, amely kilökheti magából az inkorporált hatóanyagot. Az NLC rendszereket épp ezért fejlesztették ki, hogy elkerüljék a hatóanyag kilökődését, valamint megnöveljék a mátrix hatóanyag felvevő kapacitását. Szerkezetük alapján három NLC típust különböztetnek meg:

a) hézagos típus,
b) amorf típus,
c) összetett típus.

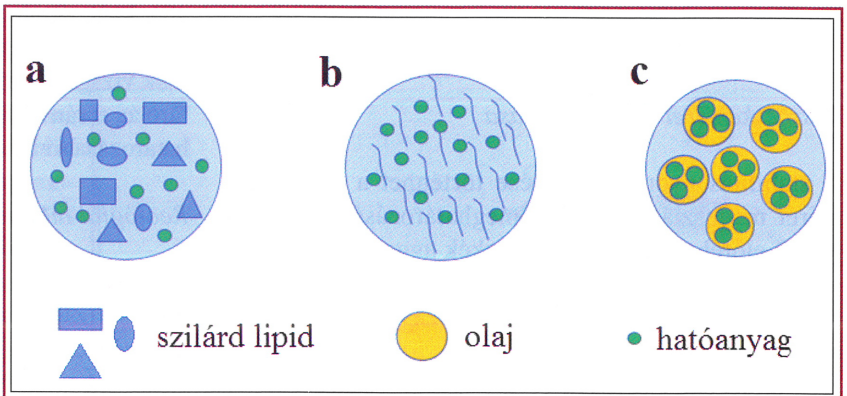

7. ábra: Az NLC három típusa: hézagos (a), amorf (b), összetett (c)

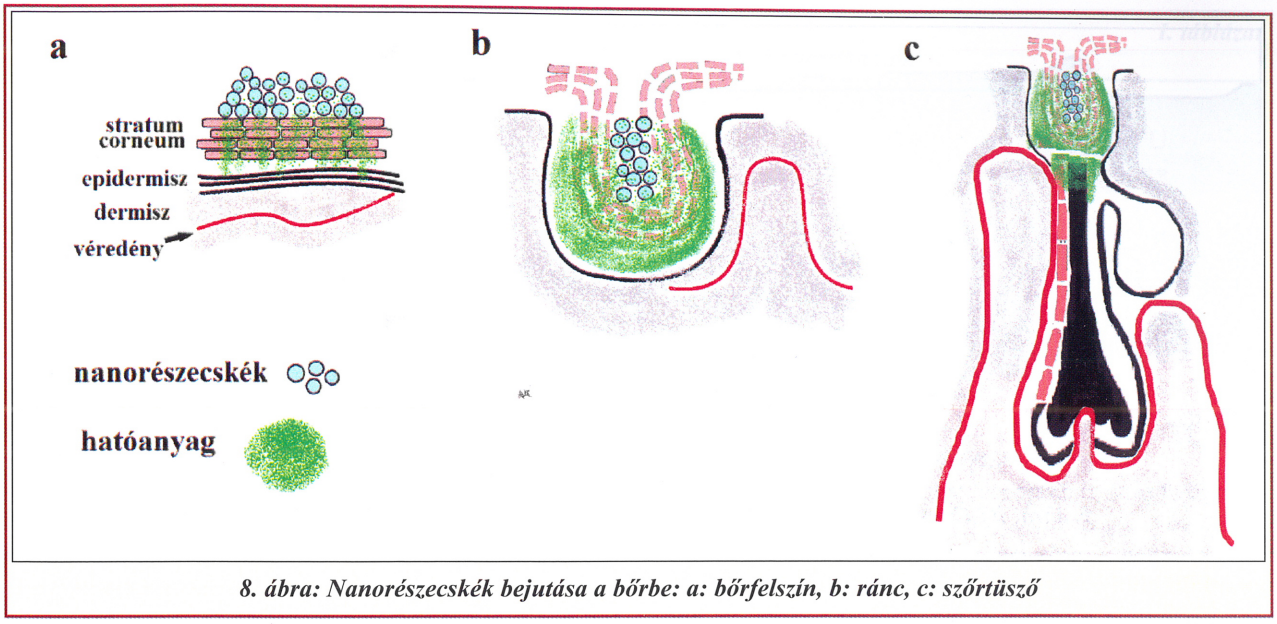

8. ábra: Nanorészecskék bejutása a bőrbe: a: bőrfelszín, b: ránc, c: szőrtüsző

A hézagos típus lényege, hogy különböző alakú és méretű lipideket alkalmaznak, így nagyobbak lesznek a hézagok, amelyek egyrészt megakadályozzák a rendezett kristályszerkezet kialakulását, másrészt a hatóanyag is „elfér". Az amorf típus esetén a lipid mátrix szilárd, de nem kristályos (amorf állapot), így megelőzhető a rendezett kristályszerkezet kialakulása. Amorf állapot alakítható ki speciális lipidek keverékéből (pl. hidroxioktakozanil-hidroxisztearát és izopropil-mirisztát elegyéből). Az összetett típus hasonlít a v/o/v emulziókra, amely ebben az esetben olaj a zsírban – zsír a vízben diszperzió. A szilárd lipid mátrix apró olajcseppeket tartalmaz (*7. ábra*) [19].

A mátrix tulajdonságai mellett a bezárni kívánt hatóanyag lipofilitása is befolyásolhatja a bezárási kapacitást. Minél nagyobb a hatóanyag lipofilitása, annál nagyobb lesz a bezárási kapacitás [10].

Az ún. bezárási hatékonyság (***Entrapment Efficiency,*** EE) megmutatja egy eljárás hatékonyságát, hogy az milyen mértékben képes a hatóanyagot inkorporálni a gyógyszerhordozó rendszerbe [30, 31]. A vizsgálat történhet direkt, vagy indirekt módszerrel. Direkt módszer esetén a szilárd lipid fázisban történik a hatóanyag meghatározása [11]. Gyakoribb az indirekt módszer, amely során a vizes fázisban lévő hatóanyagot mutatják ki, és ebből következtetnek a szilárd lipidbe zárt hatóanyag mennyiségére. A vizes fázist általában ultraszűréses centrifugálással választják le a lipid fázistól, és a bezárási hatékonyságot a (2) képlettel határozzák meg [32]:

$$EE = \left(1 - \frac{\text{bemért hatóanyag-szabad hatóanyag}}{\text{bemért hatóanyag}}\right) \cdot 100\% \quad (2)$$

A másik fontos mutató, az ún. hatóanyaggal való töltöttség (***Drug Loading,*** DL) azt mutatja meg, hogy mennyi hatóanyag található a mátrixban [31] (lásd: (3) képlet):

$$DL = \left(\frac{\text{kezdeti hatóanyagmennyiség-szabad hatóanyag mennyisége}}{\text{lipid mátrix tömege}}\right) \cdot 100\% \quad (3)$$

Biofarmáciai jellemzők

A szilárd lipid nanorészecskék kedvező hatásaik révén szinte az összes beviteli kapun keresztül lehetőséget biztosítanak a hatóanyag bevitelére. Gyors hatóanyag felszabadulás, valamint nyújtott hatású kioldódás egyaránt tervezhető szilárd lipid nanorészecskékkel attól függően, hogy a hatóanyag hol helyezkedik el a rendszerben.

A hatóanyag elhelyezkedése a nanorészecskén belül függ a szilárd és folyékony lipidek tulajdonságaitól, a hatóanyagtól, az alkalmazott tenzidektől és az előállítási technológiától is. A hatóanyag felszabadulás általában két lépésben történik a nanorészecskékből: egy kezdeti, gyors hatóanyagleadást (ún. *„burst release"*) egy lassabb, elnyújtott szakasz követ. A burst release magasabb előállítási hőmérséklet esetén kifejezettebb a „hot" módszer esetében, a „cold" technológia alkalmazásakor pedig szinte teljesen hiányzik. A „burst release" mértékét az emulgenskoncentráció is nagyban befolyásolja - minél több tenzidet alkalmaznak, az annál kifejezettebb lesz. Akkor is *„burst release"*-re kell számítani, ha a hatóanyag vízben is oldódik valamilyen mértékben [19].

Az NLC és a bőr

A bőr széleskörűen alkalmazott beviteli kapuja a lokális és szisztémás készítményeknek, és lehetséges útvonalul szolgálhat a nanorészecskéknek is. A stratum corneum (SC) képezi a bőr legfőbb fizikai barrierét,

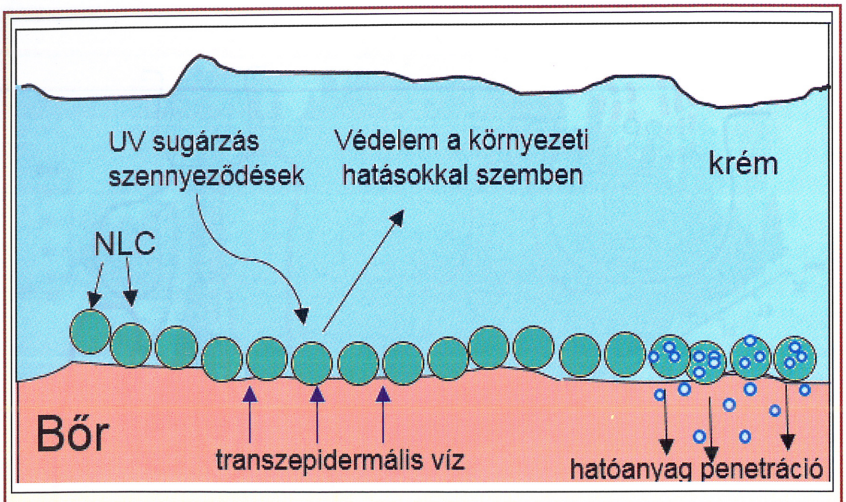

9. ábra: NLC rendszerek bőrre kifejtett hatása

így a különböző anyagok bőrbe jutásának a SC-on történő diffúziója a sebesség-meghatározó lépés. A bőrben ezen felül további függelékek találhatóak, mint a szőrtüszők a hozzájuk kapcsolódó faggyúmirigyekkel és a verejtékmirigyek. A SC-on keresztüli transzport nagyrészt passzív diffúzióval történik, amely lehet transzcelluláris, intercelluláris, illetve a transzport lehetséges a bőrfüggeléken keresztül is ***(8. ábra)*** [20].

Az NLC rendszerek számos előnyös tulajdonságát írták le bőrön való alkalmazáskor. A lipid nanorészecskék filmet képeznek a bőr felszínén, ezzel is segítve a bőr természetes lipid filmjének helyreállítását. A hatóanyagmentes NLC képes megvédeni a bőrt a káros környezeti hatásokkal szemben (UV-sugárzás, szennyeződések). A hatóanyag tartalmú NLC-k pedig képesek kémiailag stabilizálni az inkorporált molekulát (pl. fotodegradáció, oxidáció), és mélyebb bőrpentráció érhető el velük, mivel közvetlen kontaktus alakul ki a SC lipid komponenseivel (***9. ábra***) [1, 19, 21].

Az NLC rendszerek okklúzív sajátságúak, mivel a kisméretű részecskék adhezív tulajdonsággal rendelkeznek. Az adhézió mértéke fordítottan arányos a részecskék méretével. Az NLC részecskék a bőrre jutatva filmet képeznek, ezzel csökkentve a transzepidermális vízvesztést. Az okklúzív hatás alacsony olvadáspontú lipidek alkalmazásakor, erősen kristályos anyagok esetén és kis részecskeméret esetén a legkifejezettebb. Ha mikroméretű részecskéket visznek fel a bőrre, a részecskék közötti pórusok mérete relatív nagy lesz, amely hidrodinamikailag kedvez a víz párolgásának. Ezzel szemben a nanorészecskék közötti pórusok sokkal kisebbek, amelyeken keresztül a vízpárolgás hidrodinamikailag kedvezőtlen (***10.*** ábra). A víz kondenzálódik ezekben a nanoméretű pórusokban, így az NLC-film vízmegtartó sajátságokkal rendelkezik, amely elősegíti a bőr hidratáltságának megtartását, ezzel fokozva a hatóanyag-penetrációt is [19].

Az NLC rendszerekből három különböző módszer segítségével állítható elő dermális felhasználásra alkalmas forma:

a) Egy tradicionális készítmény víztartalmának egy részét lecserélik vizes lipid nanorészecskéket tartalmazó diszperzióra.
b) A lipid nanorészecskék vizes diszperziójának gélképző polimerrel történő gélesítése.
c) In situ készítéssel a koncentrált nano lipid diszperzió lehűtése után alakítják ki a félszilárd vázszerkezetet [19].

Nagyon fontos szempont, hogy a felhasznált anyagok jó bőrhidratációt eredményezzenek, de ne irritálják a bőrt, ne okozzák a SC barrier funkciójának tartós csökkenését. A barrier funkció vizsgálatára alkalmasak: a transzepidermális vízvesztés mérése Tewaméterrel, a TEWL (*transepidermal water loss*) érték meghatározása, míg bőrhidratáció mérésére corneométer használható [30, 33].

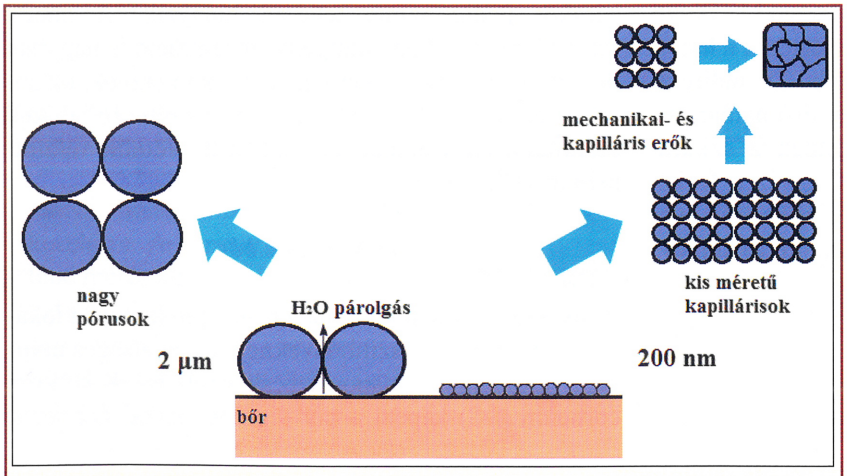

10. ábra: A részecskeméret és a transzepidermális vízvesztés kapcsolata

SLN és NLC a kozmetikai iparban

A szilárd lipid nanorészecskék és nanostruktúrált lipid hordozók dermális alkalmazásának jelentőségét mutatja, hogy számos kozmetikai készítmény van forgalomban, amely SLN/NLC rendszereket tartalmaz (***I. táblázat***) [1]. Hatóanyagot tartalmazó, gyógyszerként törzskönyvezett SLN/NLC tartalmú készítmény ismereteink szerint még nincs forgalomban, de számos hatóanyag tartalmú szilárd lipid nanorészecskével folynak kutatások.

I. táblázat

Forgalomban lévő SLN/NLC tartalmú kozmetikumok

Készítmény neve	Gyártó/forgalmazó	Piaci bevezetés	Aktív anyagok
Cutanova Cream NanoRepair Q 10	Dr. Rimpler	2005/10	Q 10, polipeptid, hibiszkusz kivonat, gyömbér kivonat, ketóz
Intensive Serum NanoRepair Q 10		2005/10	Q 10, polipeptid, mafane kivonat
Cutanova Cream NanoVital Q 10		2006/06	Q 10, TiO_2, polipeptid, urzolsav, oleanolsav, nanpraforgómag kivonat
SURMER Creme Legere Nano-Protection	Isabelle Lancray	2006/11	kókuszdió olaj, Monoi Tiare Tahiti®, kókusztej kivonat, vad gyömbér, noni kivonat
SURMER Creme Riche Nano-Restructurante			kókuszdió olaj, Monoi Tiare Tahiti®, kókusztej kivonat, vad indigó,pszeudopeptid, tamanu fa kivonat
URMER Elixir du Beaute Nano-Vitalisant			kókuszdió olaj, Monoi Tiare Tahiti®, pszeudopeptid kókusztej kivonat, vad gyömbér, noni kivonat
SURMER Masque Creme Nano-Hydratant			kókuszdió olaj, Monoi Tiare Tahiti®, kókusztej kivonat, vad indigó,pszeudopeptid, tamanu fa kivonat
SURMER Creme Contour Des Yeux Nano-Remodelante		2008/03	kukuidió olaj, Monoi Tiare Tahiti®, pszeudopeptid, hidrolizált búza protein
NanoLipid Restore	Chemisches Laboratorium Dr. Kurt Richter, CLR Berlin	2006/04	Q 10, omega-3, omega-6 zsírsavak
Nanolipid Q10		2006/07	Q 10
Nanolipid Basic		2006/07	hatóanyagmentes NLC
Nanolipid Repair		2007/02	feketeribiszke mag olaj, manuka olaj
SuperVital Cream	Amore Pacific	2006/09 2007/01	Q 10, omega-3, omega-6 zsírsavak
SuperVital Serum			
SuperVital Eye cream			
SuperVital Extra moist softener			
SuperVital Extra moist emulsion			
NLC Deep Effect Eye Serum	Beate Johnen	2006/12	Q10, oligoszacharidok
NLC Deep Effect Repair cream		2006/12	Q10, TiO_2, oligoszacharidok
NLC Deep Effect Reconstruction Cream		12/2006	Q10, acetil-hexapeptid-3, mikronizált növényi kollagén, oligoszacharidok poliszacharid mátrixban
NLC Deep Effect Reconstruction Serum			
Regenerationscreme Intensiv	Scholl	2007/06	makadám dió mag olaj, avokádó olaj, karbamid, feketeribiszke mag olaj
Swiss Cellular White Illuminating Exe Essence Swiss Cellular White Intensive Ampoules	La prairie	2007/01	glikoproteinek, gyömbér kivonat, mezei zsurló kivonat, zöld tealevél kivonat, háromszínű árvácska kivonat
Olivenöl Anti Falten Pflegekonzentrat	Dr. Theiss	2008/02	olivaolaj, pantenol, arabmézga, E-vitamin
Olivenöl Augenpflegebalsam		2008/02	olivaolaj, mandula olaj, hidrolizált tejprotein, E-vitamin, koffein, aranygyökér kivonat

Nanotoxikológiai megfontolások

Habár a levegőben található lebegő nanorészecskékkel az emberiség már az evolúció kezdetén találkozott, és azóta is ki van téve a hatásainak, nanotoxikológiával csak az elmúlt néhány évtized során kezdett el foglalkozni a tudomány. A nano mérettartományba eső részecskék mennyisége drasztikusan megugrott az ipari forradalom idején (a belső égésű motorok és a különböző erőművek megjelenése), ezek nagyrészt a levegőben jelentek meg szennyezőként. A nanotechnológia megjelenésével a szándékosan előállított nanorészecskék is bővítették ezt a palettát, amelyek környezetre és az emberi szervezetre kifejtett hosszú távú hatásairól

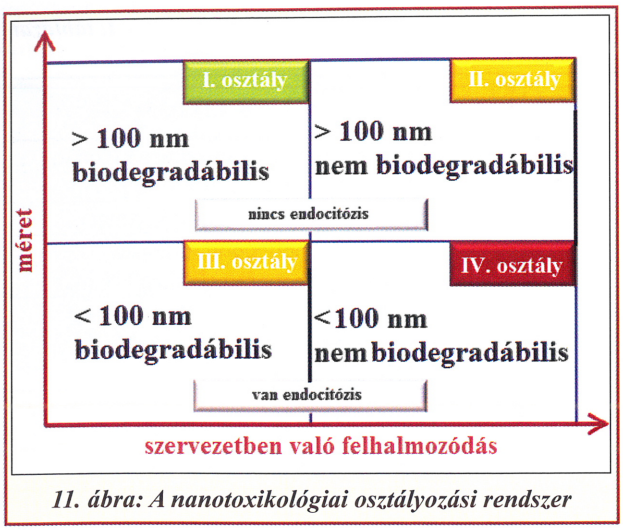

11. ábra: A nanotoxikológiai osztályozási rendszer

még hiányosak az ismereteink [34]. A kozmetikai- és az élelmiszeripar után a gyógyszeriparban is egyre nagyobb az igény olyan készítményt regisztrálni, amely részben vagy teljes egészében nanorészecskéket tartalmaz, hiszen számos alkalommal bizonyították előnyös tulajdonságaikat különböző megbetegedések terápiájában. Fontos azonban tudni, hogy milyen mellékhatásai lehetnek a nanorészecskéknek, felszaporodhatnak-e a szervezetben, és válthatnak-e ki immunválaszt kis méretüknél fogva. A kérdés a jogalkotókat és a kutatókat egyaránt foglalkoztatja. A biofarmáciai osztályozási rendszerhez (*Biopharmaceutical Classification System,* BCS) hasonlóan megalkottak egy ún. nanotoxikológiai osztályozási rendszert (*Nanotoxicological Classification System,* NCS), amely a részecskék mérete, és biodegradábilitása alapján csoportosítja a nanorészecskéket (***11. ábra***).

Mérettől függően az NLC rendszerek az első, illetve a harmadik osztályba sorolhatóak. A részecskeméret tartomány beállítása a gyógyszertechnológus feladata, kiválasztása pedig a beviteli kaputól függ. A nanorészecskék közül [35] irodalmi adatok alapján a bőrbe kizárólag a 10 nm-nél kisebb nanorészecskék képesek bejutni, az ennél nagyobb méretű részecskék felszaporodnak a bőrfüggelékekben (elsősorban a szőrtüszőkben), és ott adják le a hatóanyagot. Szignifikánsan növekszik a nanorészecskék bőrpenetrációja sérült bőrbe, illetve bizonyos bőrbetegségek esetén [20]. Mindezeket figyelembe véve megállapítható, hogy az NLC rendszerek nanotoxikológiai szempontból biztonságosnak tekinthető gyógyszerhordozó rendszerek.

Összefoglalás

Az irodalmi összefoglaló munkában a lipid nanorészecskék (LNP) formulálási szempontjait mutattuk be. Kiemeltük a nanostruktúrált lipid hordozókat (NLC), mint új, dermális terápiára igen alkalmas gyógyszerhordozó rendszereket, hiszen számos előnyös tulajdonságukat írták le bőrön való alkalmazáskor. Az NLC rendszerek filmet képeznek a bőr felszínén, így elősegítik a bőr természetes lipid filmjének helyreállítását. Hidratálják a bőrt, csökkentve a transzepidermális vízvesztést. A hatóanyagmentes NLC már magában is hozzájárul a bőr UV-sugárzással szembeni védelméhez. Az NLC rendszerek megfelelő formulálásával megoldható a hatóanyag védelme, kémiailag stabilizálják az inkorporált molekulát (pl. fotodegradáció, oxidáció), és mélyebb bőrpenetrációt tesznek lehetővé, mivel közvetlen kontaktusba lépnek a SC lipid komponenseivel.

A lipid nanorészecskék alkalmasak növelni a vízben rosszul oldódó hatóanyagok oldékonyságát, így csökkenthető a terápiás dózis, ezáltal a mellékhatások előfordulása is, továbbá formulálásukkal kontrollált hatóanyag-felszabadulás tervezhető. Számos előnyös tulajdonságuknak köszönhetően az NLC rendszerek alkalmasak lehetnek innovatív dermális készítmények formulálására.

IRODALOM

1. *Pardeike, J., Hommoss, A., Müller, R.H.*: Int J Pharm *366*(1–2), 170-184 (*2009*). – 2. *Wissing, S.A., Kayser, O., Müller, R.H.*: *Solid lipid nanoparticles for parenteral drug delivery.* Adv Drug Deliver Rev, *56*(9), 1257-1272 (*2004*). – 3. *Liu, D., et al.*: Colloid Surface B: Biointerfaces, *85*(2), 262-269 (*2011*). – 4. *Joshi, M.D., Müller, R.H.*: Eur J Pharm Biopharm *71*(2), 161-172 (*2009*). – 5. *Puglia, C., et al.*: Eur J Pharm Biopharm *81*(2), 288-293 (*2012*). – 6. *Ranpise, N.S., Korabu, S.S., Ghodake, V.N.*: Colloid Surface B: Biointerfaces, *116*, 81-87 (*2014*). – 7. *Zhuang, C.-Y.*, et al.: Int J Pharm, *394*(1–2), 179-185 (*2010*). – 8. *Patil-Gadhe, A., Pokharkar, V.*: Eur J Pharm Biopharm *88*(1), 160-168 (*2014*). – 9. *Khurana, S., Bedi, P.M., Jain, N.K.*: Chem Phys Lipids, *175-176*, 65-72 (*2013*). – 10. *Amman, H.*: Nanostructured lipid carriers (NLC) in dermal and personal care formulations, in Department of Biology, Chemistry and Pharmacy. 2009, Free University Berlin: Berlin. p. 202. – 11. *Teeranachaideekul, V., et al.*: Eur J Pharm Biopharm, *67*(1), 141-8 (*2007*). – 12. *Han, F., et al.*: Int J Pharm *439*(1–2), 349-357 (*2012*). – 13. *Zhang, W., et al.*: Int J Pharm *471*(1–2), 118-126 (*2014*). – 14. *Gonzalez-Mira, E., et al.*: Colloid Surface B: Biointerfaces, *81*(2), 412-421 (*2010*). – 15. *Araújo, J., et al.*: Int J Pharm *393*(1–2), 168-176 (*2010*). – 16. *Pardeike, J., et al.*: Int J Pharm *419*(1–2), 329-338 (*2011*). – 17. *Weber, S., Zimmer, A., Pardeike, J.*: Eur J Pharm Biopharm *86*(1), 7-22 (*2014*). – 18. *Pastor, M., et al.*: Int J Pharm *477*(1–2), 485-494 (*2014*). – 19. *Müller, R.H., Radtke, M., Wissing, S.A.*: Adv Drug Deliver Rev *54*(Suppl.) S131-S155 (*2002*). – 20. *Prow, T.W., et al.*: Adv Drug Deliver Rev *63*(6), 470-491 (*2011*). – 21. *Müller, R.H., Staufenbiel, S., Keck, C.M.*: Chemistry, *9*, 2 (*2014*). – 22. *Shah, R., et al.*: Lipid Nanoparticles: Production, Characterization and Stability. Springer, 2015. – 23. Müller-Goymann, C.C.: Eur J Pharm Biopharm *58*(2), 343-356 (*2004*). – 24. *Schäfer-Korting, M., Mehnert, W., Korting, H.-C.*: Adv Drug Deliver Rev *59*(6), 427-443 (*2007*). – 25. *Sütő, B., et al.*: *Optimization and design of an Ibuprofen-loaded nanostructured lipid carrier with a 2^3 full factorial design.* Chemical Engineering Research and Design,

2015. – 26. *Silva, A.C., et al.*: Colloid Surface B: Biointerfaces *86*(1), 158-165 (*2011*). – 27. *Pardeike, J.*: Nanosuspensions and nanostructured lipid carriers for dermal application, in Department of Biology, Chemistry and Pharmacy. 2009, Free university of Berlin: Berlin. p. 258. – 28. *Dubes, A., et al.*: Eur J Pharm Biopharm *55*(3), 279-282 (*2003*). – 29. *Esposito, E., et al.*: Mater Sci Engineer C, *48*, 328-336 (*2015*). – 30. *Kwon*, M.M.d.V.P.A.G.S., *Nanotechnology in Drug Delivery*. 2009, New York: Springer. – 31. *Abbasalipurkabir, R., Salehzadeh, A., Abdullah, R.*: Pharmaceutical Technology *35*(4), 74-79 (*2011*). – 32. *Souto, E.B., et al.*: Int J Pharm *278*(1), 71-77 (*2004*). – 33. *Wissing, S.A.*, Müller, *R.H.*: Eur J Pharm Biopharm *56*(1), p. 67-72 (*2003*). – 34. *Oberdorster, G., Oberdorster, E., Oberdorster, J.*: Environ Health Persp *113*(7), 823-39 (*2005*). – 35. *Keck, C.M.*, Müller, *R.H.*: Eur J Pharm Biopharm *84*(3), 445-8 (*2013*).

SÜTŐ B, BERKÓ SZ, CSÁNYI E: ***Application of lipid carrier systems to increase the drug penetration through the skin***

The aim of this work is to introduce lipid nanoparticles (LNPs) as potential drug delivery systems, regarding to their formulation and characterization. The second generation, nanostructured lipid carriers (NLCs) has been highlighted, as a novel drug delivery system suitable for dermal therapy, since these nanoparticles possess numerous advantages applied to the skin. The dermal use of NLC systems offers a number of advantages, such as physical stability of the applied topical formulations, enhancement of the chemical stability of the incorporated active pharmaceutical agents, improved dermal bioavailability, the skin targeting of the drugs, and film formation on the skin, accompanied by the in vivo controlled occlusion and skin hydration. The UV-reflecting properties (e.g. possible application of these carriers in sunscreens with the aim to increase their protective effect against UV light) and the possibility of the modulation of API release into the skin have also been reported.

Lipid nanoparticles avoid the disadvantages of other colloidal carriers and possess their advantages, such as the possibility of controlled drug release and drug targeting, increased drug stability, high drug payload, incorporation of both lipophilic and hydrophilic drugs, no biotoxicity of the carrier, avoidance of organic solvents and no problems with respect to large scale production and sterilization. Due to their numerous advantages, it can be concluded that NLCs are suitable drug delivery systems in the dermal therapy.

Szegedi Tudományegyetem, Gyógyszertechnológiai Intézet, Eötvös utca 6., 6720 Szeged, Magyarország

IV.

International Journal of Nanomedicine

Dovepress

open access to scientific and medical research

Open Access Full Text Article

ORIGINAL RESEARCH

Development of ibuprofen-loaded nanostructured lipid carrier-based gels: characterization and investigation of in vitro and in vivo penetration through the skin

Blanka Sütő[1]
Szilvia Berkó[1]
Gábor Kozma[2]
Ákos Kukovecz[2,3]
Mária Budai-Szűcs[1]
Gábor Erős[4,5]
Lajos Kemény[4]
Anita Sztojkov-Ivanov[6]
Róbert Gáspár[6]
Erzsébet Csányi[1]

[1]Department of Pharmaceutical Technology, Faculty of Pharmacy, [2]Department of Applied and Environmental Chemistry, [3]MTA-SZTE "Lendület" Porous Nanocomposites Research Group, [4]Department of Dermatology and Allergology, [5]Department of Oral Biology and Experimental Dental Research, [6]Department of Pharmacodynamics and Biopharmacy, University of Szeged, Szeged, Hungary

Correspondence: Erzsébet Csányi
Department of Pharmaceutical Technology, Faculty of Pharmacy, University of Szeged, Eötvös u. 6, H-6720 Szeged, Hungary
Tel +36 62 545 573
Fax +36 62 545 571
Email csanyi@pharm.u-szeged.hu

Abstract: An ibuprofen-loaded nanostructured lipid carrier (IBU-NLC) was developed for enhanced skin penetration to improve the treatment of osteoarthritis and other musculoskeletal diseases. The mean particle size was 106 nm, with a spherical morphology, a smooth surface, and a zeta potential of −18.4 mV. X-ray diffraction studies revealed the amorphous state of the lipid matrix. Both Raman spectroscopy and Fourier transformation infrared analysis indicated no major shifts in the spectra of the formulations, which suggest rapid drug dissolution from the nanoparticles. The drug loading was 9.85%, and the entrapment efficiency was 98.51%. In vitro release of the NLC dispersion, in vitro permeation, and in vivo animal studies of IBU-NLC gel all confirmed that the permeation of IBU was significantly better than that of a reference after 6 hours. In conclusion, IBU-NLC gel is of great potential to enhance drug permeation through the skin and hence the efficacy of the treatment of chronic joint inflammation.

Keywords: ibuprofen, nanostructured lipid carriers, skin penetration, SKH-1 hairless mice, osteoarthritis

Introduction

Osteoarthritis (OA), one the most prevalent chronic joint diseases, is accompanied by considerable pain.[1,2] With the current aging of the population and the epidemic of obesity, the incidence of OA is rising. The main clinical features, the pain and the loss of function, lead to treatment by nonpharmacological, pharmacological, and surgical approaches.[1] In a study involving 3,906 patients above the age of 55 years, 67% of the women and 54.8% of the men suffered from radiographic OA in at least one hand joint.[1,3] Another study confirmed that some 40% of the total population aged >70 years suffer from OA, the most common form of arthritis.[2,4] Since pain and inflammation are among the most important causes of a decline in the life quality, the primary aim of the currently available treatments is to relieve these. The American College of Rheumatology has published recommendations for the use of nonpharmacologic and pharmacologic therapy in OA. The use of nonsteroidal anti-inflammatory drugs is highly recommended.[5]

Ibuprofen (IBU) is a nonsteroidal anti-inflammatory drug that was introduced in the 1960s to replace acetylsalicylic acid in the treatment of rheumatoid arthritis, providing a more efficacious therapy and proving more tolerable for the patients. It is administered orally or topically in the form of gels, creams, and ointments. The advantages of its local application over their systemic use include the avoidance of

adverse events (bleeding and possible ulceration of the gastric mucosa) and the high concentration of the drug at the site where it is needed. The drug, usually administered in its racemic form,[6] is relatively lipophilic (log *P*=4.0) with low water solubility (21 mg/L at 25°C).[6,7] The characteristics of the permeation of IBU through the human skin have been reported by a number of research groups.[8–13] Earlier studies revealed that the topical therapeutic effectiveness of a drug is a function both of its penetration through the skin and of its potency.[7] IBU is less potent than diclofenac, for example, but the higher flux of IBU through the skin means that it is a better candidate for topical delivery, although it is still difficult to achieve its effective permeation by transdermal delivery.[14] The aforementioned physicochemical properties of IBU have hampered the preparation of a formulation satisfying the requirements of a long-lasting treatment for a chronic disease such as OA.

Nanostructured lipid carriers (NLCs) may serve as a solution to overcome the limitations of the dermal permeation of IBU. This drug delivery system offers numerous advantages for topical application.[15–19] NLCs can comprise physiological and biodegradable lipids, which were earlier reported to possess low systemic toxicity and low cytotoxicity.[20] The small size of the lipid nanoparticles ensures close contact between the lipid particles and the lipid bilayer of the stratum corneum, resulting in the penetration of an increased amount of drug into the skin. In consequence of their solid lipid matrix, controlled release is possible from these carriers. This becomes important when prolonged release of the drug is required. Burst release of the drug incorporated in the NLC system may also be achieved.[21] As a result of the film formation that occurs after topical application, occlusive properties have also been reported for NLC formulations,[22,23] and these favor further enhanced penetration through the dermal layers.

The aim of the present study was to develop a hydrogel based on an IBU-loaded NLC (IBU-NLC) system, with improved drug release properties (for the potential treatment of OA or musculoskeletal disorders) as compared with those of a traditional IBU gel formulation and to characterize this hydrogel by means of techniques such as X-ray diffraction (XRD), atomic force microscopy (AFM), Raman spectroscopy, and Fourier transformation infrared (FT-IR) spectroscopy in order to attain a better understanding of its properties.

Materials and methods

Materials

IBU was provided by PannonPharma Ltd. (Pécsvárad, Hungary), Witepsol E85 and Miglyol 812 were gifts by Sasol GmbH (Hamburg, Germany), and Lutrol F68 was kindly supplied by BASF SE Chemtrade GmbH (Ludwigshafen, Germany). Acetonitrile (high-performance liquid chromatography [HPLC] grade), K_2HPO_4, KH_2PO_4, and H_3PO_4 (85%) (analytical grade) were purchased from VWR Int Ltd (Radnor, PA, USA). Carbopol 971P NF was supplied by Azelis Ltd (Budapest, Hungary). Macrogol 400 was obtained from Hungaropharma Ltd (Budapest, Hungary). Purified water (HPLC grade) produced with a TKA Smart2Pure system (TKA GmbH, Niederelbert, Germany) was used to prepare all the formulations.

Preparation of the samples

The NLC formulations were prepared by a hot high-pressure homogenization method,[17,18,24,25] using an Emulsiflex C-3 High Pressure Homogenizer (Avestin Europe GmbH, Mannheim, Germany). Briefly, 1% IBU was dissolved in the mixture of the solid and liquid lipids (Witepsol E85 and Miglyol 812, ratio 7:3) at ~10°C above the melting point of the solid lipid. The surfactant, Lutrol F68, was dissolved in purified water at the same temperature. The aqueous phase was added to the lipid phase, and the mixture was stirred with a Heidolph DIAX 900 homogenizer (Heidolph Instruments GmbH & Co. KG, Schwabach, Germany) for 1 minute at 12,500 rpm. The pre-emulsion was subjected to high-pressure homogenization, applying five cycles at 600 bar and 65°C. The hot oil-in-water pre-emulsion was cooled in an ice bath to recrystallize the lipid and form the NLC.

An IBU suspension containing 1% of IBU dispersed in purified water was prepared as a reference for in vitro diffusion studies of IBU-NLC. For the in vitro penetration and in vivo permeation studies, IBU-NLC was gelled with a previously prepared 3% Carbopol 971P NF gel in a ratio of 1:1. For comparison, 0.5% IBU was dissolved in Macrogol 400 and gelled with the same polymer.

Particle size characterization and zeta potential measurements

The particle sizes of the prepared blank NLC and IBU-NLC formulations were analyzed by photon correlation spectroscopy (PCS) (Zetasizer Nano ZS; Malvern Instruments, Malvern, UK). The presence of particles in the micrometer range was excluded by laser diffraction (LD) (Mastersizer 2000; Malvern Instruments). The diameters of 10%, 50%, and 90% ($d(0.1)$, $d(0.5)$, and $d(0.9)$) of the particles were evaluated. The medium was purified water.

To obtain information concerning the stabilities of the prepared samples, their zeta potentials were determined with

a Zetasizer Nano ZS (Malvern Instruments). The medium was double-distilled water.

Atomic force microscopy

The particle size of the blank and IBU-NLC samples was also determined by AFM for comparison with the results obtained by PCS and LD measurements. The tapping mode was used on a SOLVER Scanning Probe Microscope (NT-MDT Co, Moscow, Russia) under ambient conditions. PPP-NVHAuD-10 (NANOSENSORS™; NanoWorld AG, Neuchatel, Switzerland) AFM tips with a nominal radius of curvature of 2 nm and a length of 15 µm were used.

XRD analysis

Diffractograms of the raw materials (IBU, Witepsol E85, and Lutrol F68), the melted physical mixtures of the raw materials with or without IBU, and the blank NLC and IBU-NLC were obtained with a Bruker D8 Advance diffractometer (Bruker AXS GmbH, Billerica, MA, USA) system with Cu K λI radiation (λ =1.5406 Å). Each sample was scanned at 40 kV and 40 mA in the interval 3°–40° 2θ, at a scanning speed of 0.1/second and a step size of 0.010°.

DXR Raman spectroscopy measurements

IBU, Witepsol E85, Miglyol 812, and Lutrol F68 (as standard components of the NLC), blank, and IBU-NLC samples were characterized. Raman spectra were recorded with a Thermo Fisher DXR Dispersive Raman spectrometer (Thermo Fisher Scientific Inc., Waltham, MA, USA) attached to an Olympus MPlan ×10/0.25 BD microscope (Olympus Corporation, Tokyo, Japan). At least five measurements were made at 532 nm with the in-built fluorescence and cosmic ray correction to ensure low background noise. Measurement conditions were as follows: power on the surface of the sample, 3 mW; diameter spot (×10 magnification objective), 3 µm; and aperture of the pinhole with 50 µm. Samples were packed onto an aluminum sample holder, and spectra were collected for a total of 48 scans at a spectral resolution of 4 cm^{-1}. For the characterization of IBU and NLC samples, the full spectral range (3,000–200 cm^{-1}) was used. IBU-NLC and blank NLC compositions were investigated by Raman mapping to localize the IBU inside the formulation. To identify the individual components in the Raman spectra, the vibrational chemical images were processed by a multivariate curve resolution – alternating least squares chemometric method. The NLC compositions were dried overnight on the aluminum surface to stabilize the NLC droplets for the Raman analysis. The 200–220 µm ×60 µm flat surfaces were analyzed at a step size of 10 µm. The acquisition time was 3 seconds per spectrum. Twenty-four spectra were accumulated and averaged at each measured point, ensuring an acceptable signal-to-noise ratio. The Raman spectra were then normalized to eliminate the intensity deviation between the measured areas.

FT-IR spectroscopy

FT-IR measurements of the pure drug and the NLC dispersions (blank and IBU-NLC) were performed with a Bio-Rad Digilab Division FTS-65A/896 FTIR spectrometer (Bio-Rad Laboratories Inc., Hercules, CA, USA) in the wavelength range 4,000–400 cm^{-1}, 128 scan size, and at an optical resolution of 4 cm^{-1}. The operating conditions were Harrick's Meridian SplitPea single reflection, diamond, and attenuated total reflectance accessory. The spectrum of the drug-loaded composition was processed to deconvolution in the range 1,800–1,660 cm^{-1} by a curve-fitting algorithm with a Gaussian–Lorentzian function. The best curve-fitting procedure was performed by iterative fits toward a minimum standard error. Thermo Scientific GRAMS/AI Suite software (Thermo Fisher Scientific Inc.) was used for the spectral analysis.

Drug loading and entrapment efficiency measurements

Drug loading (DL%) and entrapment efficiency (EE%) were evaluated by an indirect method, with measurement of the free drug concentration in the external aqueous phase:[26,27]

$$DL\% = \frac{W_{\text{initial drug}} - W_{\text{free drug}}}{W_{\text{lipid}}} \times 100\% \quad (1)$$

$$EE\% = \frac{W_{\text{initial drug}} - W_{\text{free drug}}}{W_{\text{initial drug}}} \times 100\% \quad (2)$$

where W is the weight in milligrams.

One hundred microliters of the IBU-NLC sample and 400 µL of phosphate-buffered saline (PBS) were transferred into a Nanosep 3K ultrafilter Eppendorf tube having an molecular weight cut-off of 3 kDa (Pall Co, Port Washington, NY, USA) and centrifuged at 5,055 rpm for 10 minutes. The solution obtained was filtered through a 0.20 µm polyethersulfone syringe membrane filter and injected directly into the HPLC system.

The IBU content was quantified with an Agilent 1260 HPLC system (chimically pure [QP], diode array detector, alternating least squares). IBU was measured on a 100 mm ×4.6 mm

column packed with 3 µm Luna C18, 100 Å (Phenomenex Inc., Torrance, CA, USA). Isocratic elution was performed with 40:60 (v/v) MeCN-PBS (0.025 M) (pH adjusted to 2.7 with orthophosphoric acid) at a flow rate of 1 mL/min. The buffer was prepared from KH_2PO_4 and K_2HPO_4. Before use, the eluent was degassed. The run time was 10 minutes. Detection was performed via the absorption at 215±4 nm. Ten microliters of sample was injected, and the elution was carried out at a sample temperature of 27°C and a column temperature of 35°C. Qualitative determination was achieved by comparison with the spectra of standards. The stock solution of IBU (0.5 mg/mL) was prepared in methanol and stored at 4°C. Working standards (1, 5, 10, 25, 50, and 100 µg/mL) were prepared freshly by diluting the stock solution with the mobile phase prior to the HPLC analysis. Calibration plots were freshly prepared and were highly linear (R^2>0.9998) in the concentration range 1.0–100.0 µg/mL (n=3–4).

In vitro release, in vitro permeation, and in vivo animal studies

The in vitro drug release study was carried out by using the dialysis bag method.[24,28,29] Briefly, 200 µL of the IBU-NLC formulation was sealed in a Spectra/Por® 4 dialysis membrane (Spectrum Laboratories, Inc., Rancho Dominguez, CA, USA), with Spectra/Por® Closures (Spectrum Laboratories, Inc.), and placed into 25 mL of PBS (pH 7.4). The system was held at 37°C to mimic in vivo conditions and continuously stirred at 450 rpm. At selected time intervals during 6 hours, 1 mL of bulk solution was taken. The withdrawn samples were each replaced by 1 mL of PBS to maintain sink conditions. Blank NLC served as blank and was analyzed in the same way as IBU-NLC. A previously prepared 1% IBU suspension was subjected to the same procedure, to serve as a reference.

The ex vivo permeation studies were performed with a vertical Franz diffusion cell system (Hanson Microette TM Topical & Transdermal Diffusion Cell System; Hanson Research Corporation, Chatsworth, CA, USA). A 0.300–0.400 g of 0.5% IBU-NLC gel or 0.5% IBU gel (which served as a reference) was measured as donor phase on pretreated excised human skin[10,30] supported by a Porafil® CM membrane (pore diameter 0.45 µm; Macherey-Nagel GmbH & Co. KG, Düren, Germany). The effective diffusion surface area was 1.3 cm^2. PBS (pH 7.4) was used as acceptor phase. The rotation of the magnetic stirbar was set to 450 rpm. The receptor medium was thermostated at 37°C±0.5°C to ensure the physiological skin temperature, 32°C at the site of the sampling. Experiments were performed for 6 hours. Samples of 0.8 mL were taken from the acceptor phase at given times by the autosampler (Hanson Microette Autosampling System; Hanson Research Corporation) and replaced with fresh receiving medium.

The samples from both experiments were analyzed at 263 nm with a Unicam Evolution 201 UV/Vis spectrophotometer (Thermo Fisher Scientific Inc.).

The in vivo animal studies were performed on 11- to 13-week-old male SKH-1 hairless mice (body weight: 28–34 g). The procedures and protocols applied were approved by the Ethical Committee for the Protection of Animals in Scientific Research at the University of Szeged (license number: V./145/2013). The modified dorsal skin fold chamber was used to determine IBU penetration through living animal skin by a previously described method.[31] This experimental setup provides an effective means of performing in vivo examinations of permeation.

The mice were randomly allocated into the following groups. The animals in group 1 (n=5) received IBU gel. In group 2 (n=7), IBU-NLC gel was used. 0.1 g of the study formulation was applied to the skin. One milliliter of PBS (pH 7.37) was added as the chamber acceptor phase. The observation period lasted for 6 hours. At given time points, the PBS was replaced by fresh PBS. The concentration of the penetrated drug was measured by means of HPLC. Previous tests of the blank NLC gel indicated that the components of this gel do not interfere with HPLC detection of the active agent. At the end of the experiment, the animals were euthanized with an overdose of ketamine.

The HPLC instrumentation included a Shimadzu CBM-20A/20Alite system controller, a Shimadzu LC-20AD solvent delivery system, a Shimadzu DGU-20A3 on-line degasser, a Shimadzu SPD-M20A UV/VIS photodiode array detector, and a Shimadzu CTO-20A column oven (Shimadzu Corp, Kyoto, Japan). The chromatographic system was equipped with a Rheodyne Model 7725i injector (IDEX Corp, Lake Forest, IL, USA) with a 20 µL loop. The chromatographic data were collected and processed by means of Shimadzu LCsolution software (Shimadzu Corp).

Statistical analysis

The results were evaluated and analyzed statistically with the two-way analysis of variance test (Bonferroni's multiple comparison), using Prism for Windows 5 software (GraphPad Software Inc., La Jolla, CA, USA). The data are the averages of the results of at least five experiments ± standard deviation (*P<0.05, **P<0.01, ***P<0.001, and ****P<0.0001 versus the control).

Results

Results of particle size and zeta potential measurements

Particle size determination by PCS demonstrated that both samples were in the nanometer range, with an effective particle size (Z_{ave}) of 114 nm for the blank NLC and 106 nm for IBU-NLC. LD measurements confirmed that larger particles (>1 μm) were not present in the formulations, and 90% of the particles measured <205 nm. The surface charge was negative for both the blank (−15.9 mV) and IBU-NLC (−18.4 mV) (Table 1).

Results of AFM measurements

Both samples were measured by AFM to confirm the PCS and LD results. The data were evaluated by grain analysis, and size distribution histograms were made (Figure 1A and B). The *Z* values of most of the blank NLC particles were between 109 and 124 nm, while those of the IBU-NLC were between 95 and 118 nm (Figure 1C and D), verifying the PCS and LD results.

AFM has been widely used to acquire information on the size, shape, and surface morphology of nanoparticles.[32] In all the present samples, the separated lipid particles were spherical or nearly spherical with a smooth surface (Figure 2). No major differences were detected between the blank and IBU-NLC samples, although some larger lipid agglomerates were found in the IBU-NLC. This is probably due to the sample preparation process: the pretreatment (sonication) was unable to disperse the previously dried lipid particles completely.

Results of XRD

XRD measurements were carried out to determine the possible changes in the crystallinity of the components during the hot high-pressure homogenization procedure. Diffractograms of the pure, untreated components (IBU, Witepsol E85, and Lutrol F68) are depicted in Figure 3. Diffractograms were also recorded of the melted lipid mixture (Witepsol E85 and Miglyol 812 in a ratio of 7:3) with or without IBU, the melted total physical mixture, the blank, and IBU-NLC. The crystallinity of the solid lipid (plot 2) decreased to such an extent after the addition of the excipients (plots 4 and 6) and the drug (plot 5) that the material became amorphous in the cases of the prepared blank (plot 7) and IBU-NLC (plot 8) formulations. This suggests that both of the NLC formulations have a structureless solid amorphous matrix and belong to the amorphous NLC type.[33] The XRD pattern of pure racemic IBU (plot 1) exhibited characteristic diffraction peaks at various diffraction angles (6°, 12.3°, 16°, 20.4°, and 22.3° 2θ), indicating the presence of crystallinity.[34] These peaks also appeared in the plot of the melted mixture of the lipid matrix and the active pharmaceutical ingredient (plot 5) but were absent from those of the total mixture (plot 6) IBU-NLC (plot 8).

Results of DXR Raman spectroscopy measurements

Raman spectroscopy was employed to confirm the physical state of the IBU and to study the possible physicochemical interactions between the components. The Raman spectra of dried free racemic IBU, Lutrol F68, Witepsol E85, and Miglyol 812 are presented in the wavenumber range 2,000–200 cm^{-1} in Figure 4A. As model solutions, IBU was dissolved in Miglyol 812 in two concentrations (10% and 25%, w/w), to observe the principal differences in the physical state of the IBU (Figure 4B). The spectra of IBU, the blank NLC, and IBU-NLC are presented in Figure 4C.

The selected Raman bands of IBU, the IBU-containing Miglyol model solutions, and the IBU-NLC composition with the vibrational assignments (cm^{-1}) are presented in Table 2. The chemical structure of Miglyol is very similar to those of the other lipid components, and therefore, the bands from the IBU-NLC sample, Raman spectrum characteristic of Miglyol 812, could be overlapped by the bands characteristic of other lipids.

The IBU spectrum exhibited characteristic peaks at 1,608, 1,576, 1,208, 1,182, 1,008, 959, 834, 746, 638, and 415 cm^{-1}. These peaks are attributed mainly to aryl ring stretching and C_{24}-Ar-C_{11} conformational stretching and wagging. Medium sharp peaks are attributed to Ar and Ar-CH in-plane and out-of-plane bending. In spite of the many free racemic IBU peaks, the Raman spectra of the model solutions and the NLC composition were characteristic of the auxiliary

Table 1 Particle size, zeta potential, polydispersity index, span value, and average *Z* (height) value of the blank NLC and IBU-NLC formulations (the measurements were performed in triplicate, n=3)

Sample	Z_{ave} (nm)	ZP (mV)	PDI	*d*(0.1) (nm)	*d*(0.5) (nm)	*d*(0.9) (nm)	Span value	Average *Z* (nm)
Blank NLC	114±2.2	−15.9±0.7	0.15±0.1	67±0	118±0	204±0.6	1.16±0	113.67±15.5
IBU-NLC	106±1.7	−18.4±1.3	0.18±0.3	74±0	122±0	205±0.6	1.07±0	107.47±14.4

Abbreviations: NLC, nanostructured lipid carrier; IBU-NLC, ibuprofen-loaded nanostructured lipid carrier; ZP, zeta potential; PDI, polydispersity index.

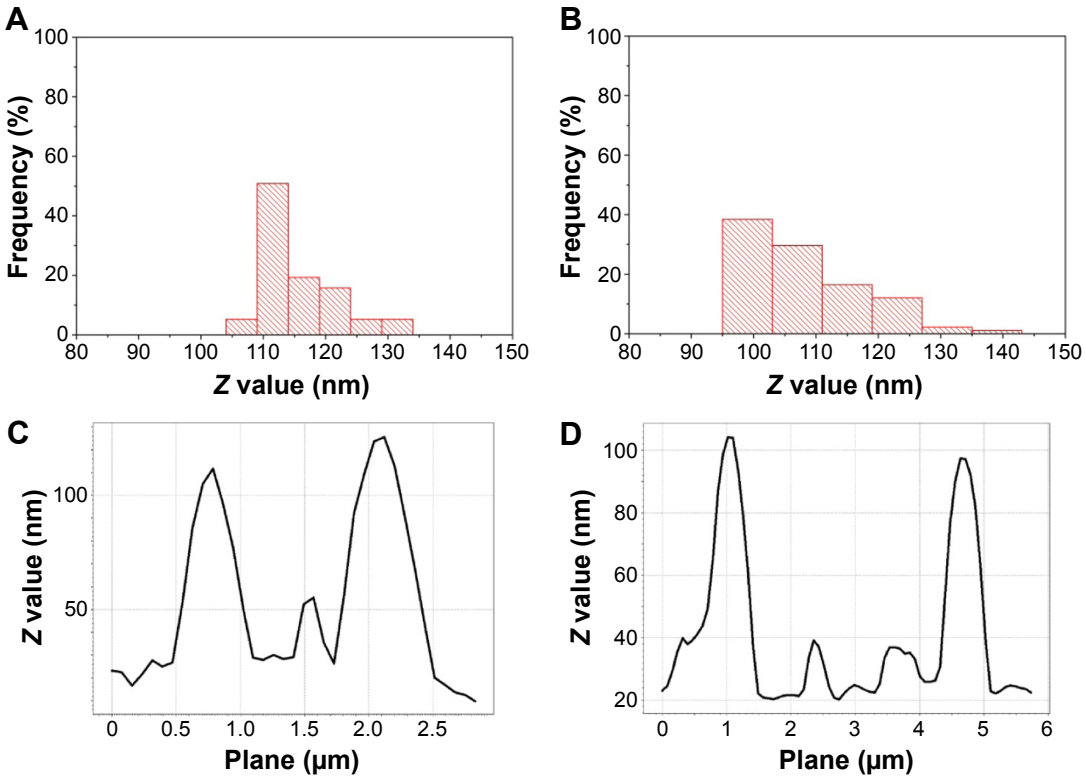

Figure 1 *Z* value distribution (height) of blank NLC (**A**) and IBU-NLC (**B**) and *Z* value (height) of blank NLC (**C**) and IBU-NLC (**D**) (n=3).
Abbreviations: NLC, nanostructured lipid carrier; IBU-NLC, ibuprofen-loaded nanostructured lipid carrier.

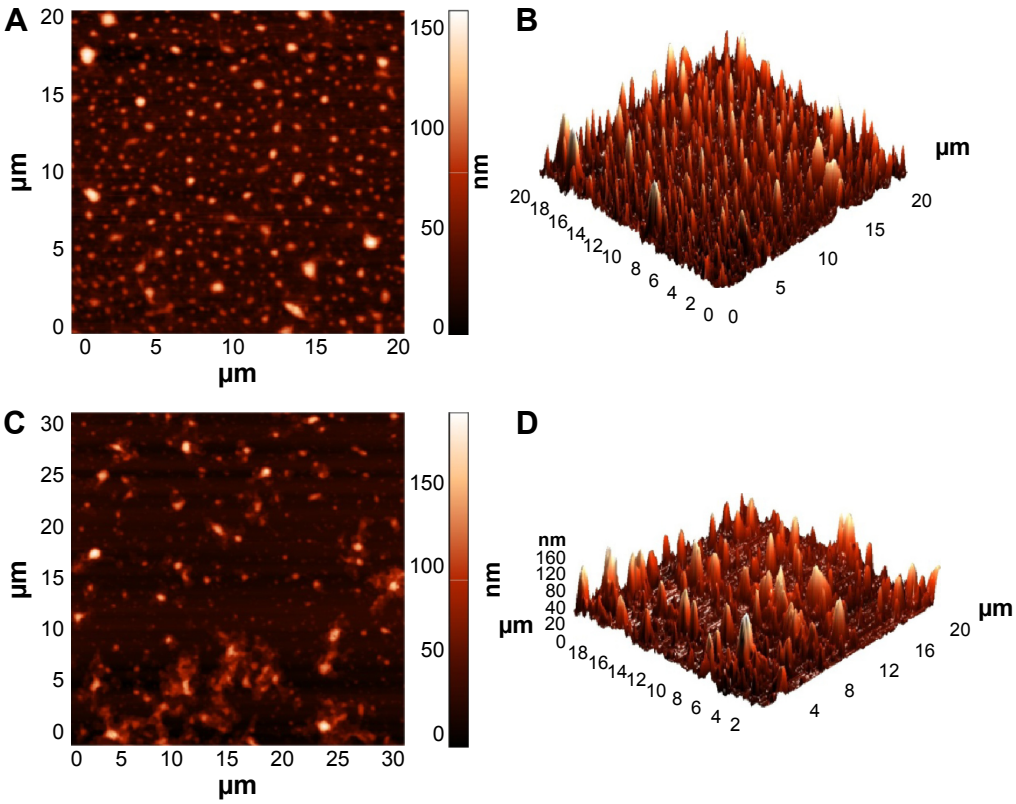

Figure 2
Notes: 2D images of blank NLC (**A**) and IBU-NLC (**C**). 3D images of blank NLC (**B**) and IBU-NLC (**D**) revealing the morphology and size of the formulations (n=3).
Abbreviations: 2D, two dimensional; NLC, nanostructured lipid carrier; IBU-NLC, ibuprofen-loaded nanostructured lipid carrier; 3D, three dimensional.

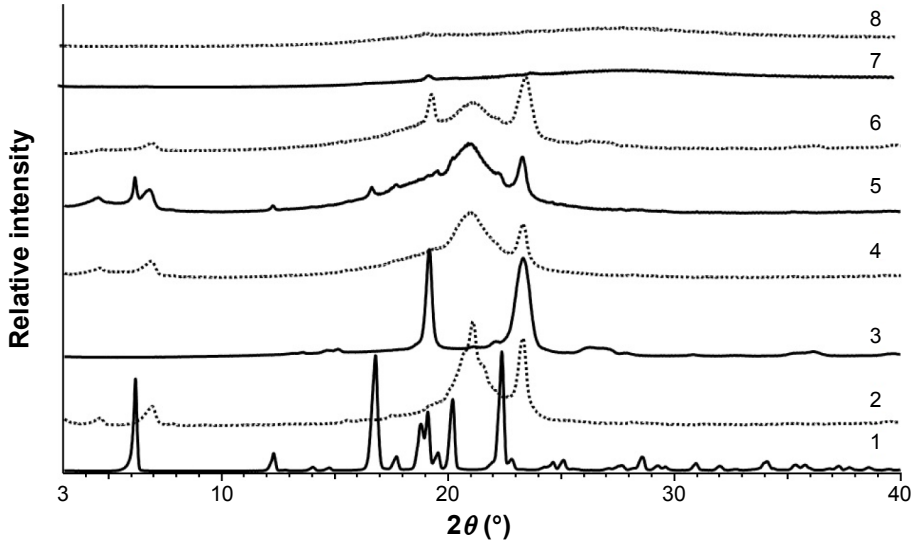

Figure 3 XRD diffractograms of IBU (1), Witepsol E85 (2), Lutrol F68 (3), bulk mixture of Witepsol E85:Miglyol 812 mixture in ratio 7:3 (4), Witepsol E85:Miglyol 812:IBU mixture in ratio 7:3:1 (5), Witepsol E85:Miglyol 812:IBU:Lutrol F68 mixture in ratio 7:3:1:5 (6), blank NLC (7) and IBU-NLC (8).
Abbreviations: XRD, X-ray diffraction; IBU, ibuprofen.

materials. The medium-intensity IBU peaks at 1,452, 1,341, 1,116, 943, 820, 662, 784, and 269 cm^{-1} (C_x–H_y bending, twisting, or rocking) were absent from the spectra of the IBU-containing model solutions and NLC composition. Comparison of the Raman peaks of the IBU and the model solutions (10% and 25%) revealed small shifts in the wavenumbers of the characteristic IBU peaks. Moreover, the Raman spectrum of the IBU-NLC composition (with less characteristic IBU peaks) revealed the same small shifts, indicating the occurrence of weak interactions between

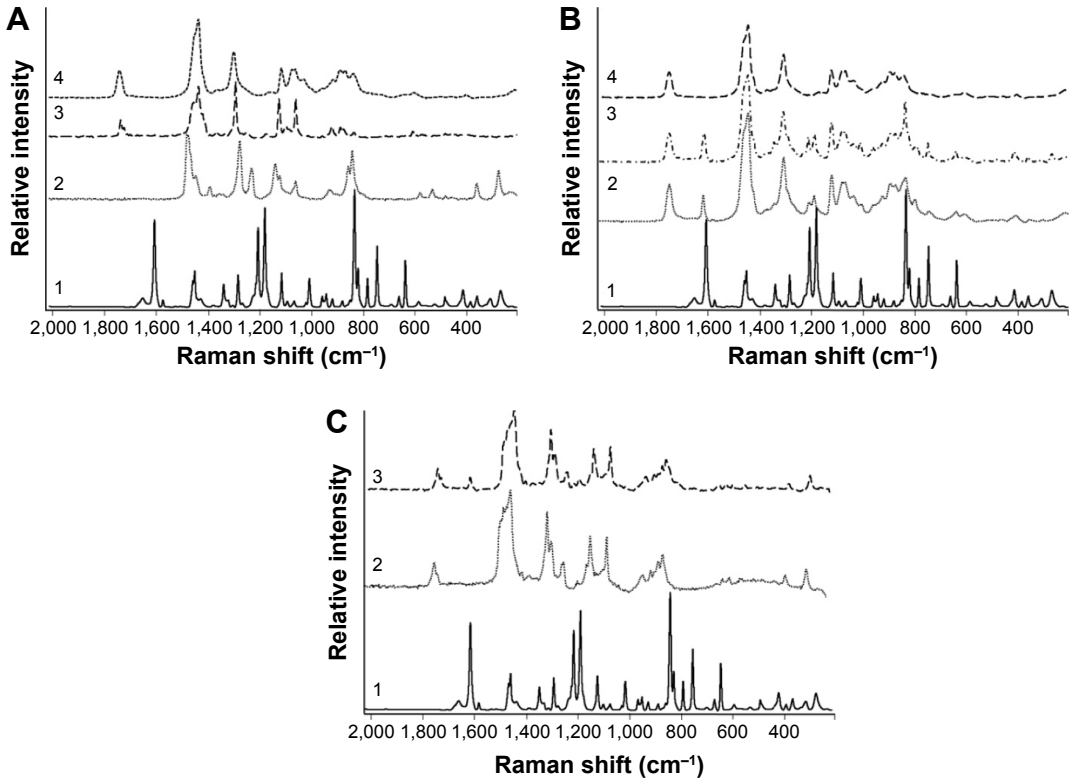

Figure 4
Notes: (**A**) Raman spectra of individual components, as IBU (1), Lutrol F68 (2), Witepsol E85 (3), and Miglyol 812 (4). (**B**) Raman spectra of IBU (1) and the model mixtures of 10% IBU (2) and 25% IBU (3) both dissolved in Miglyol 812 (4). (**C**) Raman spectra of IBU (1), drug-free NLC composition, as blank NLC (2), and IBU-containing composition, as IBU-NLC (3) in the range of 2,000–200 cm^{-1} (n=3).
Abbreviations: IBU, ibuprofen; NLC, nanostructured lipid carrier; IBU-NLC, ibuprofen-loaded nanostructured lipid carrier.

Table 2 Observed Raman peaks (in cm^{-1}) and peak assignments of free racemic IBU and IBU-containing model solutions and NLC compositions

IBU (literature)	Assignment	10%	25%	IBU-NLC
1,608	s(C–C)Ar	1,613	1,609	1,616
1,576	s(C–C)Ar and v(C=C)Ar	1,574	1,574	–
1,208	t(CH_2) (C_{11}–C_{12}–C_{13})	1,207	1,206	1,208
1,182	s(C_6–C_{11})	1,185	1,182	1,185
1,008	in(CH)Ar	1,004	1,007	1,004
959	r($C_{26}H_3$) and antisymmetric s(C_{26}–C_{24}–C_{30})	957	957	955
834	out(CH)Ar	832	833	–
746	r(CH_3) and out(CH)Ar	739	745	–
638	out(CO–H) and in(Ar)	637	636	–
415	d(C_{15}–C_{14}–C_{19})	405	412	–

Notes: Assignments have been compared with those found in the literature in order to seek for peak shifts (n=3). Significant shifts appear in bold.
Abbreviations: IBU, ibuprofen; NLC, nanostructured lipid carrier; IBU-NLC, ibuprofen-loaded nanostructured lipid carrier; s, stretching; Ar, aromatic; v, vibration; t, twisting; in, in-plane bending; r, rocking; out, out-of-plane bending; d, deformation.

IBU and the lipids. A significant change in the spectrum of interacted IBU was the shift in the peak corresponding to the aryl C–C stretching from 1,608 to 1,609–1,616 cm^{-1}. This latter shift indicates that the aryl ring is affected by the interaction with the lipid molecules and not the C=O group of IBU. In Table 3, the Raman spectra of the lipid components are compared with those of IBU-NLC and the blank NLC. The lipid components used in this study have similar chemical structures and therefore similar Raman bands. The Raman spectra of the lipid components in the range 3,000–200 cm^{-1} displayed characteristic peaks, which are assigned to vibrations of the fatty acid hydrocarbon chains. The sharp and intense peaks at 2,881 and 2,850 cm^{-1} and the medium peaks at 1,128 and 1,062 cm^{-1} in all the NLC compositions confirmed the ordered acyl chains in the lipid structure. The incorporation of IBU did not lead to the disappearance of the sharp bands at 2,881 and 2,850 cm^{-1} in the Raman spectrum of IBU-NLC.

In order to confirm the homogeneity of the IBU, Raman mapping of the NLC was performed. Figure 5A shows the distribution map of IBU in the NLC composition at ×10 magnification. The characteristic bands obtained for IBU at ~1,608 cm^{-1} were used to visualize the spatial distribution of IBU from Raman chemical mapping. The IBU was found homogeneously in the dried, round areas. The purpose of this analysis was to estimate the distribution of the individual ingredients in the scanned area. The spectra of the estimated "Components" were compared with the reference ingredient spectra (Figure 5B). The spectra of components 1 and 4 were identified as the Raman spectrum of Lutrol F68, with characteristic Raman band regions of 1,750–1150, 900–750, and 400–200 cm^{-1}. The resolved spectrum of component 2 does not correspond to the reference spectra but contains similar Raman bands to those of Miglyol 812. The spectrum of component 2 displays several other peaks; the reason may be the low signal-to-noise ratio. Component 3 corresponds to Witepsol E85, with very characteristic Raman band regions of 1,500–1,400 and 1,150–1,000 cm^{-1}. The Raman spectra of each component contain the characteristic Raman peaks of IBU at 1,614–1,608 cm^{-1}.

Table 3 Observed Raman peaks (in cm^{-1}) and peak assignments of individual lipid components and NLC compositions (n=3)

Assignment	Lutrol F68	Witepsol E85	Miglyol 812	Blank NLC	IBU-NLC
s(CH)	2,934	2,935	2,931	2,936	2,935
s(CH_2) antisymmetric	2,884	2,880	–	2,881	2,881
s(CH_2) symmetric	–	2,846	2,853	2,850	2,850
s(CH)	–	2,724	2,728	2,724	2,725
s(C=O)	–	1,739	1,745	1,741	1,742
CH_2 scissoring and s(C–O)	–	1,438	1,439	1,441	1,441
t(CH_2) and s(C–O)	–	1,295	1,302	1,297	1,297
s(C–C) symmetric and s(C–O–C) asymmetric	1,125	1,126	–	1,128	1,128
s(C–C) asymmetric and s(C–O) symmetric	1,062	1,062	1,063	1,063	1,063
r(CH_3)	–	889	889	889	892
r(CH_3)	843	–	841	844	845

Abbreviations: NLC, nanostructured lipid carrier; IBU-NLC, ibuprofen-loaded nanostructured lipid carrier; s, stretching; t, twisting; r, rocking.

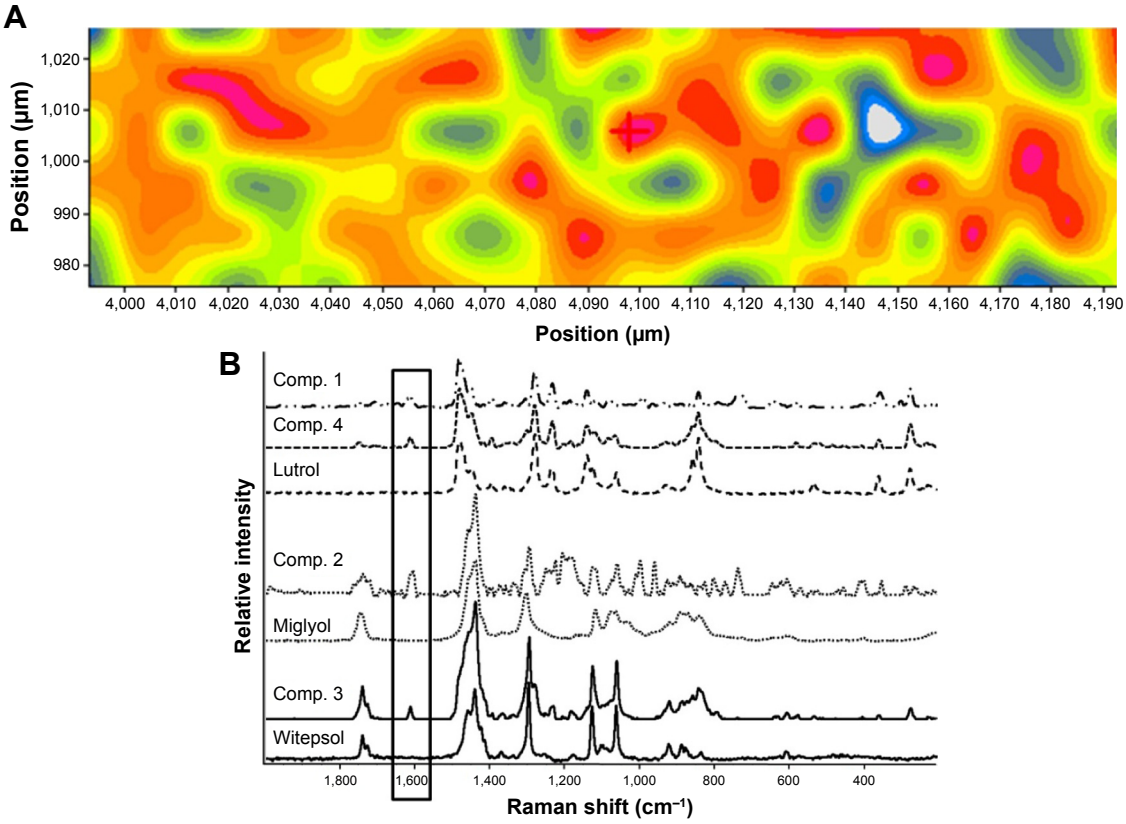

Figure 5
Notes: (**A**) Raman distribution map of IBU in the IBU-NLC composition (×10 magnification). (**B**) Multivariate curve resolution of IBU-NLC Raman chemical mapping. Spectra of the estimated ingredients, "Components", are compared to reference spectra of individual ingredients (n=3).
Abbreviations: IBU, ibuprofen; IBU-NLC, ibuprofen-loaded nanostructured lipid carrier.

Results of FT-IR

The FT-IR spectra of the excipients, blank NLC, and IBU-NLC were recorded to obtain information about the possible interactions between IBU and the matrix of the nanoparticles. Analysis of the spectrum of IBU-NLC clearly indicates that there are no strong interactions between the drug and the excipients (Figure 6A). Comparison of the FT-IR spectra of the blank NLC and the drug-loaded IBU-NLC at 1,700 and 1,550 cm^{-1} revealed two peaks (which are characteristic of the drug) as shoulders in the spectrum of IBU-NLC (Figure 6A, marked peaks). After the deconvolution of the wavelength range 1,800–1,660 cm^{-1},

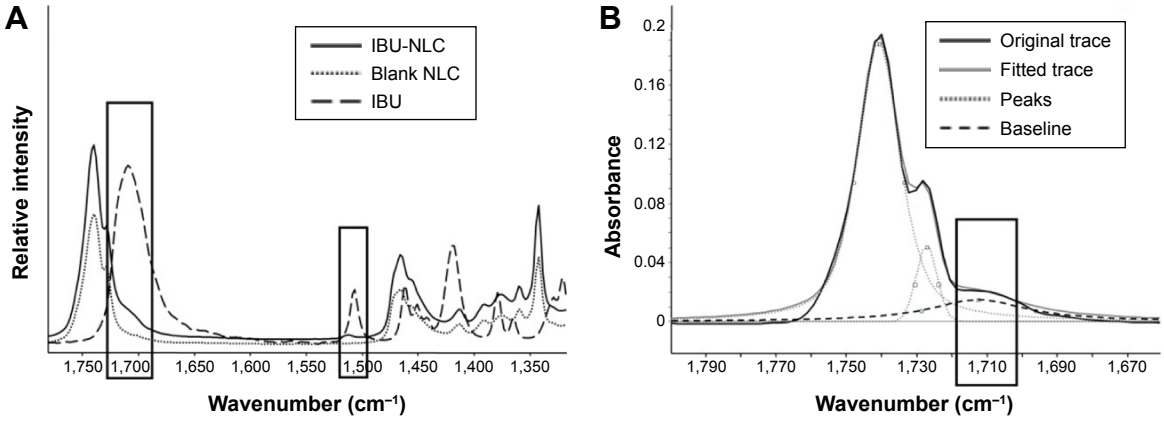

Figure 6
Notes: (**A**) FT-IR spectra of IBU-NLC, blank NLC, and IBU. (**B**) Deconvolution of IBU-NLC from 1,800 to 1,665 cm^{-1} (n=3). The boxes highlight the small peaks/shoulders, which are characteristic to the drug, and a significant shift has occurred in their position compared to the native spectrum of ibuprofen.
Abbreviations: FT-IR, Fourier transformation infrared; IBU-NLC, ibuprofen-loaded nanostructured lipid carrier; NLC, nanostructured lipid carrier; IBU, ibuprofen.

the characteristic peak of IBU at 1,721 cm^{-1}, described as the vibration of the C=O bond,[35] could be characterized (Figure 6B). The intensity of this peak is low, which means that nondissolved IBU is present in low concentrations. The presence of drug crystals could be due to the pretreatment of the samples before the measurement (the NLC dispersions were dried in air).

Results of drug loading and entrapment efficiency

From the results of the applied HPLC method, DL was found to be 9.85%±4.10% and EE 98.51%±4.10% for the prepared IBU-NLC composition, since 1.49%±4.10% of the IBU was measured in the outer aqueous phase.

Results of in vitro release, ex vivo permeation, and in vivo animal studies

The in vitro diffusion of IBU through the artificial membrane from IBU-NLC and the IBU suspension was calculated in terms of the mean cumulative amount diffused at each sampling time point during a period of 6 hours (Figure 7A). The amount of IBU diffused from the IBU-NLC after 6 hours was significantly higher (2.59-fold) than that from the IBU suspension.

The ex vivo penetration of the drug from the prepared IBU-NLC gel and IBU gel through excised human skin was calculated in the same way as for the in vitro measurements (Figure 7B). The permeation of IBU through the excised human skin was 12.78-fold higher from the IBU-NLC gel than from the traditional IBU gel. These findings correlate with those of the in vitro diffusion study, since after 6 hours, much higher drug permeation could be observed from the IBU-NLC gel than from the IBU gel.

Finally, the in vivo permeation of IBU from the IBU-NLC gel and the IBU gel was determined with a murine model, using a modified dorsal skin chamber; the results are presented in Figure 7C. The drug penetration was significantly higher (1.87-fold, $P>0.001$) from the IBU-NLC gel

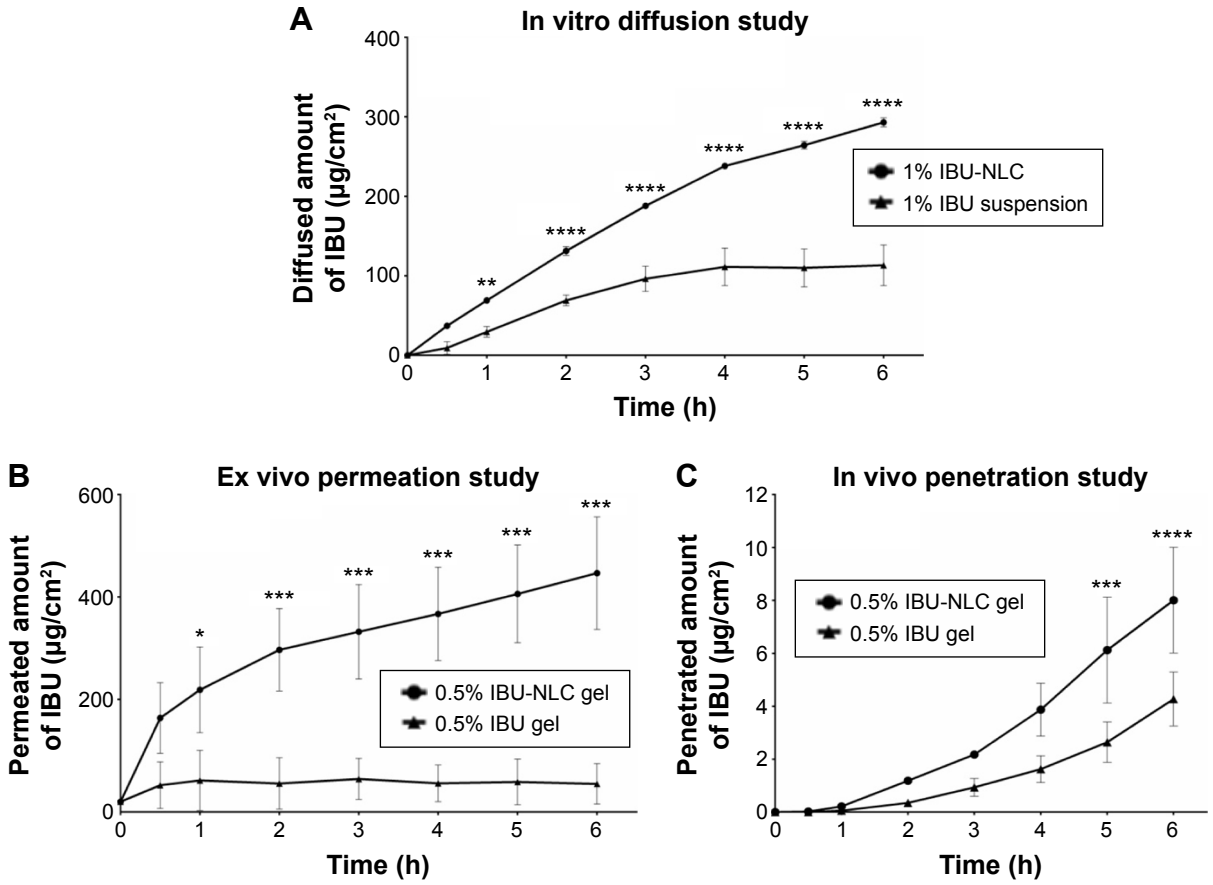

Figure 7

Notes: (**A**) In vitro diffusion of IBU from IBU-NLC (filled circle) and IBU suspension (filled triangle) (n=5). (**B**) Ex vitro permeation through excised human epidermis of IBU from IBU-NLC gel (filled circle) and IBU gel (filled triangle) (n=5). (**C**) In vivo permeation through living animal skin of IBU from IBU-NLC gel (filled circle) and IBU gel (filled triangle) (n=5–7).

Abbreviations: IBU, ibuprofen; IBU-NLC, ibuprofen-loaded nanostructured lipid carrier; h, hours.

formulation than from the IBU gel, as found in the previous in vitro and ex vivo studies.

Discussion

An NLC-based gel of IBU was produced. Characterization of the IBU-NLC dispersion by PCS, LD, and AFM proved the appropriate size range and morphological properties of the lipid nanoparticles, which are essential for the stability and the desired performance of the formulation. XRD measurements and the high EE (98.51%) both confirmed the presence of IBU as a molecular dispersion in the lipid matrix of the final formulation. The results of Raman spectroscopy and FT-IR analysis indicated that the ordered lipid structure was not affected by the presence of the IBU molecules. The homogeneous distribution of the IBU in the lipid matrix and the weak interactions between the drug and the excipients predicted rapid drug liberation, since there is no need for energy to break the bonds between the drug and the excipients. These findings were confirmed by drug diffusion and permeation studies. The in vitro diffusion study demonstrated higher drug permeation from the IBU-NLC than from the IBU suspension. The permeation of IBU through the excised human skin was also significantly higher from the IBU-NLC gel than from the IBU gel. The higher penetration rate is probably due to the direct contact between the lipid nanoparticles and the lipids of the stratum corneum, which results in the increase of the penetration channels through the skin. The NLC carrier-based gel facilitated the drug permeation through the living animal skin even under physiological conditions.

It can be concluded that the IBU-NLC gel is of great potential to increase drug permeation through the skin and enhance the efficacy of the treatment for OA and other musculoskeletal inflammations.

Acknowledgments

The authors would like to thank Miss Gabriella Farkas for analyzing the FT-IR spectra, Péter Sipos, PhD, for the Raman measurements and analysis, as well as Piroska Révész, PhD, DSc, for revising the manuscript critically for important intellectual content.

The authors would also like to thank Azelis Ltd, Sasol GmbH, and BASF SE for the gift samples.

The financial support of the Hungarian National Research Fund projects OTKA NN 110676 and K 112531 is acknowledged.

Disclosure

The authors report no conflicts of interest in this work.

References

1. Bijlsma JWJ, Berenbaum F, Lafeber FP. Osteoarthritis: an update with relevance for clinical practice. *The Lancet*. 2011;377(9783):2115–2126.
2. Zeng C, Li H, Yang T, et al. Electrical stimulation for pain relief in knee osteoarthritis: systematic review and network meta-analysis. *Osteoarthritis Cartilage*. 2015;23(2):189–202.
3. Dahaghin S, Bierma-Zeinstra SM, Ginai AZ, Pols HA, Hazes JM, Koes BW. Prevalence and pattern of radiographic hand osteoarthritis and association with pain and disability (the Rotterdam study). *Ann Rheum Dis*. 2005;64(5):682–687.
4. Dieppe PA, Lohmander LS. Pathogenesis and management of pain in osteoarthritis. *The Lancet*. 2005;365(9463):965–973.
5. Hochberg MC, Altman RD, April KT, et al. American College of Rheumatology 2012 recommendations for the use of nonpharmacologic and pharmacologic therapies in osteoarthritis of the hand, hip, and knee. *Arthritis Care Res (Hoboken)*. 2012;64(4):465–474.
6. Potthast H, Dressman JB, Junginger HE, et al. Biowaiver monographs for immediate release solid oral dosage forms: ibuprofen. *J Pharm Sci*. 2005;94(10):2121–2131.
7. Patel A, Bell M, O'Connor C, Inchley A, Wibawa J, Lane ME. Delivery of ibuprofen to the skin. *International Journal of Pharmaceutics*. 2013;457(1):9–13.
8. Akhter SA, Barry BW. Absorption through human skin of ibuprofen and flurbiprofen; effect of dose variation, deposited drug films, occlusion and the penetration enhancer N-methyl-2-pyrrolidone. *J Pharm Pharmacol*. 1985;37(1):27–37.
9. Bock U, Krause W, Otto J, Haltner E. Comparative in vitro and in vivo studies on the permeation and penetration of ketoprofen and ibuprofen in human skin. *Arzneimittelforschung*. 2004;54(9):522–529.
10. Csizmazia E, Erős G, Berkesi O, Berkó S, Szabó-Révész P, Csányi E. Penetration enhancer effect of sucrose laurate and Transcutol on ibuprofen. *Journal of Drug Delivery Science and Technology*. 2011;21(5):411–415.
11. Hadgraft J, Valenta C. pH, pKa and dermal delivery. *International Journal of Pharmacology*. 2000;200(2):243–247.
12. Watkinson RM, Guy RH, Hadgraft J, Lane ME. Optimisation of cosolvent concentration for topical drug delivery – II: influence of propylene glycol on ibuprofen permeation. *Skin Pharmacol Physiol*. 2009;22(4):225–230.
13. Watkinson RM, Herkenne C, Guy RH, Hadgraft J, Oliveira G, Lane ME. Influence of ethanol on the solubility, ionization and permeation characteristics of ibuprofen in silicone and human skin. *Skin Pharmacol Physiol*. 2009;22(1):15–21.
14. Rhee YS, Chang SY, Park CW, Chi SC, Park ES. Optimization of ibuprofen gel formulations using experimental design technique for enhanced transdermal penetration. *Int J Pharm*. 2008;364(1):14–20.
15. Müller RH, Mäder K, Gohla S. Solid lipid nanoparticles (SLN) for controlled drug delivery – a review of the state of the art. *European Journal of Pharmaceutics and Biopharmaceutics*. 2000;50(1):161–177.
16. Mehnert W, Mäder K. Solid lipid nanoparticles: production, characterization and applications. *Advanced Drug Delivery Reviews*. 2001;47(2–3):165–196.
17. Müller RH, Radtke M, Wissing SA. Solid lipid nanoparticles (SLN) and nanostructured lipid carriers (NLC) in cosmetic and dermatological preparations. *Advanced Drug Delivery Reviews*. 2002;54 Suppl 1:S131–S155.
18. Müller RH, Petersen RD, Hommoss A, Pardeike J. Nanostructured lipid carriers (NLC) in cosmetic dermal products. *Advanced Drug Delivery Reviews*. 2007;59(6):522–530.
19. Joshi M, Patravale V. Nanostructured lipid carrier (NLC) based gel of celecoxib. *Int J Pharm*. 2008;346(1–2):124–132.
20. Müller RH, Rühl D, Runge S, Schulze-Forster K, Mehnert W. Cytotoxicity of solid lipid nanoparticles as a function of the lipid matrix and the surfactant. *Pharmaceutical Research*. 1997;14(4):458–462.

21. Yang X, Zhao L, Almasy L, et al. Preparation and characterization of 4-dedimethylamino sancycline (CMT-3) loaded nanostructured lipid carrier (CMT-3/NLC) formulations. *Int J Pharm*. 2013; 450(1–2):225–234.
22. Wissing SA, Müller RH. The influence of the crystallinity of lipid nanoparticles on their occlusive properties. *Int J Pharm*. 2002; 242(1–2):377–379.
23. Wissing SA, Müler RH. Solid lipid nanoparticles as carrier for sunscreens: in vitro release and in vivo skin penetration. *J Control Release*. 2002;81(3):225–233.
24. Araujo J, Garcia ML, Mallandrich M, Souto EB, Calpena AC. Release profile and transscleral permeation of triamcinolone acetonide loaded nanostructured lipid carriers (TA-NLC): in vitro and ex vivo studies. *Nanomedicine*. 2012;8(6):1034–1041.
25. Farboud ES, Nasrollahi SA, Tabbakhi Z. Novel formulation and evaluation of a Q10-loaded solid lipid nanoparticle cream: in vitro and in vivo studies. *Int J Nanomedicine*. 2011;6:611–617.
26. How CW, Rasedee A, Manickam S, Rosli R. Tamoxifen-loaded nanostructured lipid carrier as a drug delivery system: characterization, stability assessment and cytotoxicity. *Colloids Surf B Biointerfaces*. 2013;112:393–399.
27. Shi F, Zhao J-H, Liu Y, Wang Z, Zhang Y-T, Feng N-P. Preparation and characterization of solid lipid nanoparticles loaded with frankincense and myrrh oil. *Int J Nanomedicine*. 2012;7:2033–2043.
28. Kheradmandnia S, Vasheghani-Farahani E, Nosrati M, Atyabi F. Preparation and characterization of ketoprofen-loaded solid lipid nanoparticles made from beeswax and carnauba wax. *Nanomedicine*. 2010;6(6):753–759.
29. Xie S, Zhu L, Dong Z, Wang Y, Wang X, Zhou W. Preparation and evaluation of ofloxacin-loaded palmitic acid solid lipid nanoparticles. *Int J Nanomedicine*. 2011;6:547–555.
30. Kligman AM, Christophers E. Preparation of isolated sheets of human stratum corneum. *Arch Dermatol*. 1963;88(6):702–705.
31. Erős G, Hartmann P, Berkó S, et al. A novel murine model for the in vivo study of transdermal drug penetration. *Scientific World Journal*. 2012; 2012:543536.
32. Neupane YR, Srivastava M, Ahmad N, Kumar N, Bhatnagar A, Kohli K. Lipid based nanocarrier system for the potential oral delivery of decitabine: formulation design, characterization, ex vivo, and in vivo assessment. *Int J Pharm*. 2014;477(1–2):601–612.
33. Üner M, Yener G. Importance of solid lipid nanoparticles (SLN) in various administration routes and future perspectives. *Int J Nanomedicine*. 2007;2(3):289–300.
34. de Villiers MM, Liebenberg W, Malan SF, Gerber JJ. The dissolution and complexing properties of ibuprofen and ketoprofen when mixed with N-methylglucamine. *Drug Dev Ind Pharm*. 1999;25(8):967–972.
35. Matkovic SR, Valle GM, Briand LE. Quantitative analysis of ibuprofen in pharmaceutical formulations through FTIR spectroscopy. *Latin American Applied Research*. 2005;35:189–195.